The Thesis Committee for Mark Timothy Eason
Certifies that this is the approved version of the following thesis:

Experimental Performance of High Mast Illumination Poles with Pre-Existing Cracks

APPROVED BY
SUPERVISING COMMITTEE:

Michael Engelhardt, Supervisor

Todd Helwig

Experimental Performance of High Mast Illumination Poles with Pre-Existing Cracks

by

Mark Timothy Eason, B.S.C.E.

Thesis

Presented to the Faculty of the Graduate School of

The University of Texas at Austin

in Partial Fulfillment

of the Requirements

for the Degree of

Master of Science in Engineering

The University of Texas at Austin

December 2016

Dedication

I dedicate this work to:

My family, for your constant love, guidance, and support.

Heather, for your love, prayers, and patience throughout the last year.

Acknowledgements

I would like to thank Dr. Michael Engelhardt and Dr. Todd Helwig. It has been a pleasure learning from and working for both of you. Your guidance is immeasurable and your jokes are like no others.

Thank you also to the Texas Department of Transportation for funding this research project and in turn, my education.

To John Kintz and Heather Wilson, thank you for your friendship. You are truly wonderful people and I am lucky to have both of you in my life. Your help in classes and around the lab will never be forgotten. We have become a great team and even better friends. I look forward to continuing our friendships for many years to come.

To the staff Ferguson Structural Engineering Laboratory, thank you for all of the help. In particular, thank you Blake Stasney, David Braley, Mike Brown, and Dennis Phillip. You were always patient and willing to help, even when I was unsure of how things should be done.

Finally, thank you to all of my friends, both at the Ferguson Lab and elsewhere. You have all been there when I've needed you and are all part of fantastic memories. We have become family and for that I am grateful.

Abstract

Experimental Performance of High Mast Illumination Poles with Pre-Existing Cracks

Mark Timothy Eason, M.S.E

The University of Texas at Austin, 2016

Supervisor: Michael Engelhardt

High Mast Illumination Poles (HMIPs) are tall structures used to provide lighting along highways. There are a large number of in-service HMIPs in Texas that have pre-existing cracks at the weld that joins the pole shaft with the baseplate. Previous research has shown these pre-existing cracks occur during the galvanizing process, before the poles are put into service. Once in service, these pre-existing cracks can grow under repeated loading generated by wind, and most notably by vortex shedding. While none of these HMIPs in Texas have failed, the presence of the pre-existing cracks and potential for wind-induced crack growth raises safety concerns. .

The work reported in this thesis is part of TxDOT Research Project 0-6829: "Fatigue Resistance and Reliability of High Mast Illumination Poles (HMIPs) with Pre-Existing Cracks." TxDOT Project 0-6829 is aimed at generating data and information to support a probabilistic based assessment of the remaining life of pre-cracked HMIPs. The scope of Project 0-6829 includes laboratory fatigue tests on galvanized HMIPs with pre-existing cracks, field studies and measurements to characterize the wind response of

Texas HMIPs, the development of a reliability based framework to assess the fatigue life of in-service pre-cracked HMIPs, and recommendations for possible retrofit techniques for in-service HMIPs. The research reported in this thesis focuses on the task of conducting laboratory fatigue tests of galvanized HMIP specimens with pre-existing cracks at the shaft to baseplate weld. The objective of this work was to develop additional experimental data, to supplement experimental data collected in earlier studies, to characterize the fatigue performance of galvanized HMIPs with pre-existing cracks. A more specific objective was to collect fatigue test data on pre-cracked HMIPs at low stress ranges, representative of the stress ranges seen by in-service HMIPs subject to vortex induced vibration. This thesis reports the results of a series of fatigue tests on HMIP specimens, including a description of the test setup and test procedures, a presentation of ultrasonic test results that measured crack growth during the course of the fatigue tests, and the test results.

Table of Contents

List of Tables

List of Figures

Chapter 1: Introduction

This chapter provides background for a fatigue study on high mast illumination poles conducted at the University of Texas at Austin's Ferguson Structural Engineering Laboratory. It will describe the problem being studied and provide the necessary background knowledge to understand the research and conclusions discussed in the chapters following.

1.1 BACKGROUND

This study addresses the fatigue performance of High Mast Illumination Poles (HMIPs) in Texas, with pre-existing cracks at their base. HMIPs are tall multi-sided galvanized steel structures commonly used to provide lighting along highways and at highway interchanges. While poles vary in height from one site to the next, typical Texas HMIPs have heights of 100, 125, 150, or 175 feet. A 150 foot tall specimen can be seen in Figure 1.1.

To facilitate their shipment and construction, HMIPs are constructed out of several sections that nest upon one another. These sections are tapered along their height. This tapering both reduces weight and improves the efficiency of the connection between sections, as it allows each upper section to be placed on top of the section below.

At the top of the final section is the lighting fixture used to provide illumination. The lighting fixture is composed of eight or more lights fixed to a sliding circular mount (Stam, 2009). This mount can be lowered for maintenance or replacement using a winch system located within the pole. This system is accessible via a small hatch near the base of the pole.

Figure 1.1: A Typical High Mast Illumination Pole

At the base of the pole, the pole's shaft is welded to a thick baseplate. This baseplate is connected to a concrete foundation through the use of anchor rods. The number of anchor rods ranges from 6 rods to 16 rods, with increases occurring at changes in pole height and designed wind speed. The foundation, light fixtures, and splices can be seen in Figure 1.1. Splices are marked to assist in the identification of their locations.

In the state of Texas, standard HMIP designs have been developed by the Texas Department of Transportation, hereafter called TxDOT. Plans for these designs can be found in design drawing HMIP 98, *High Mast Illumination Poles 100' –125' – 150' – 175'*. TxDOT plans are based upon the design documentation published by the American Association of State Highway and Transportation Officials (AASHTO). Specifically this is the *LRFD Specification for Structural Supports for Highway Signs, Luminaires, and Traffic Signals* (AASHTO, 2015). For the remainder of this thesis, these standards will simply be referred to as the AASHTO specifications.

A number of collapses of HMIPs have been reported in recent years, including the collapse of a 140 ft. HMIP along Interstate 29 in Sioux City, Iowa in 2003 and the collapse of a 150 ft. HMIP in Rapid City, South Dakota in 2005. These collapses have occurred by fracture at the shaft-to-baseplate joint. An example of a failed HMIP is shown in Figure 1.2. Collapses have also been reported for HMIPs used at schools and at outdoor stadiums, including an incident of a HMIP falling through the roof of a school gymnasium (Magenes 2011). These collapses have been attributed to fatigue failures at the shaft-to-base plate connection (Rios 2007).

No collapses of HMIPs have been reported in Texas. However, recent studies have shown that many galvanized HMIPs in Texas have pre-existing cracks at their shaft-to-base plate connection, most likely caused by the galvanization process (Kleineck 2011). Research (Rios 2007, Stam 2009, Pool 2010) has also shown that pre-existing cracks may significantly reduce the fatigue life of galvanized HMIPs. The potentially poor performance of in-service galvanized HMIPs with pre-existing cracks in Texas is a significant concern. Collapse of an HMIP can cause fatalities or serious injuries. In addition, inspection, monitoring, repair and replacement of HMIPs may be a significant cost, particularly in light of the large number of HMIPs in Texas. Because of the serious safety and cost concerns, better methods are needed to identify the remaining fatigue life of in-service TxDOT HMIPs with pre-existing cracks.

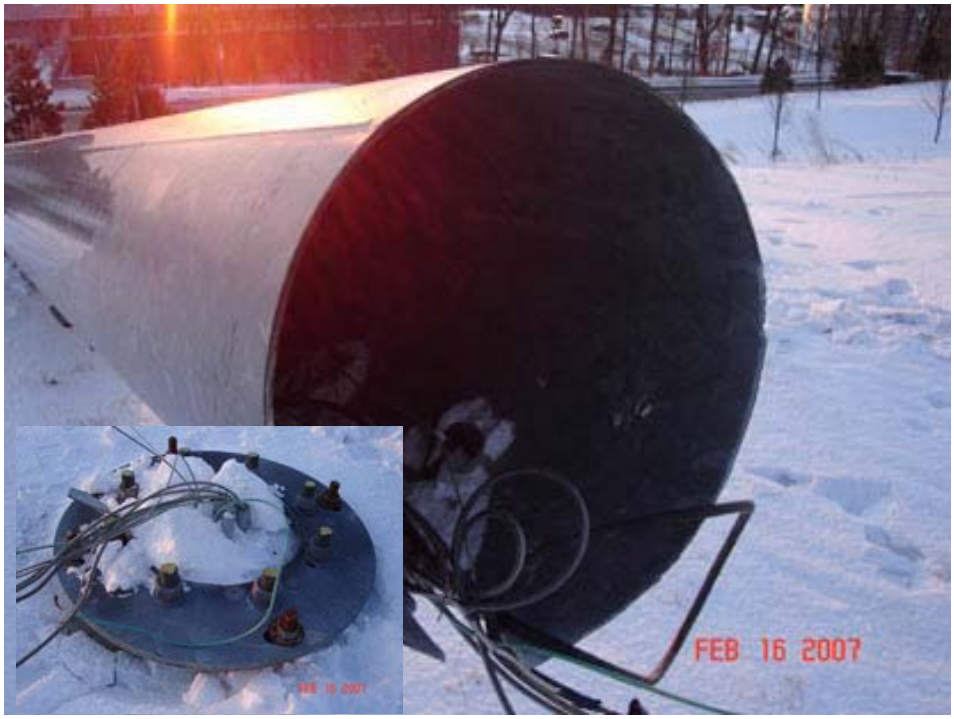

Figure 1.2: Failure of an HMIP in Colorado (Rios, 2007)

1.2 RESEARCH OBJECTIVES

The work reported in this thesis is part of TxDOT Research Project 0-6829: *Fatigue Resistance and Reliability of High Mast Illumination Poles (HMIPs) with Pre-Existing Cracks.* TxDOT Project 0-6829 is aimed at generating data and information to support a probabilistic based assessment of the remaining life of pre-cracked HMIPs. The scope of Project 0-6829 includes laboratory fatigue tests on galvanized HMIPs with pre-existing cracks, field studies and measurements to characterize the wind response of Texas HMIPs, the development of a reliability based framework to assess the fatigue life of in-service pre-cracked HMIPs, and recommendations for possible retrofit techniques for in-service HMIPs.

The research reported in this thesis focuses on the task of conducting laboratory fatigue tests of galvanized HMIP specimens with pre-existing cracks at the shaft to baseplate weld. The objective of this work is to develop additional experimental data, to supplement experimental data collected in earlier studies, to characterize the fatigue performance of galvanized HMIPs with pre-existing cracks. A more specific objective is to collect fatigue test data on pre-cracked HMIPs at low stress ranges, representative of the stress ranges seen by in-service HMIPs subject to vortex induced vibration. As discussed in Chapter 2, adequate fatigue data at low stress ranges, on the order of 1 to 6 ksi, is currently lacking, based on previous test programs. An additional objective of the work reported in this thesis is to conduct a limited number of monotonic load tests to failure of HMIP specimens that have previously experienced significant fatigue cracking. The purpose of these tests is to evaluate to what extent the static strength of the HMIP

shaft to baseplate connection has been affected by the presence of a significant degree of fatigue cracking.

1.3 THESIS SCOPE AND ORGANIZATION

The primary objective of this thesis is to provide an overview of the laboratory fatigue tests run on pre-cracked HMIP specimens as part of TxDOT Project 0-6829. At the time of the writing of this thesis, these tests are still ongoing. Thus this thesis will only provide a partial summary of these fatigue tests. The remaining tests will be reported in subsequent reports on Project 0-6829.

This thesis is organized as follows. A brief overview of previously completed HMIP fatigue test programs will be reviewed in chapter 2. Chapter 3 describes the test setups used for the fatigue tests and monotonic tests of HMIP specimens. Chapter 4 will present the design details for the test specimens in addition to covering the procedures used during specimen preparation and testing. The results of these fatigue tests will then be discussed in chapter 5. Finally, chapter 6 will briefly present a summary of the fatigue tests that have been run at this time.

Chapter 2: Literature Review

This chapter will provide an overview of previously completed research projects related to the current research study on High Mast Illumination Poles (HMIPs). Although a significant number of research studies on HMIPs have been conducted at universities and other research laboratories throughout the U.S., this literature review will focus on previous studies conducted at the University of Texas at Austin Ferguson Structural Engineering Laboratory. This is because the current research study is largely an extension of previous work at the University of Texas at Austin. For more complete literature reviews, see for example Connor et. Al. (2012) and Roy et. Al. (2011).

This research study is a continuation of earlier fatigue investigations on high mast illumination poles at the University of Texas at Austin. This study is the seventh phase of research studying the shaft-to-baseplate connection. Previous phases studied many factors involving the fatigue resistance of these connections. This chapter will examine the previous tests run at the University of Texas at Austin Ferguson Laboratory and discuss their significance to the study currently underway.

2.1 Overview

In recent years, failure of HMIPs have been documented in many states within the United States (Magenes, 2011). These failures have raised concern over whether or not the current design and fabrication procedures for these poles are adequate. Many of these concerns arise from the lack of knowledge about the behavior of these poles. With these concerned in mind, research agencies across the US combined resources to fund a

nationally Pooled Fund Study. This Pooled Fund Study was conducted to study the fatigue behavior of HMIPs. The initial Pooled Fund Study provided much needed knowledge, but left several questions unanswered. To answer these questions, the Texas Department of Transportation (TxDOT) has funded subsequent research studies investigating HMIPs.

These TxDOT funded studies have been focused on many factors affecting the fatigue life of HMIPs. These have included full scale laboratory tests, parametric finite element analytical (FEA) studies, and field studies. They have identified the source of cracks, the influence of baseplate and wall thicknesses on cracking, crack initiation points, and many other significant factors. Details of these studies and their goals will be discussed in the following sections. Ultimately, details of the previous studies relating to the current research study will be highlighted.

2.2 PHASE 1 – POOLED FUND STUDY

The first phase of research conducted on HMIPs at the University of Texas at Austin focused predominately on large scale experiments. In these experiments, multiple variables were changed to study their effects. These variables included baseplate thickness, number of anchor rods, and shaft-to-baseplate connection type. Four connection types were studied: (1) A fillet welded socket connect, (2) A Texas full penetration welded connection, (3) A Wyoming full penetration welded connection, and (4) A stool base connection. Connection details for each of these details are described in sections 2.2.1 through 2.2.4.

2.2.1 Fillet Welded Socket Connection Details

The fillet welded socket connection involved the use of an unequal-leg fillet weld. This weld is run along the exterior of the pole shaft, connecting the shaft to the baseplate. Following the completion of the primary weld, a seal weld is run along the inside of the shaft to protect the specimen from zinc intrusion during galvanization.

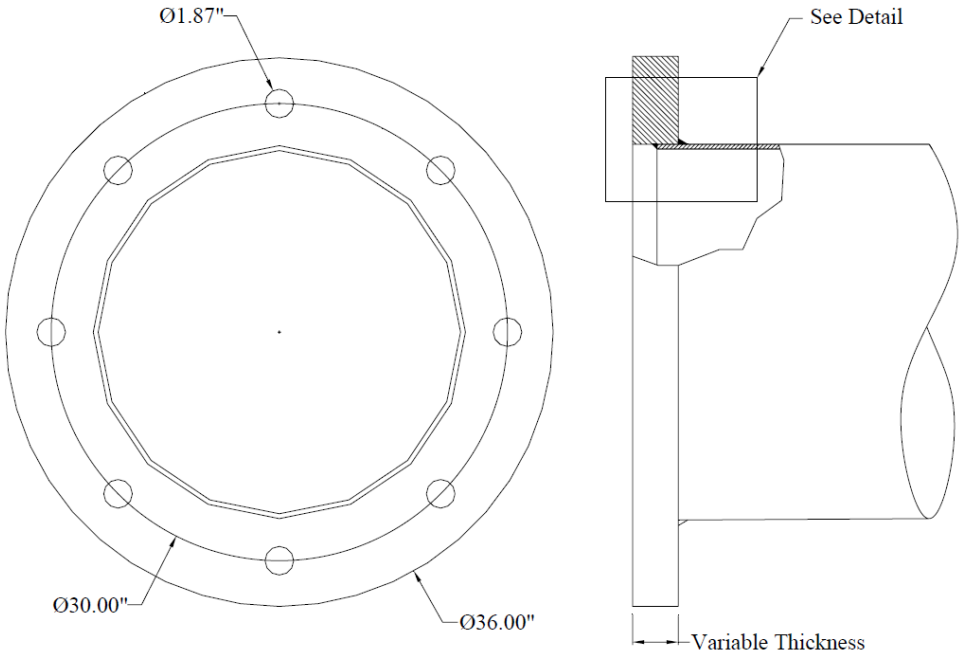

Figure 2.1: Fillet Welded Socket Connection Detail (Rios, 2007)

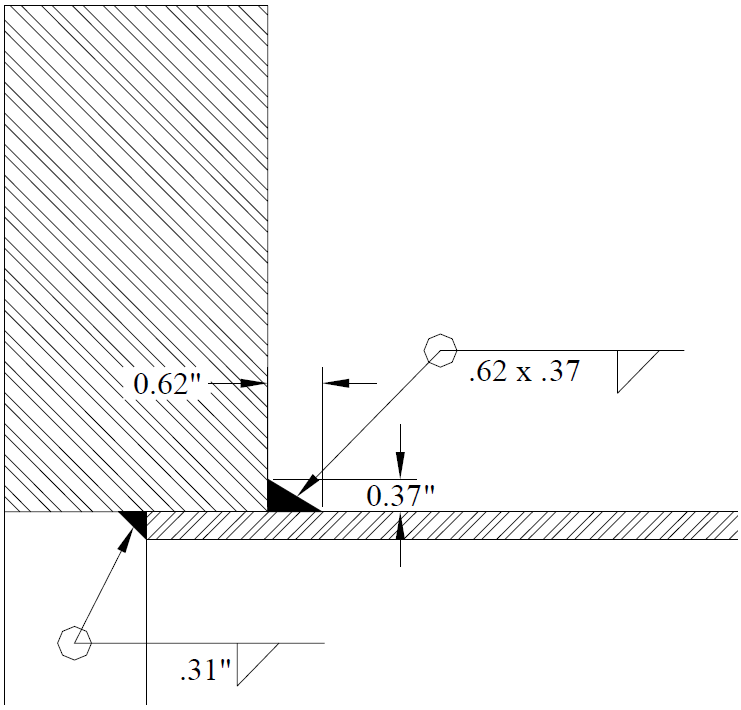

Figure 2.2: Socket Connection Weld Detail (Rios, 2007)

2.2.2 Wyoming Full Penetration Welded connection Details

The Wyoming full penetration welded connection is used throughout the state of Wyoming on high mast illumination poles. In this connection, a backing bar is welded to the pole's baseplate. The pole is then mated with the baseplate. Before the pole can be attached to the baseplate, its shaft wall is beveled on the exterior. This bevel is filled and welded with an unequal-leg full penetration weld. Details for this connection can be seen in Figures 2.3 and 2.4.

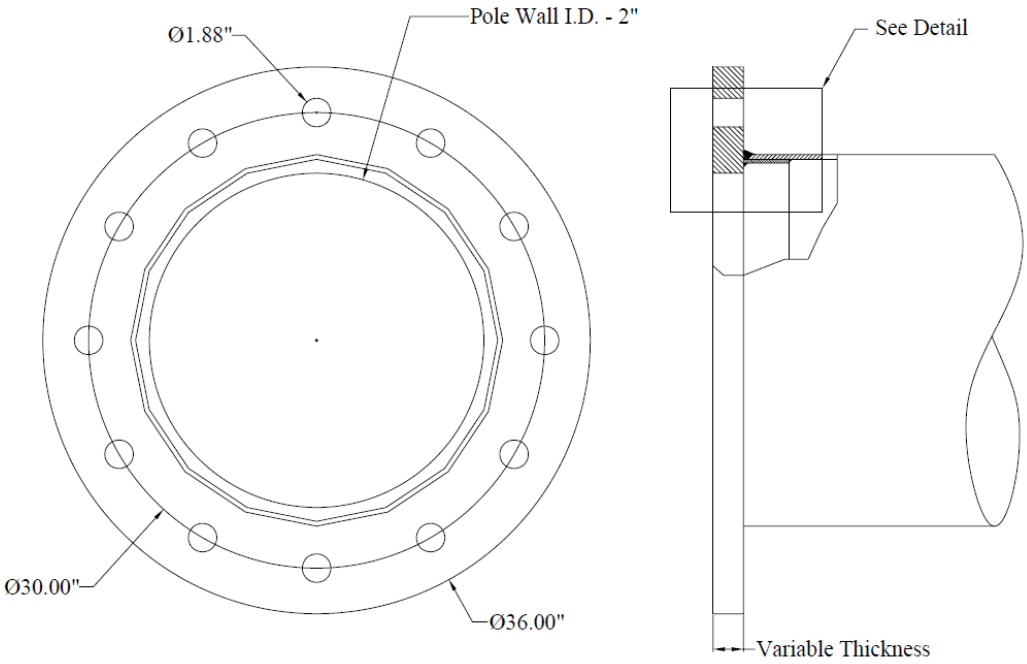

Figure 2.3: Wyoming Connection Detail (Rios, 2007)

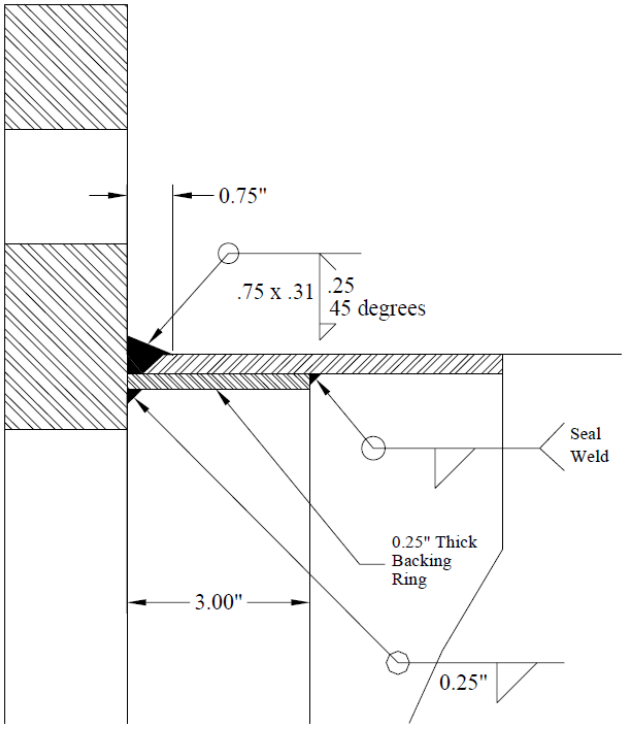

Figure 2.4: Wyoming Connection Weld Detail (Rios, 2007)

2.2.3 Texas Full Penetration Welded connection Details

The Texas full penetration welded connection is similar to the Wyoming connection, but does not include the backing bar. Instead of the backing bar, the interior of the pole shaft is welded to the baseplate. This weld serves essentially the same purpose as the backing bar in the Wyoming detail. Before the backing weld is created, the exterior of the pole is beveled. This bevel is filled with weld material to create the full penetration weld. Details for this connection can be seen in Figures 2.5 and 2.6.

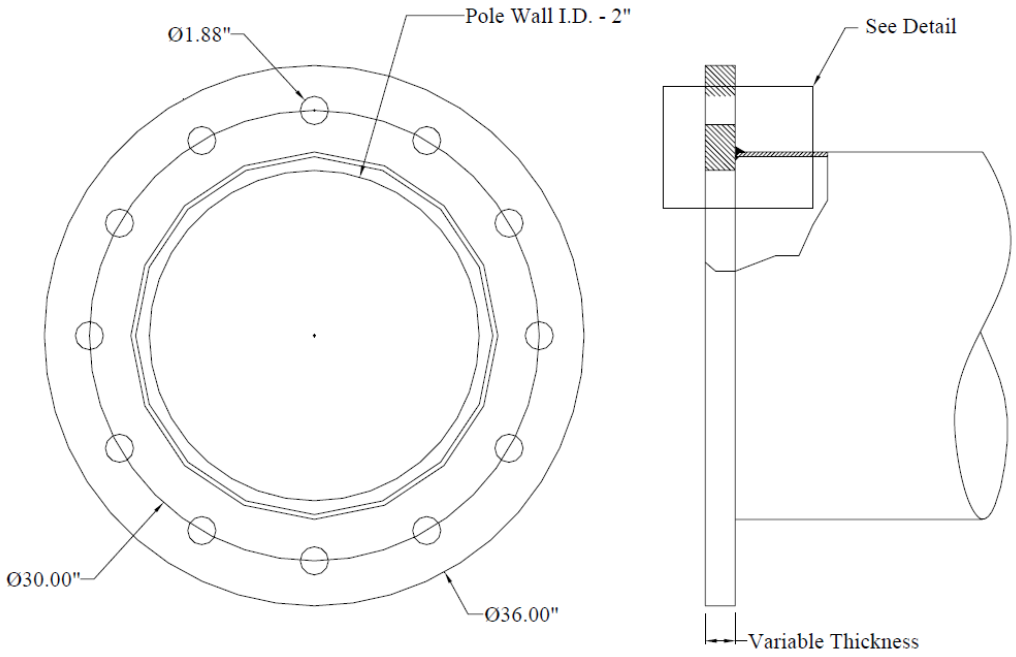

Figure 2.5: Texas Connection Detail (Rios, 2007)

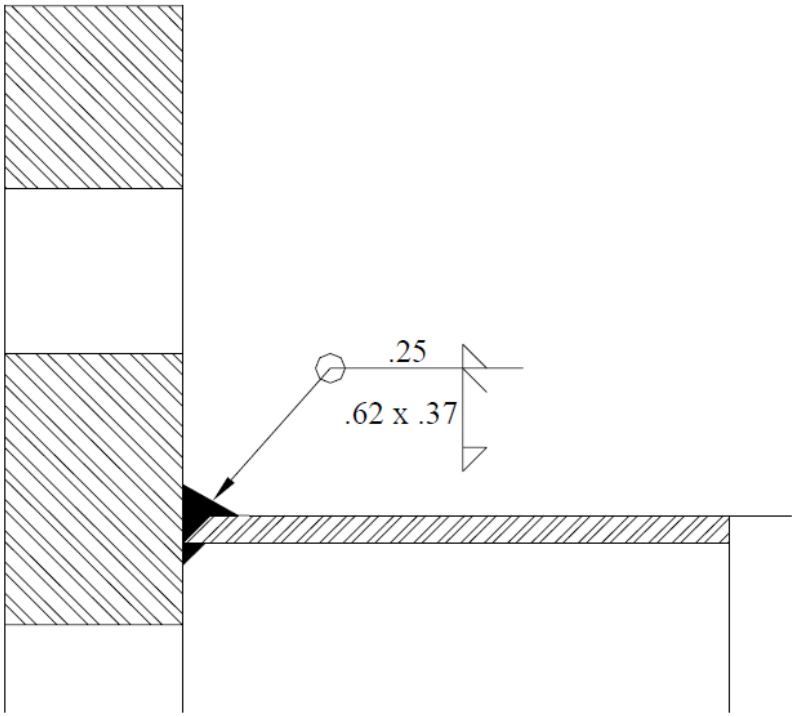

Figure 2.6: Texas Connection Weld Detail (Rios, 2007)

2.2.4 Stool Base connection Details

The final connection used during the first phase of research was dubbed the stool base connection. This connection used vertical plates to stiffen the shaft-to-baseplate connection. These stiffeners were installed with a cap plate to create a bearing surface for the nuts attaching the pole to its foundation. Figures 2.7 and 2.8 below show the details for the stool base connection.

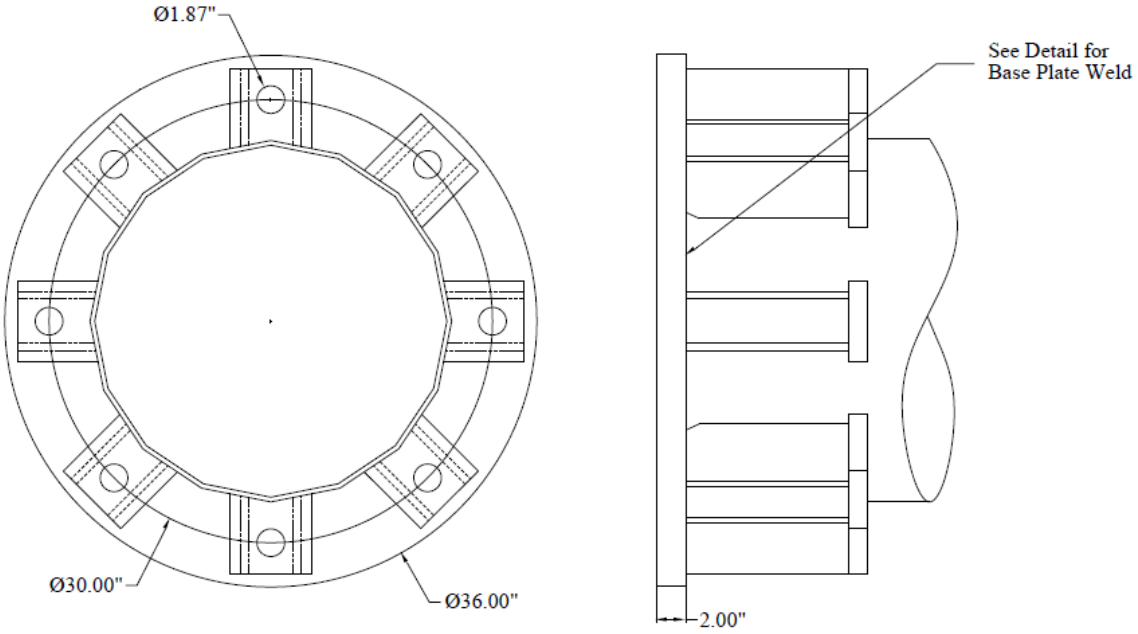

Figure 2.7: Stool Base Connection Detail (Rios, 2007)

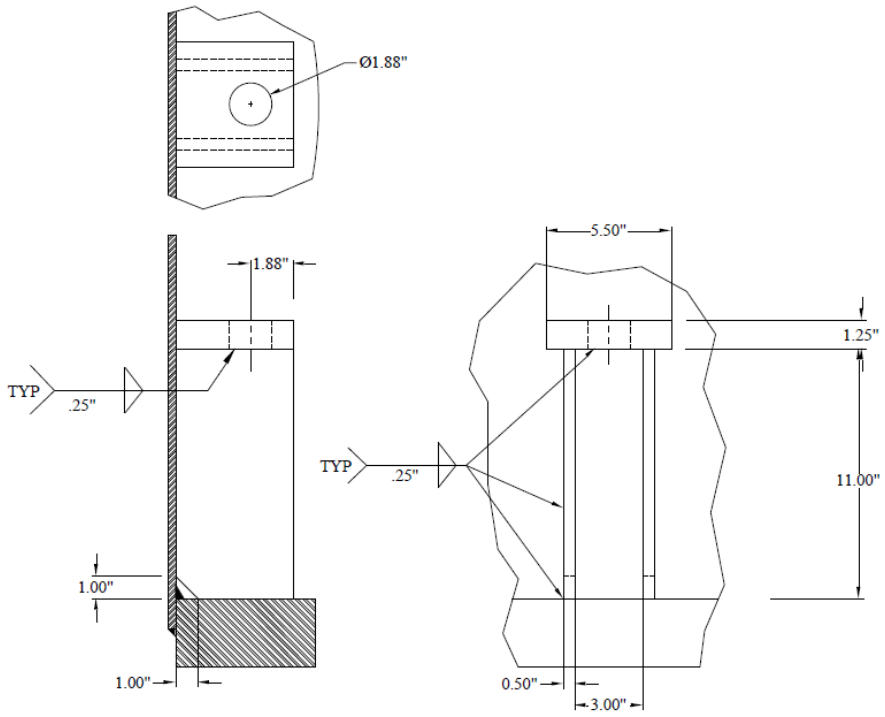

Figure 2.8: Stool Chair Detail (Rios, 2007)

2.2.5 Phase 1 Results

The results from the research in Phase 1 are presented in a combined plot below. This figure presents this data in an S-N plot. This graph takes the stress range that specimens were tests at and plots them again the number of cycles taken to fail the specimens. This failure criteria was defined as a 10-percent reduction in specimen stiffness. Also plotted on the S-N plot are the fatigue category limits from A through E'. These limits are simply linear relationships with a lower bound value called a Constant Amplitude Fatigue Limit (CAFL). These categories are taken from the AASHTO specifications. Note that in the S-N plot below, specimens are reported using a specific naming convention. The naming convention used in Phase 1 is presented in Figure 2.10.

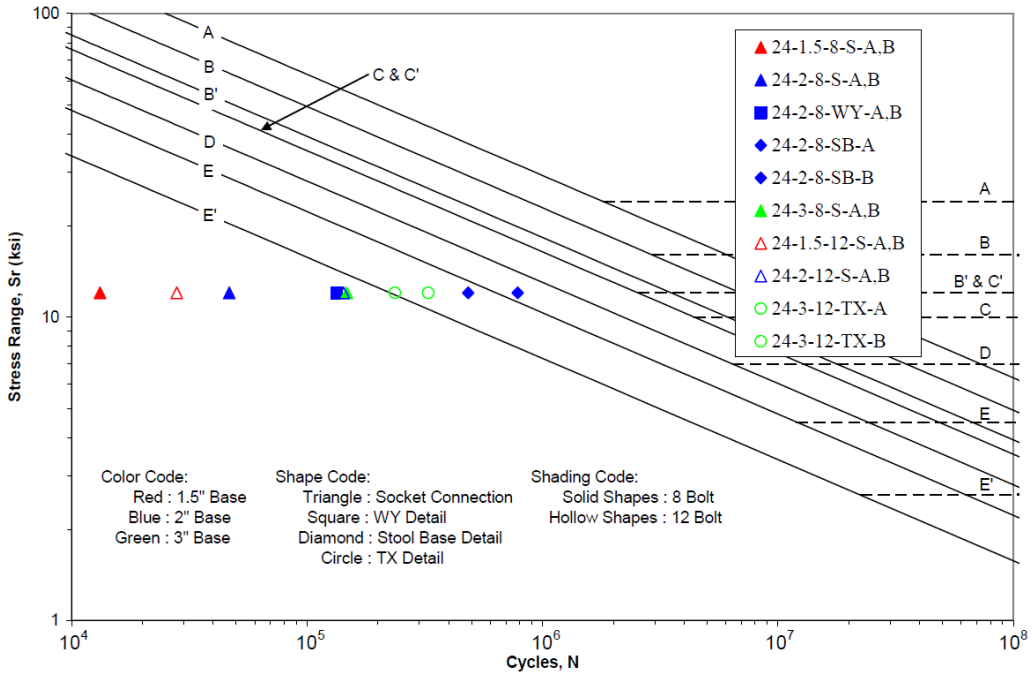

Figure 2.9: S-N Plot of Phase 1 Fatigue Test Results (Rios, 2007)

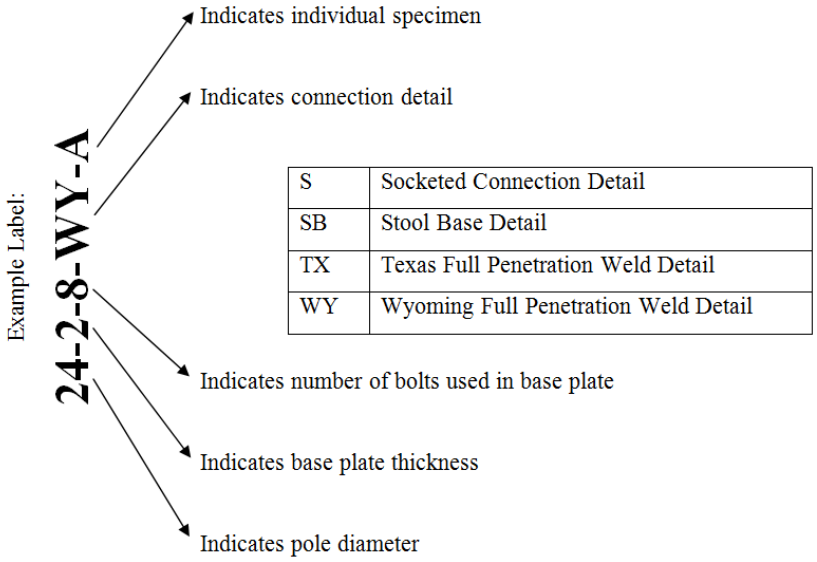

S	Socketed Connection Detail
SB	Stool Base Detail
TX	Texas Full Penetration Weld Detail
WY	Wyoming Full Penetration Weld Detail

Figure 2.10: Naming Convention Used During Phase 1 Research (Rios, 2007)

Phase 1 testing resulted in several conclusions. Perhaps the most significant conclusion of this test was that many of the details tested showed very poor fatigue performance that was significantly worse than Category E'. The specimens that showed the best fatigue performance, among all of the details tested, were the Texas Full Penetration Connection and Stool Base Connection. For each of these connections, the specimens with thicker baseplates showed fatigue performance. Likewise, specimens with more anchor bolts also showed better fatigue performance.

2.3 PHASE 2 – POOLED FUND STUDY

The work completed in Phase 2 was a continuation of the work completed in Phase 1 and is documented by Stam (2009). Phase 1 concluded that the fatigue resistance of HMIPs was related to the stiffness of the pole at its base. As discussed, this stiffness is a function of the connection type, the base plate thickness, whether or not the connection was stiffened (by a backing bar, ground sleeve or something similar) and the number of anchor rods used. During Phase 2, a series of additional laboratory tests and FEA models were developed to study the fatigue performance of the high mast poles (Stam, 2009).

2.3.1 Phase 2 – Experimental Results

As Phase 2 was simply a continuation of previous research, the topics studied during this phase were similar to those studied during Phase 1. The Phase 2 study tested specimens using many of the same connections types that were previously tested during Phase 1. Phase 2 added two additional connection types. These were both specimens with

external collars, also referred to as ground sleeves. Details for these connections can be seen in Figures 2.11 through 2.14.

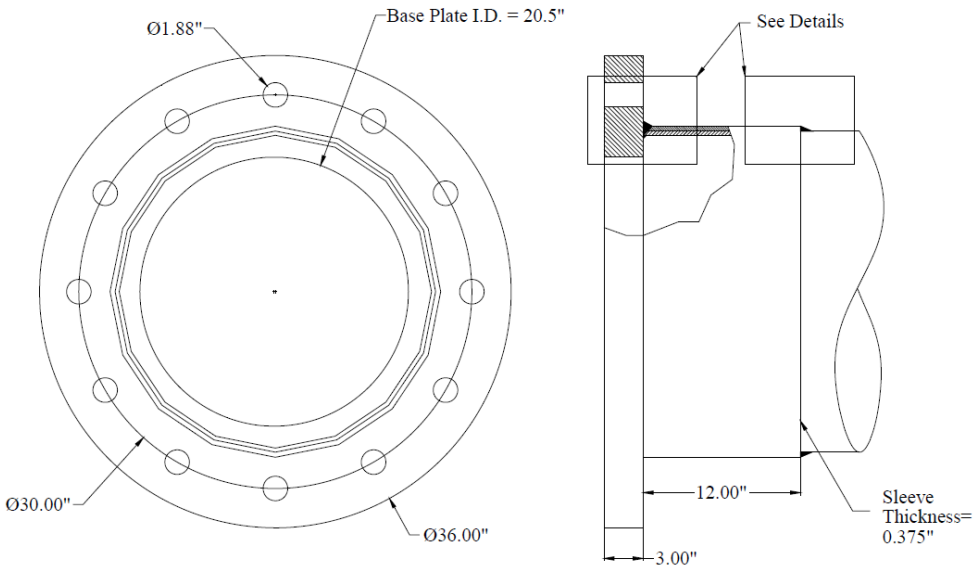

Figure 2.11: Texas External Collar Connection (Stam, 2009)

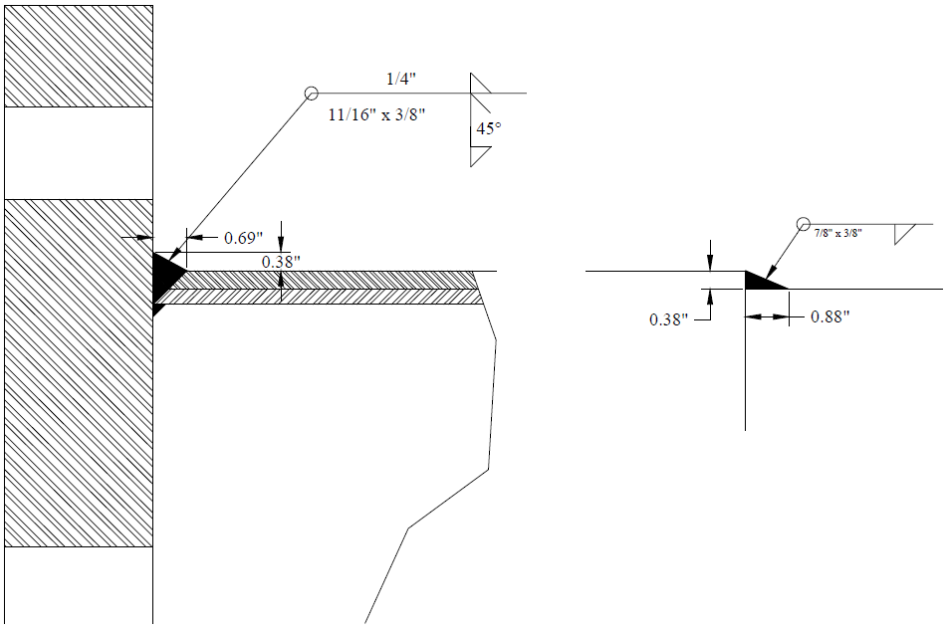

Figure 2.12: Texas External Collar Connection Details (Stam, 2009)

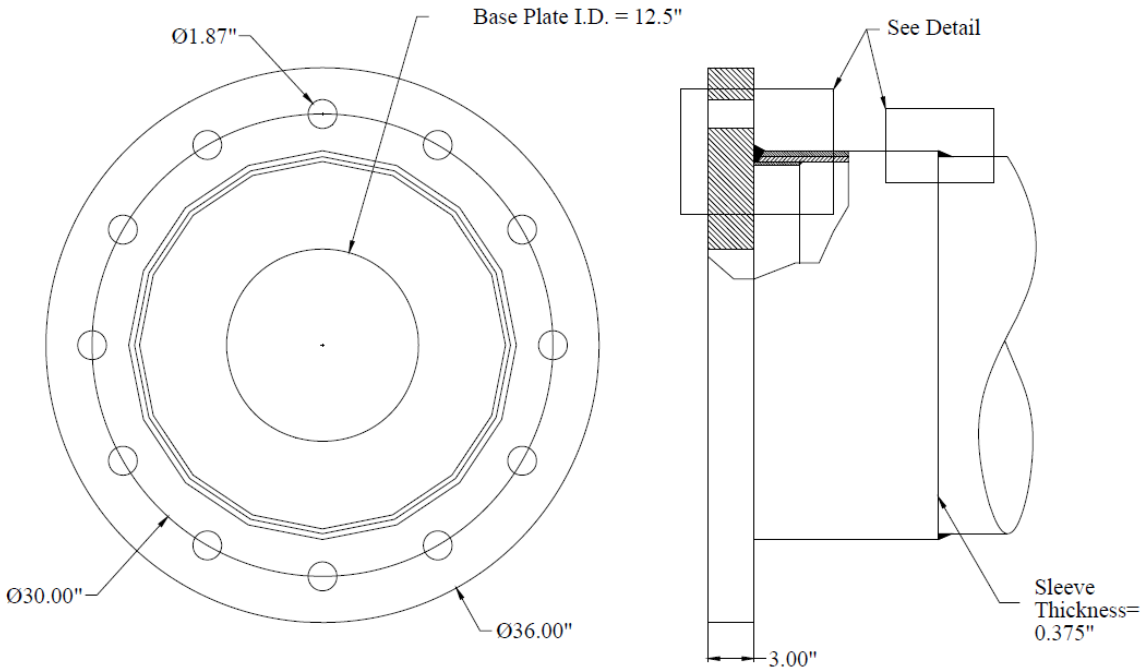

Figure 2.13: Wyoming External Collar Connection (Stam, 2009)

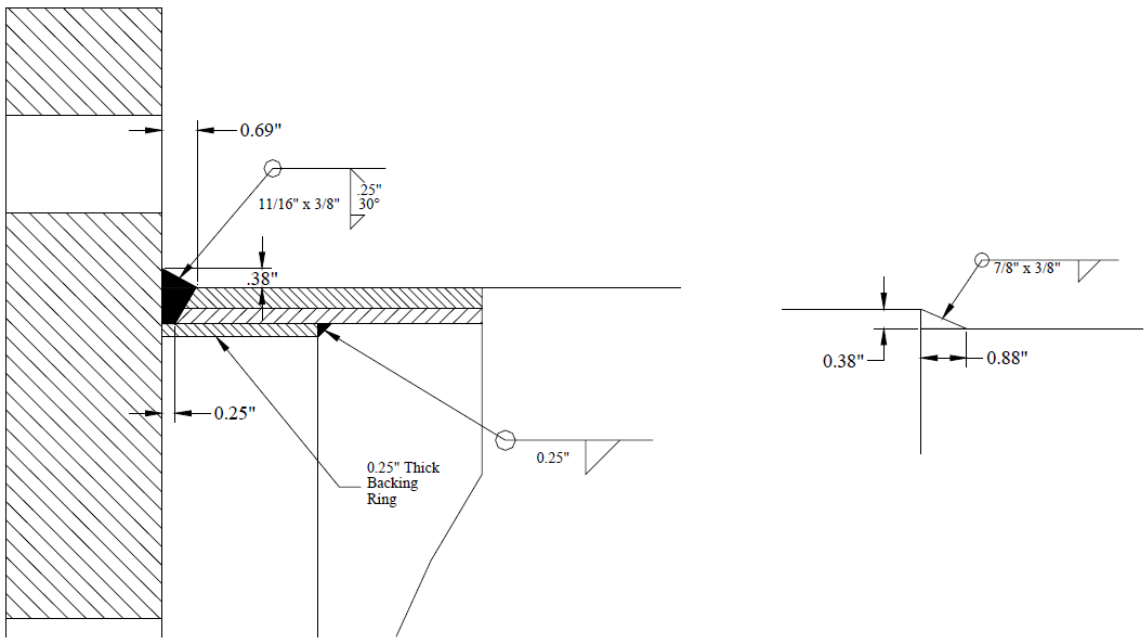

Figure 2.14: Wyoming External Collar Connection Details (Stam, 2009)

Note that these connections are very similar. Both start with the full penetration connection, where the detail differed between the Texas and Wyoming connections. Those connections are built upon by the addition of a plate on the external side of the specimen. This external plate or external collar is welded to the specimen and the baseplate through the use of a full penetration weld at one end. At the other end, the collar is fillet welded to the pole shaft.

In addition to these connection types, Phase 2 also experimented with baseplate thickness and the number of anchor rods, as Phase 1 had done. The experimental results complete by Stam (2009) during Phase 2 are presented in an S-N plot shown in Figure 2.15. Stam went on to combine these results with the results of Phase 1 tests to reinforce the findings of that phase. S-N plots of this combined data can be seen in Figure 2.16 through Figure 2.19. Figures 2.16 to 2.19 show fatigue test results from Phases 1 and 2, as presented in Belivanis (2014).

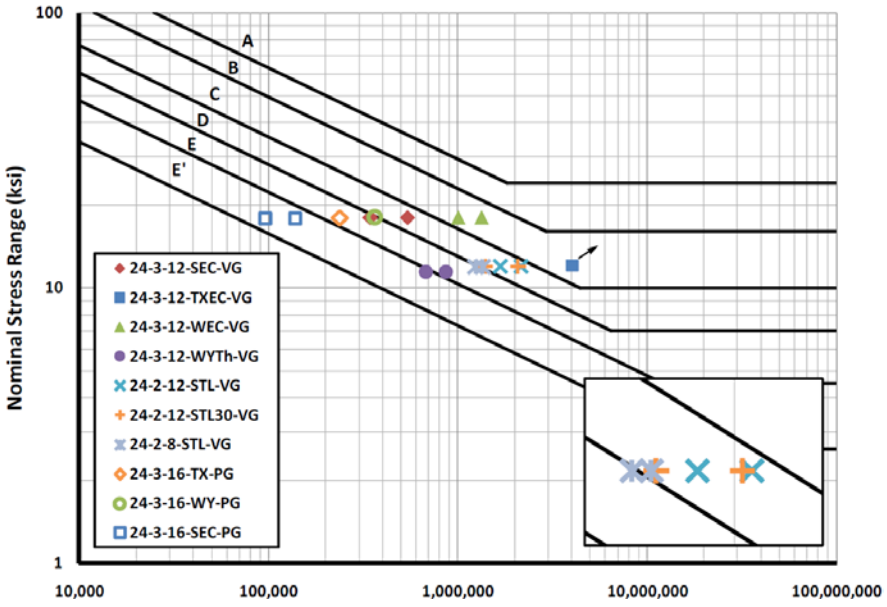

Figure 2.15: Phase 2 Fatigue Test Results (Stam, 2009)

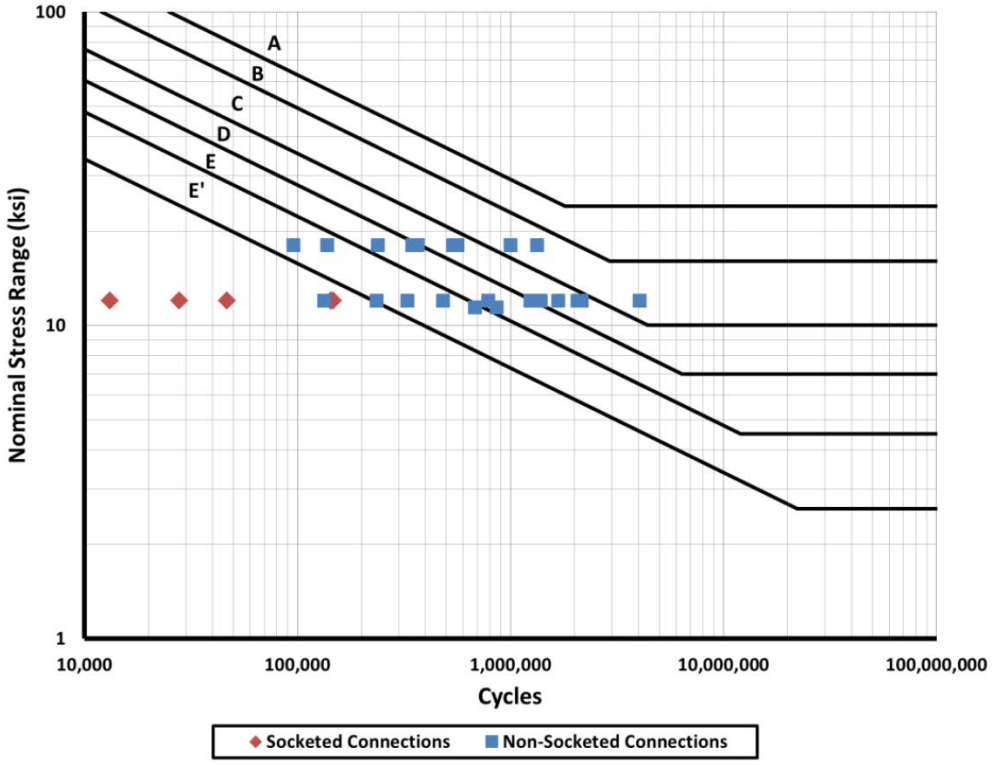

Figure 2.16: S-N Plot for Socketed vs. Non-Socketed Connection (Belivanis, 2014)

Note that “Non-Socketed Connections” refer to all connection details that were not fabricated using a socket connection. This includes the full penetration welded connections, the stool base connection, and the external collar connections.

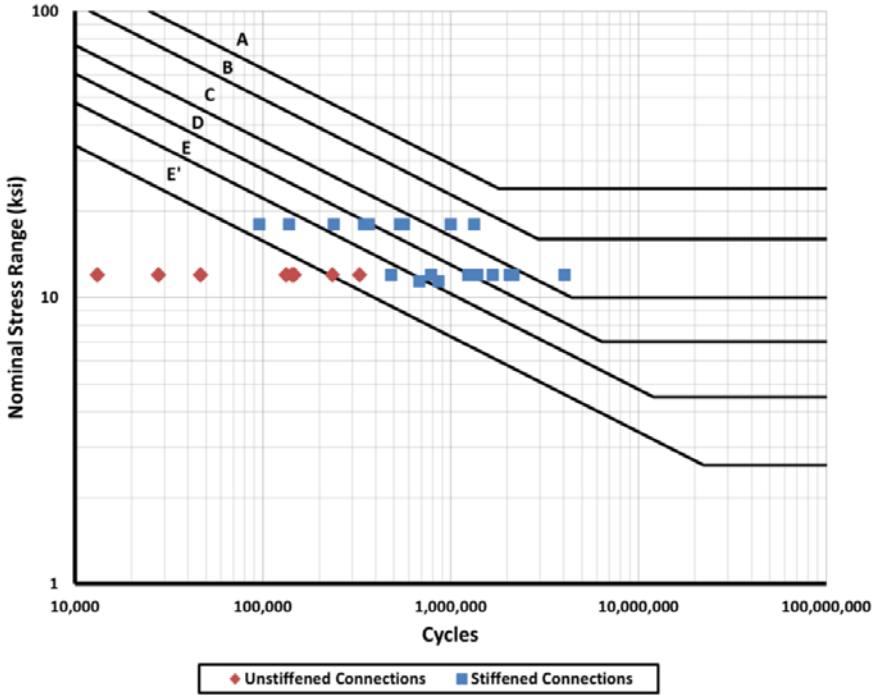

Figure 2.17: S-N Plot for Stiffened vs. Unstiffened Connections (Belivanis, 2014)

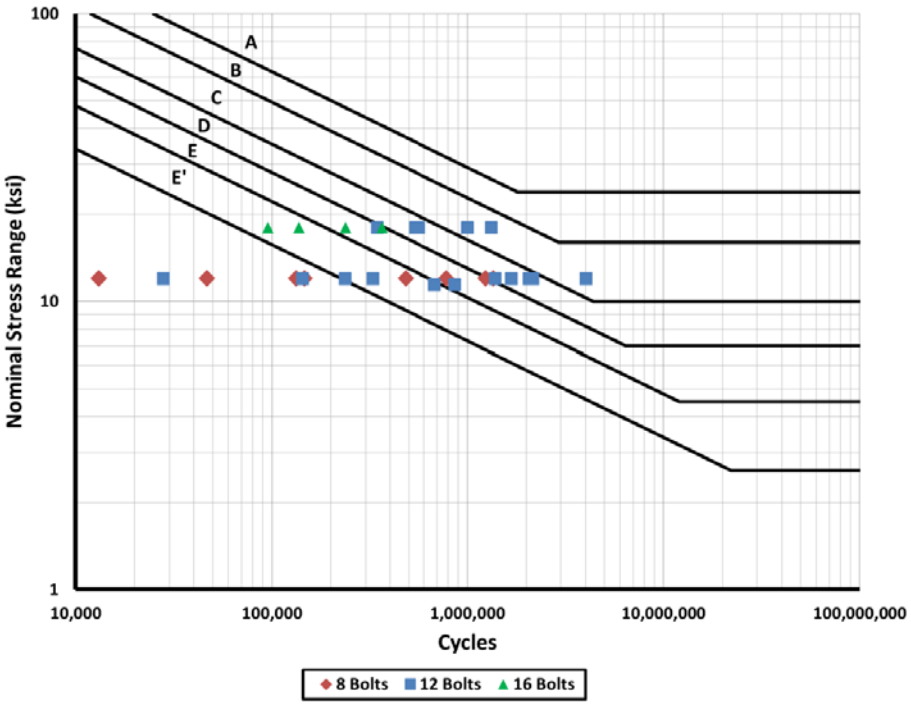

Figure 2.18: S-N Plots for Amount of Anchor Bolts (Belivanis, 2014)

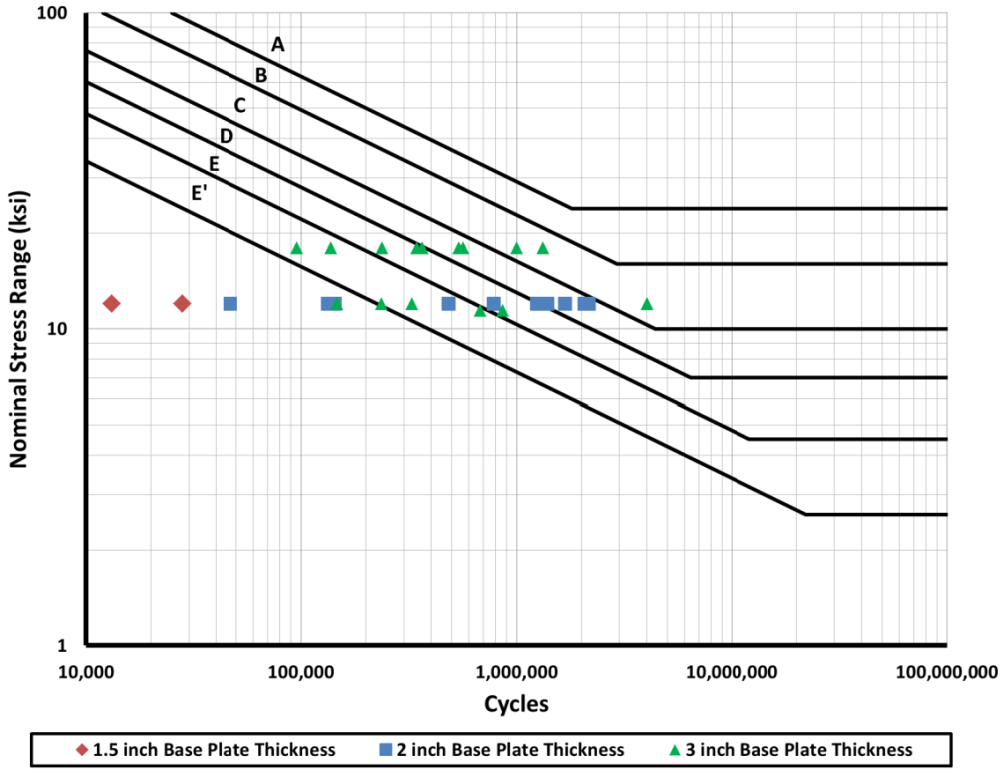

Figure 2.19: S-N Plot for Baseplate Thickness (Belivanis, 2014)

For Phase 2 research, the specimen naming convention was nearly identical to that which was used during Phase 1. As the external collar connections were added, two new connection detail abbreviations had to be added. These were TXEC for the Texas External Collar Connection and WYEC for the Wyoming External Collar Connection. The stool base designation was also modified from SB to STL for the standard stool base and to STL30 for a specialized stool base detail. Phase 2's naming scheme also included the addition the manufacturer to the end of the specimen name. For more details on the changes made to the naming scheme, consult Stam (2009).

The Phase 2 experiments showed many results similar to those seen during Phase 1. These results indicated that fillet welded socket connections generally had the

worst fatigue performance. Improvements in fatigue performance were found by increasing the thickness of the baseplate and the number of anchors rods, though it was discovered that too many anchor rods could be used. Ultimately this research recommended the use of HMIPs with non-socketed connections, three inch thick baseplates, and 8 or 12 anchor rods.

2.3.1 Phase 2 –Analytical Results

To further study the factors affecting fatigue performance of HMIPs, a parametric FEA analysis was performed (Stam 2009). In this analysis, multiple finite element models were constructed with varied section parameters. The parameters that were varied were the pole diameter, shaft thickness, baseplate thickness, and the connection type. Since socket connections were shown to not resist fatigue well during the full scale tests, non-socketed connections were primarily examined.

The models showed many results similar to the findings of the full scale tests. The analysis results supported that increases in the baseplate thickness improved performance. Connections stiffened with backing bars, stool bases, and external collars were also shown to improve performance. The analysis also suggested that 36-inch diameter poles may show worse fatigue performance than 24-inch diameter poles.

2.4 PHASE 3

Phase 3 studies of HMIPs were documented by Pool (2010). As Stam's (2009) analytical models showed a decrease in performance in specimens with large diameter, this phase focused on testing specimens with larger diameters than those of previous

phases. Phases 1 and 2 tested specimens with diameters of 24 inches. Phase 3 tested specimens conforming to TxDOT specifications for a 150 foot tall specimen designed for 80 mile and hour winds. These specifications call for a specimens with a 32 5/8" base diameter (Pool, 2010). Both Texas full penetration weld and external collar connections were tested during this phase.

In addition to studying fatigue performance of HMIP specimens, this phase also studied the effects that arise when different manufacturers fabricate the specimens. In varying the manufacturers, the galvanizers were varied as well. These variations were made to examine the possible influence of galvanization on fatigue performance. As part of this study, one of the tested specimens was left "black" or ungalvanized. Every experiment consisted of one galvanized specimen and one black specimen. This allowed researchers to directly compare a galvanized and an ungalvanized specimen.

After considering the results of the experiments, no significant differences could be found between the differing fabricators and galvanizers. This was not the case for the comparisons between galvanized and black specimens, however. In all cases, ultrasonic tests showed that only the galvanized specimens contained initial cracks. These initial cracks greatly reduced the fatigue lives of specimens and caused them to fail before the black specimens in all tests. This led Pool to conclude that the galvanization process damaged the specimens in some way.

The results of the fatigue tests of Phase 3 can be seen in Figure 2.20. All of this data represents galvanized specimens. The naming scheme for this phase is the same as that used in Phase 2. One thing worth noting on this plot is the inclusion of two repaired

specimens. After two specimens were tested to failure, they were repaired using two weld repair procedures. To learn more about these procedures, consult Pool (2010).

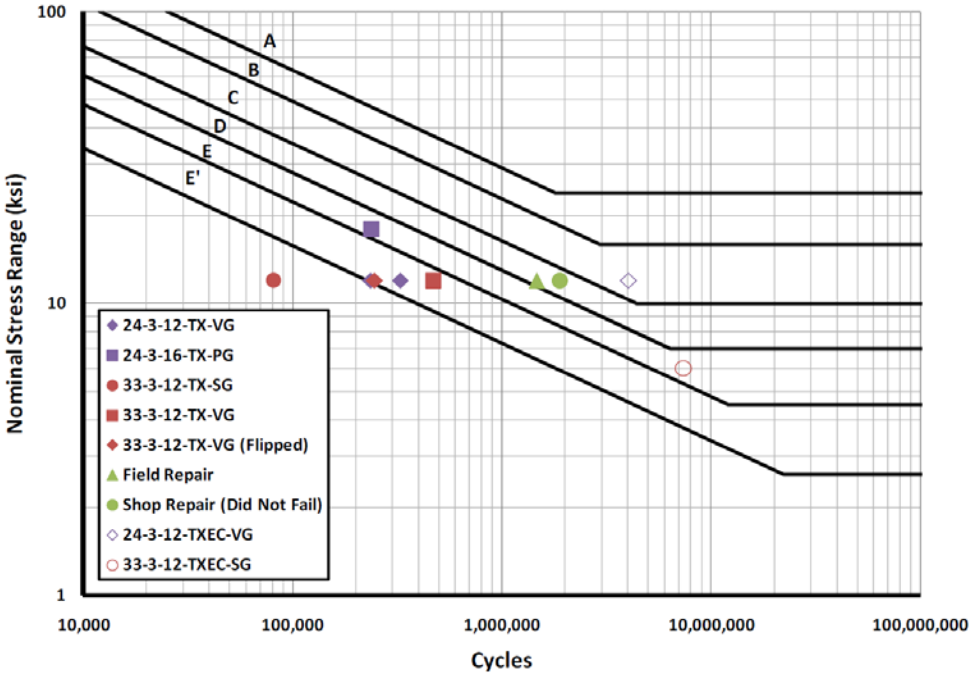

Figure 2.20: S-N Plot of Phase 3 Test Results (Pool, 2010)

2.5 PHASE 4

Following Pool's conclusion that galvanization caused fatigue cracks, Phase 4 research was devoted to studying the galvanizing process. The results of Phase 4 are documented by Kleineck (2011). This phase included both analytical studies and instrumentation of specimens during galvanization.

2.5.1 Results of Instrumentation of HMIPs during Galvanizing

Several factors were explored when determining the underlying reason for crack formation during galvanization. These included bend radius, weld geometry, chemical

composition of the galvanizing compound, and thermally induced stresses during galvanization. The first three variables were determined to have less significance to crack formation. The thermally induced stress and their effects on initial crack formation, however, were studied in greater detail.

To study these thermal effects, HMIP specimens were instrumented with thermocouples prior to galvanization. These thermocouples enabled the measurement of thermal gradient and resulting thermal strains that developed when HMIPs were dipped in the zinc galvanization bath. Thermocouples were installed at several locations along the specimen's length to measure temperatures. Strain gauges were installed at the top of the specimens to measure thermally induced strains. Because of the high temperatures of the bath, these gauges were not expected to and did not measure strain throughout the entire galvanization process. They simply measured strains as the specimens were dipped in the galvanization bath, becoming unreliable once submerged.

After galvanization was completed, this data was analyzed. It showed that significant thermal gradients develop near the shaft-to-baseplate connection during galvanization. This is primarily the result of the significant differences between the baseplate thickness, 3 inches, and the pole shaft thickness, 5/16 of an inch. This information was stored and reserved for the development of finite element models made latter during the phase.

2.5.2 Analytical Results

Following the results observed during the instrumentation of the HMIP, the researchers during this phase decided to create analytical models to further investigate

thermal effects. A parametric study was run to study the effect of various pole geometries when subjected to the measured thermal strains. One significant result of this study was the confirmation that the thermal stresses varied throughout the specimens. The highest stresses were seen at the shaft-to-baseplate connection, specifically at the bends of the specimen. This can be seen in Figure 2.21. This result was expected, as the 3 inch thick baseplates took longer to heat than the 5/16 inch thick pole shaft. Improved behavior was noticed when the model's pole shaft thickness was increased from 5/16 inch to 7/16 inch or 1/2 inch thicknesses. After concluding the parametric study, researchers concluded that the ratio of the pole diameter to pole thickness played a substantial role in determining whether or not a specimen will crack during galvanization. The lower this ratio is, the less likely a specimen is develop cracks from galvanization.

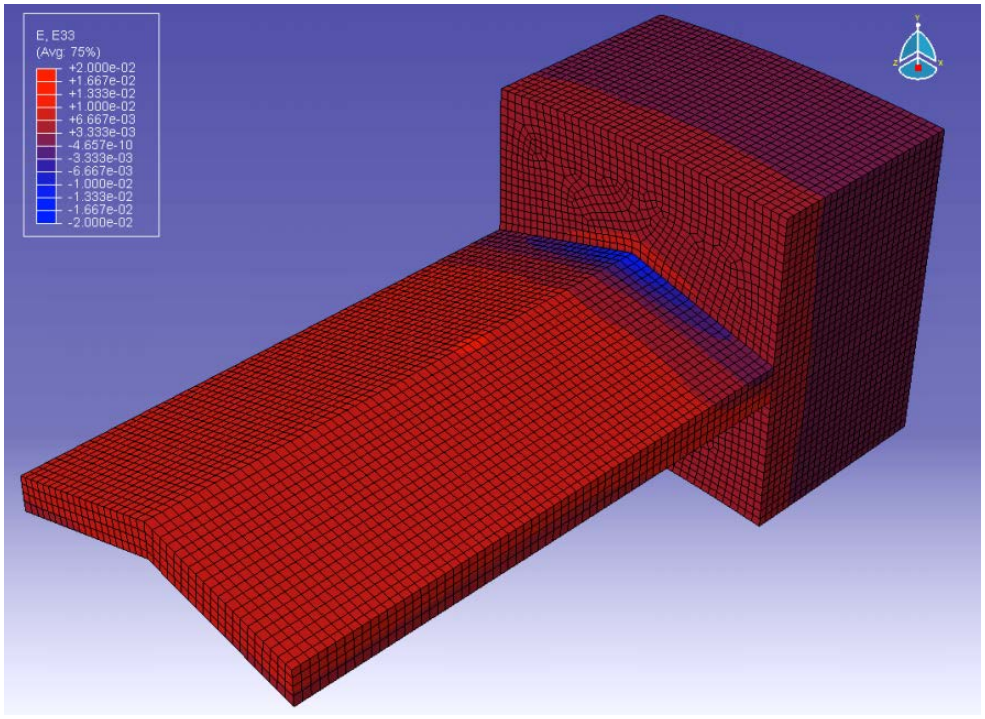

Figure 2.21: A Typical Submodel Showing the Concentration of Forces at the Shaft-to-Baseplate Connection (Kleineck, 2011)

2.6 PHASE 5

Having concluded that galvanization was the source of initial HMIP cracks during the previous studies, attention was turned toward yet another area that had not been investigated. Phase 5 of research at the University of Texas at Austin was devoted to field study of wind effects on HMIPs. The results of this phase were documented by Magenes (2011). The primary focus of this study was to determine the stresses experienced at the base of in-service HMIPs. The end goal of this research was to provide estimates of HMIP fatigue lives using the collected field data.

Five total HMIPs were instrumented throughout four cities to capture some of the many different wind environments seen in Texas. The selected poles were instrumented with both strain gauges and anemometers. Strain gauges were placed near the shaft to baseplate connection and were used to capture the stresses seen in this area. Anemometers were placed higher on the poles to capture wind speeds and directions. This information was then combined with strain gauge data to determine the wind speeds of vortex shedding, buffeting, and gusting.

Analysis of the field data showed that vortex shedding induced stresses that were much lower than those at which specimens had been tested in the first three phases. Magenes concluded that this induced stress was typically around 1 ksi, not the 12 ksi stress that most specimens had been tested at. Figure 2.22 shows the typical daily stress values that were measured during the field monitoring phase. Note that the wind induced stresses typically dropped off after around 5 to 6 ksi. This would cause researchers to reconsider testing stresses in future experimental phases.

Phase 5 concluded with researchers proposing a model to estimate HMIP fatigue life. This model was created modifying AASHTO specification-based equations. Phase 6 focused on evaluating the model's accuracy.

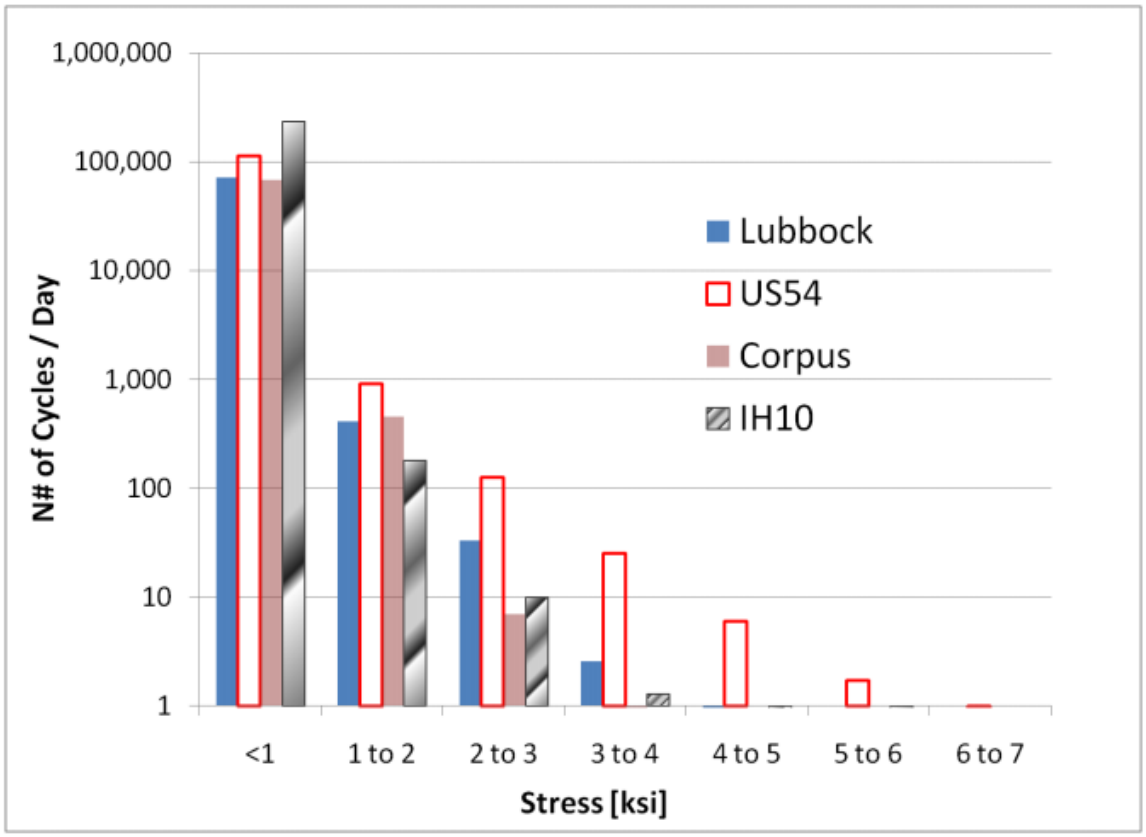

Figure 2.22: HMIP Daily Stresses and Cycles (Magenes, 2011)

2.7 PHASE 6

During the field instrumentation study of Phase 5, one of the instrumented poles was found to be severely cracked. This pole was removed from service and tested during Phase 6. The results of this phase are documented by Belivanis (2014). The primary purpose for this phase was to investigate the fatigue life of a severely cracked pole that

had been removed from service. This investigation was accomplished through full scale fatigue tests on the pole and a partner specimen.

While the main focus of Phase 6 was to test in service poles, work was also conducted to evaluate ultrasonic testing procedures to detect cracks and to evaluate a weld repair technique. Further details are provided by Belivanis (2014).

The Phase 6 full scale testing concluded with three fatigue tests on the specimen that was removed from service and two on its partner specimen. The results of these tests are displayed in the S-N plot shown in Figure 2.23. In this plot, tests 1, 2, and 3 correspond with the specimen that was removed from the field. S&S1 and S&S2 correspond with the partner specimen. During testing, this partner specimen failed before the field specimen and required weld repairs. After weld repairs, the specimen showed no signs of failure. Its second point on the plot corresponds to the number of cycles that the specimen had been tested to at the time of the projects conclusion. The three tests represented for the field specimen correspond to three orientations at which the specimen was tested. All tests were conducted at a stress range of 5 ksi.

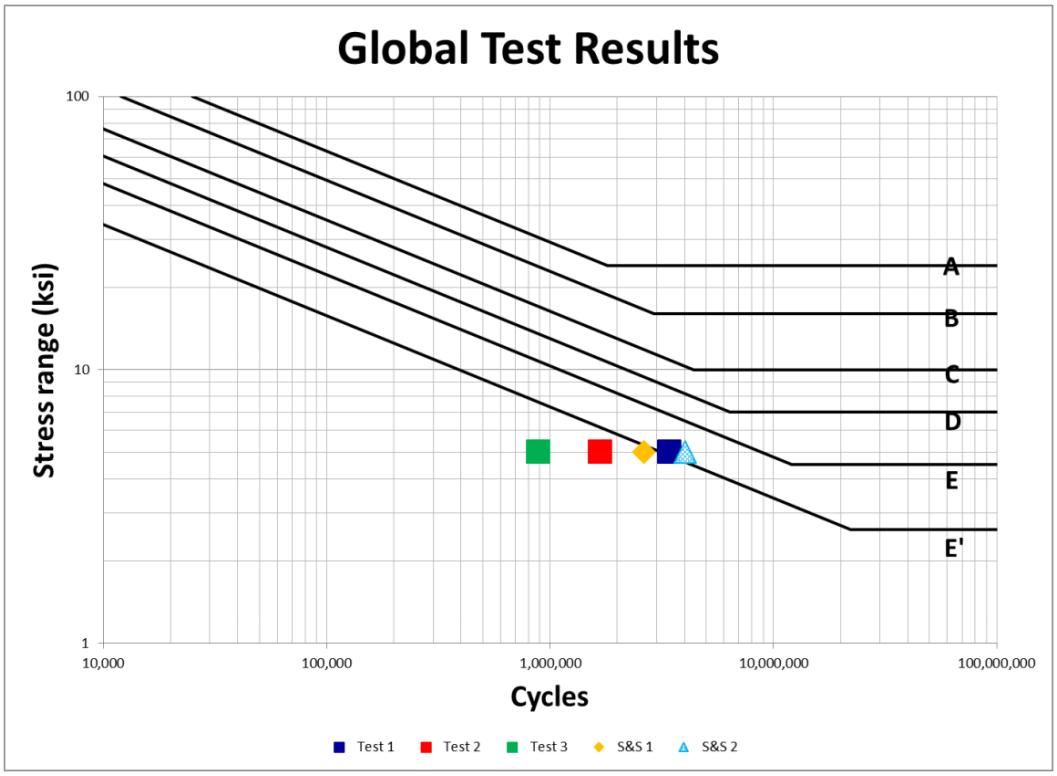

Figure 2.23: S-N Plot of Phase 6 Testing Results (Belivanis, 2014)

Chapter 3: Test Setup Design

This chapter outlines the details for the test setup and procedures used to test HMIP specimens in this research program. The primary purpose of the experimental tests is to provide data on the fatigue life of HMIP specimens with pre-existing cracks, with an emphasis on the fatigue life at low stress ranges. An additional purpose is to provide data on the ultimate capacity of HMIP specimens with pre-existing cracks under monotonic loading.

3.1 HORIZONTAL TEST SETUP

Two test setups were constructed in this phase of the research. The first test setup is similar to those which were used in previous fatigue investigations of HMIP specimens, as described in Chapter 2. The setup consists of a portal loading frame that tests the HMIP specimens horizontally. Compared to previous investigations, the testing frame has been expanded so that it is capable of handling two tests at a time in lieu one test, where each test consists of two specimens. This original testing setup was designed by researchers for earlier HMIP tests at the University of Texas at Austin (Rios, 2007). It is a large scale replication of the testing setup used to test traffic signal mast arms at the University of Texas (Koenigs, 2003). A schematic of this testing setup can be seen in Figure 3.1.

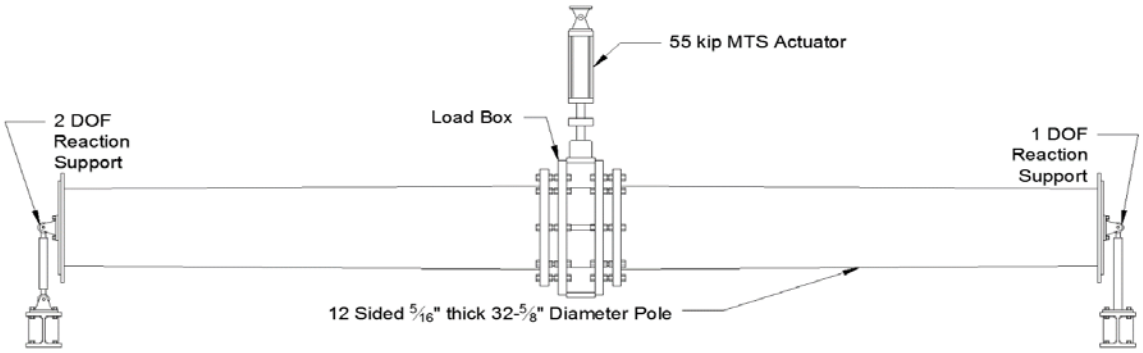

Figure 3.1: Horizontal Test Setup

Since vertical testing limits this experiment to one specimen at a time, the horizontal configuration was selected. This configuration allows for two specimens to be tested at one time, provided they have the same or similar stiffness. The ability to test multiple specimens at the same time was important, as these specimens are being tested at stress ranges from 2-6 ksi and experiments can take months to complete. The setup shown in Figure 3.1 can be modeled as a simply supported beam with zero moments at its ends. When two identical specimens are tested in this setup and a stiff load box is used, rotation at the midpoint can be assumed to be zero. This effectively makes it a test of two back-to-back cantilevers.

For the test setup in Figure 3.1, an elevated rod eye at one provides a single rotational degree of freedom. Meanwhile, a steel rod with a rod eye at each end is provided at the other end to create a two degree of freedom roller. This roller permits rotation and longitudinal translation of specimens. See Figure 3.2 for schematics of these end supports.

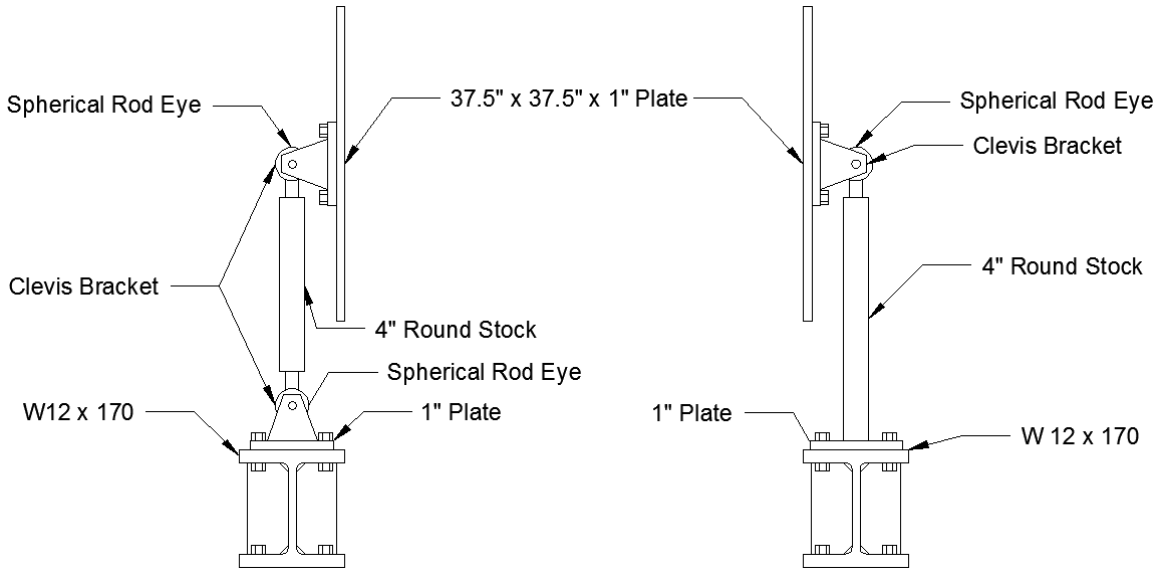

Figure 3.2: Test Setup End Supports

Vertical loads are imparted by a 55-kip MTS actuator. These loads are resisted by a portal frame that was designed accommodate two test setups simultaneously, allowing four HMIP specimens (two HMIP specimens per setup) to be tested simultaneously. The frame consists of two wide-flange column sections, one coped wide flange section connecting the columns, and two diagonal bracing elements, all of which are ultimately tied down to the laboratory strong floor. The portal frame, specimens, and loading boxes can all be seen in Figure 3.3.

Figure 3.3: Portal Loading Frame with Four Specimens Attached

The overall length of this testing setup is 32 feet. This was chosen based on the practical limits of available laboratory space, limits of the loading equipment, and to be consistent with previous investigations.

Because the actuators have a clevis at each end, tests must be run in a manner where the actuators are always in tension. This is done in order to maintain stability of the test setup. Consequently, the actuators are always pulling up on the specimens, placing the top half of a specimen in tension, and the bottom half in compression. Thus, for each test, a mean stress was chosen to provide the target stress range, and to always provide a minimum stress value at the top fiber that was in tension. Correspondingly, the

bottom fibers of the test specimen were always in compression. In some cases, when fatigue failure occurred at the top fibers, the specimen was rotated 180 degrees, to provide an additional fatigue test on the side of the specimen that as previously cycled in compression.

3.1.1 Load Box Connections

The specimens were bolted back to back to a built up stiff loading box previously designed in Phase 1 and then redesigned in Phase 3 to accommodate larger diameter specimens. This loading box needed to be rigid to minimize rotation at the base of each specimen.

The load box was fabricated out of two vertical 3” thick plates welded to two horizontal 2” thick plates. Two internal 2” internal plates were welded within the box in a cruciform shape to provide additional stiffness. The 3” thick plates were drilled with twelve 1-7/8” holes sized to accommodate the 1-3/4” diameter threaded rods used to connect the box to the high mast baseplate. The design schematics for the load box can be seen in Figure 3.4.

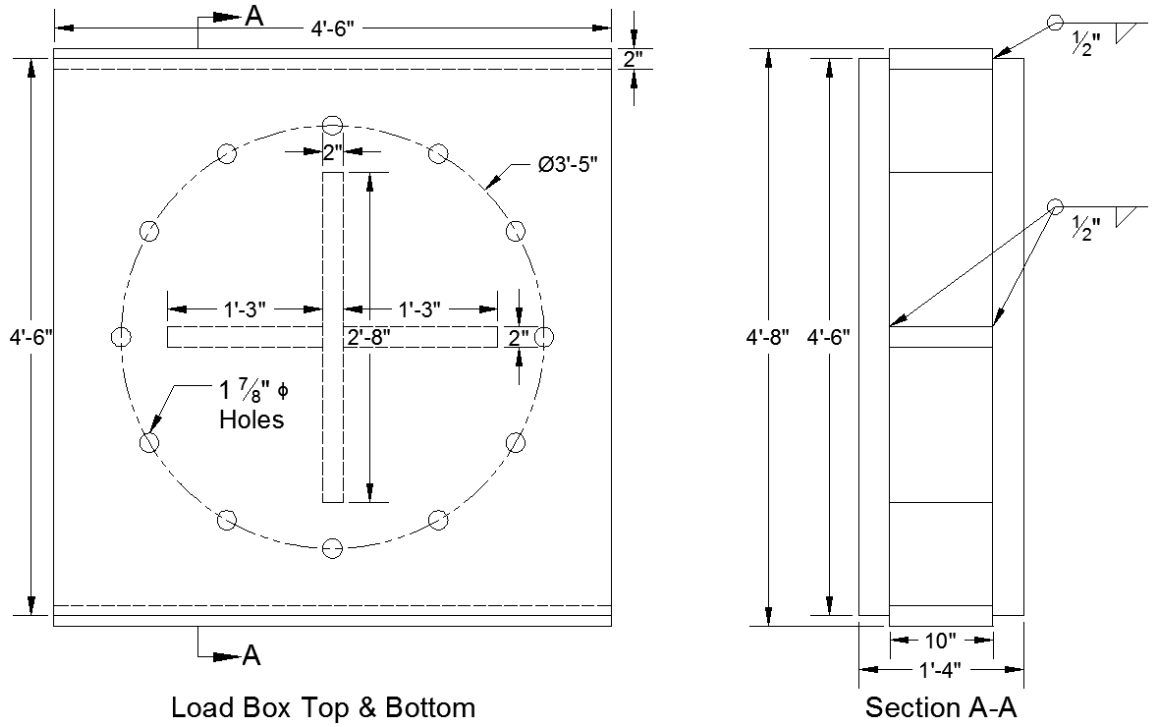

Figure 3.4: Schematic Design of Load Box

A double nut configuration was used at the connection between the loading box and the HMIP specimen. This is consistent with the field connection, as threaded rods are embedded into a concrete footing and connected to the High Mast Poles using a double nut configuration of heavy hex nuts. See Figure 3.5 for a picture of this connection as well as a description of nomenclature.

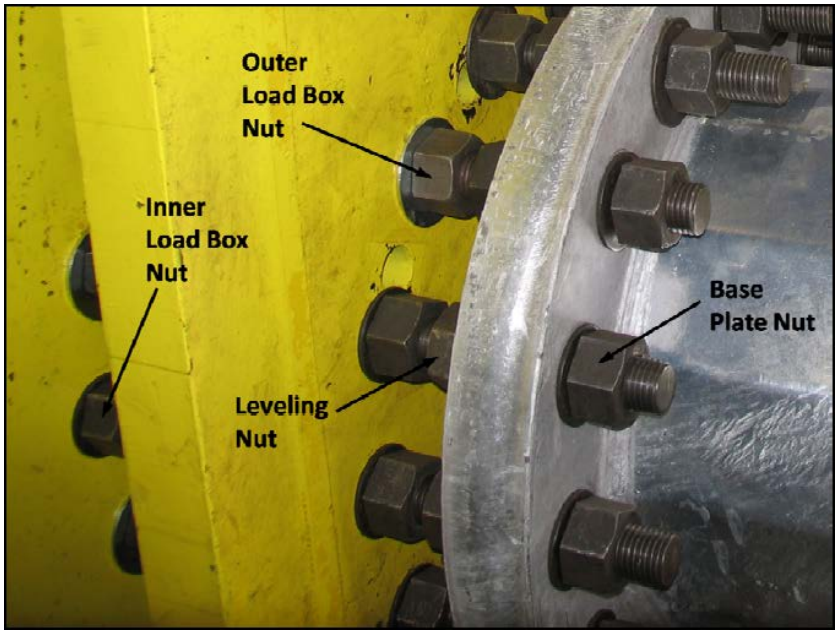

Figure 3.5: Double-Nut Connection and Nomenclature (Stam, 2009)

3.1.2 Hydraulic Systems – Horizontal Setup

A hydraulic actuator was used to provide cyclic loading to the specimens at a variety of tensile stress ranges varying from 2 ksi to 6 ksi. Forces were applied by a 55 kip MTS hydraulic actuator and measured via an inline 55 kip MTS load cell. Hydraulic pressure was applied using an MTS SilentFlo Hydraulic Power unit operating at 3000 psi. The power unit was connected in line with two servo valves and a hydraulic manifold.

An MTS FlexTest SE Controller was connected a personal computer, which in turn was used to control the test. The controller monitored and controlled displacement, force, error, and cyclic frequency of the actuator. A screen capture of this controlling computer can be seen in Figure 3.6. To avoid system resonance, this frequency was kept below 4.0 Hz. This decision was made based on calculations made during phase one for a similar specimen (Rios, 2007). The researchers estimated that the setup's resonance

frequency was about 6.67 Hz. While the specimens used in this research are not the same as those used previously, the previous estimation was deemed conservative, as the specimens used in this test are significantly stiffer, but are not much more massive than those previously tested.

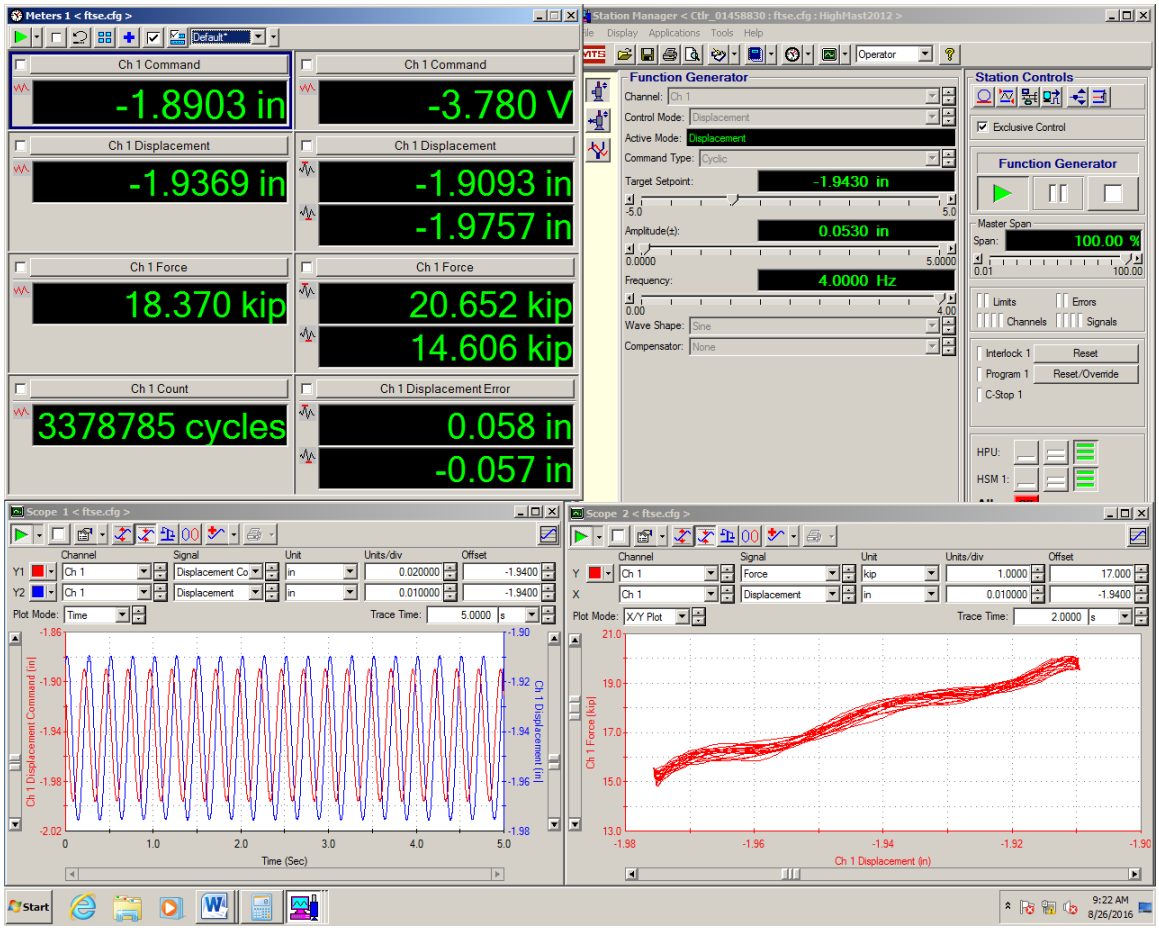

Figure 3.6: Screen Capture of Test Controls and Actuator Feedback

3.1.3 Control Methodology – Horizontal Setup

Due to programming limitations, displacement control was used in lieu of force control for these tests. Displacement levels were chosen so that the targeted nominal stress range could be met. Despite only using displacement control during these, two methods of test management were employed.

The first method of test management was to set the displacement command and simply run the test without adjustments. This is pure displacement control. No adjustments were made to the control throughout the test unless changes to the testing frame required them. This method was used in previous tests as it reduced dynamic effects and prevented the system from becoming unstable as the specimens were tested. Similar to previous tests, failure was defined as a 10-percent reduction in the load.

The second method of test management was a modification of displacement control. This method allowed adjustment of the displacement command gradually during the test. These adjustments were made throughout the test to maintain constant forces and a constant nominal stress range. Failure was defined as the point when the displacement command had to be increased by 10-percent, relative to the beginning command, to maintain the same force range. This method of test management was designed to emulate force control. Since this method was only a modification of displacement control, all benefits of displacement control were maintained.

While full tests have yet to be completed in the vertical setup at the time of this thesis, it is expected that similar control methodologies will be used to control that test.

3.2 VERTICAL TEST SETUP

The second setup used in this phase of research allowed researchers to tests HMIP specimens in the vertical orientation. This configuration involved testing specimens with the baseplate fixed against the laboratory reaction floor and a hydraulic actuator reacting against a reaction wall. A schematic of this setup can be seen in Figure 3.7.

While tests were being run on the horizontal test setup, researchers undertook the task of designing a setup that would be capable of testing the HMIP specimens in a vertical orientation. Two main advantages led researchers to construct this setup. The first is that this setup could be used to test specimens in a full stress reversal. The second advantage is that this setup can be used for ultimate strength tests in addition to fatigue tests. Specimens that have been tested to failure in the fatigue tests can be placed in this setup and pushed in one direction to determine the remaining static strength. These tests provide an estimate of the remaining static ultimate strength an HMIP with significant fatigue damage.

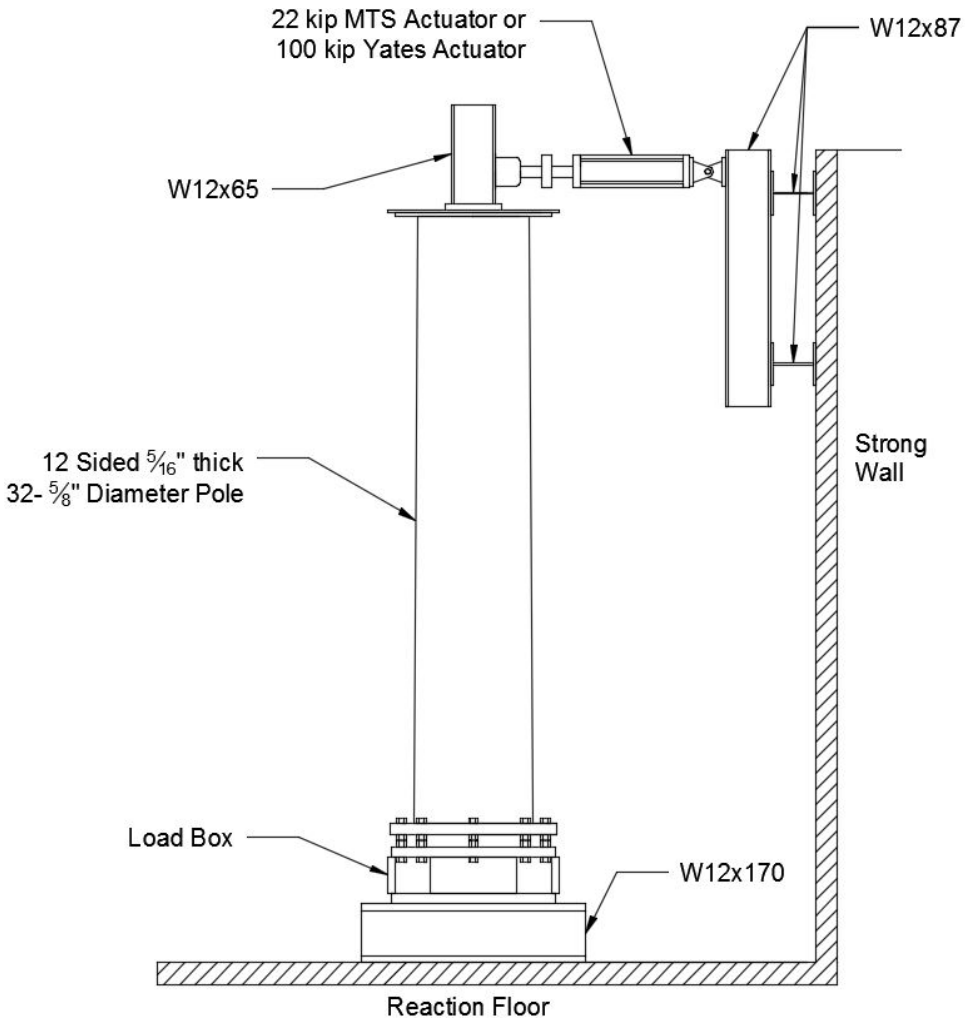

Figure 3.7 Vertical Test Setup

3.2.1 Vertical Test Setup Connections

To maintain a rigid base, the HMIP specimens were bolted to a stiff load box repurposed from earlier experimental phases at Ferguson Lab. Despite being smaller than the other load boxes used in this phase, this load box was large enough to accommodate these specimens. All connection methods previously discussed were kept for the vertical setup.

The bottom of the load box was bolted to two stiff wide flange sections which were in turn bolted to the laboratory's floor. To allow a wide range of possible fatigue loads on a vertical specimen, the tie downs to the floor were post tensioned at 40 kips. This load corresponds to 80 percent of the strong floor's capacity. Figures of the repurposed loading box can be seen in Figure 3.8.

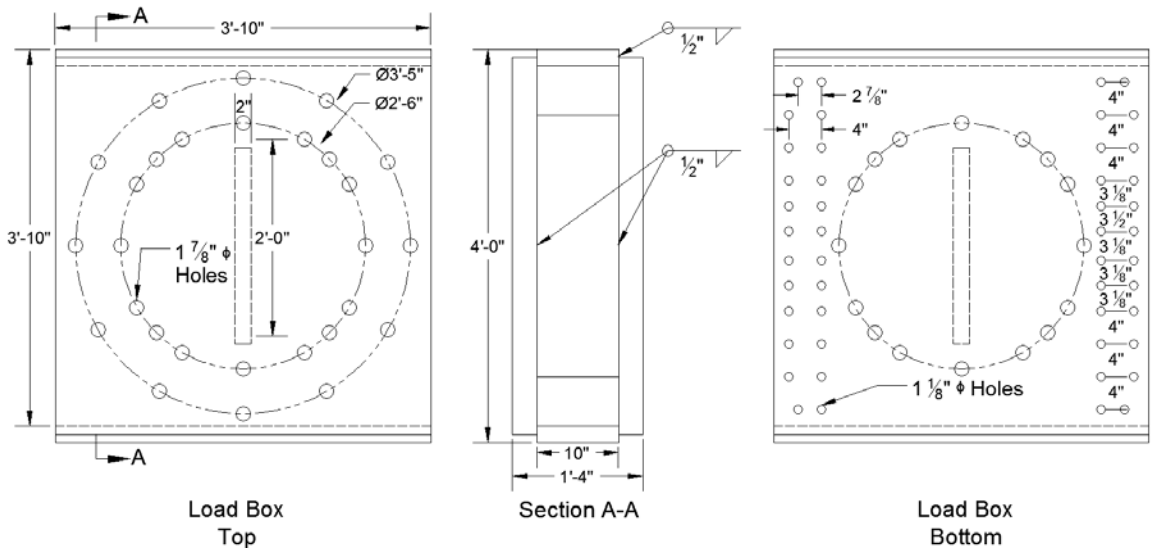

Figure 3.8 Load Box Repurposed for the Vertical Setup

To transfer the load from the actuator to the HMIP specimen, built up connection points were constructed out of several wide flange sections. To the top of the specimen, a plate is bolted. On this plate is a vertical wide flanged shape that has been welded to a baseplate, allowing it to be bolted to the specimen setup. This wide flange section is used to help transmit load to the specimen setup. The load is imparted by one of two actuators. These actuators were bolted to the laboratory's strong wall through the use of three wide flange sections. A vertically oriented wide flange section directly connected to the other

side of the actuator. This section was then bolted to two horizontally running wide flange sections that were connected directly to the strong wall. Where permissible, these connections were slotted to allow for any errors that arose in fabrication. An isometric drawing of this setup is available in Figure 3.9.

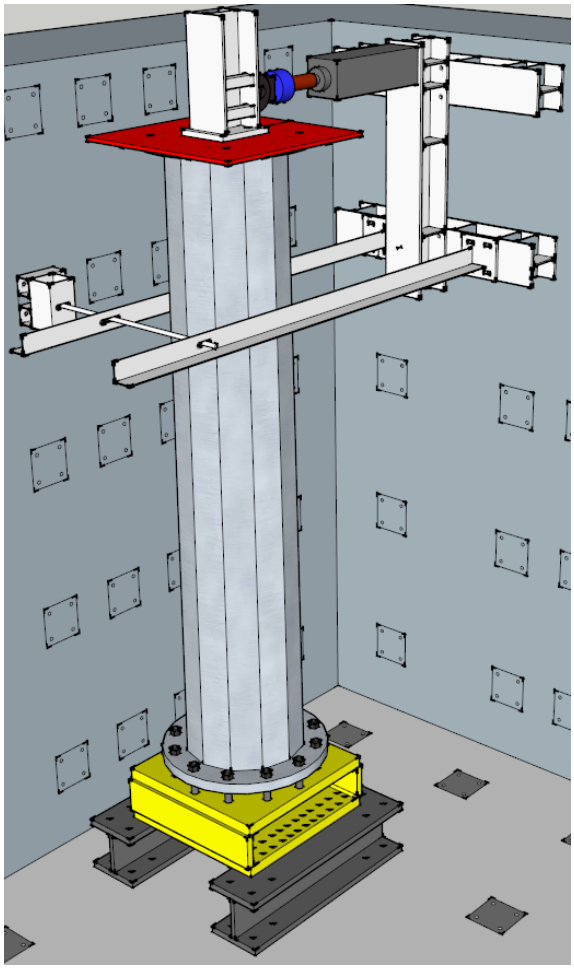

Figure 3.9: Vertical Test Setup Isometric View

The specimen is restrained laterally to prevent damage to the actuator. The lateral restraint system consists of an angle on each side of the specimen. Each of these angles is welded to a baseplate with slotted holes. These baseplates make use of the primary

loading system by bolting to the lower wide flange section on the strong wall. At the free end of these angles, there is a slotted hole. Through these holes, a threaded rod is fit. This threaded rod is in turn tied back to a tube section that is connected to the strong wall. This system is adjustable to account for imperfect specimens and the displacements corresponding with different loading ranges. This system is pictured above in Figure 3.9. Detailed drawings can be seen in Figure 3.10.

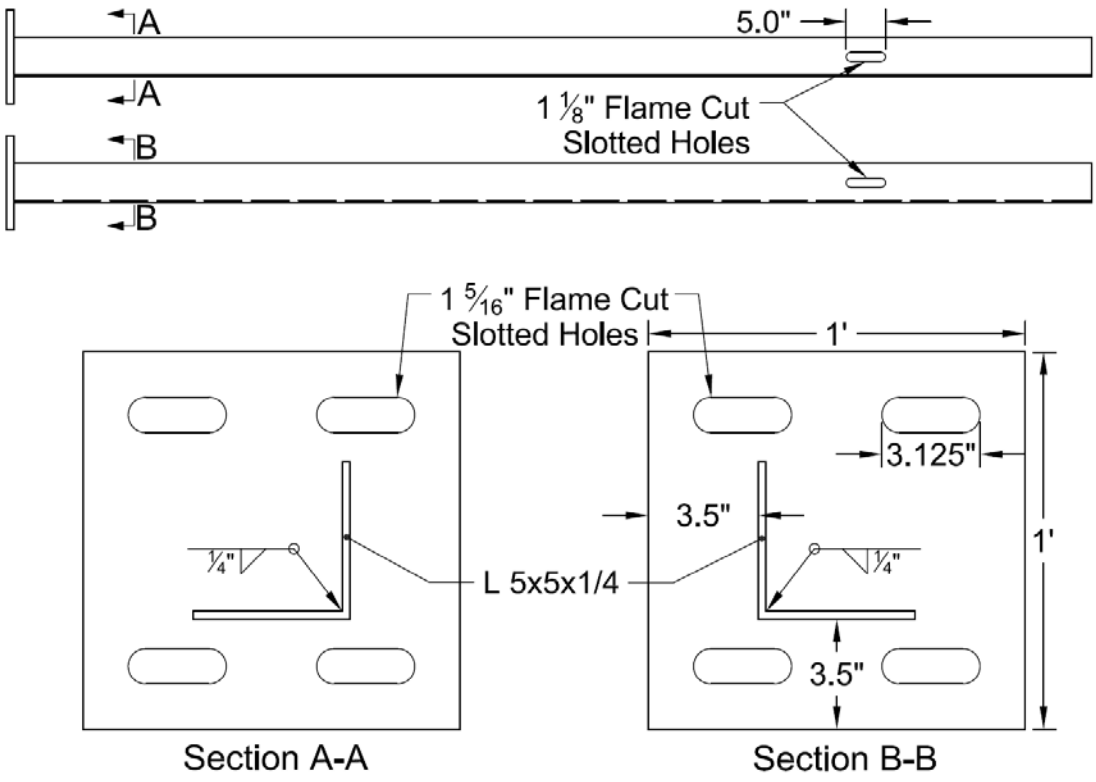

Figure 3.10: Lateral System Restraint Details

3.2.2 Hydraulic Systems – Vertical Setup

As this setup was made to be capable of handling both fatigue and ultimate strength tests, it was necessary to use two hydraulic actuators and therefore two hydraulic loading systems.

The first system consists of a hydraulic actuator used to provide cyclic loading to a specimen at a variety of stress ranges varying from 1 ksi to 4 ksi. Forces are applied by a 22 kip MTS hydraulic actuator and measured via an inline 22 kip MTS load cell. Hydraulic pressure is applied using an MTS SilentFlo Hydraulic Power unit operating at 3000 psi. The power unit is connected in line with two servo valves and a hydraulic manifold.

The second system consists of a hydraulic actuator used to provide unidirectional loading to a specimen until failure. Forces are applied using a Yates actuator model H6C-B8.0N-16.00N3.50T2-11. This actuator is capable of applying a force of nearly 100 kips. Thus a 100 kip Interface load cell was used in line with the actuator to measure the applied load. Hydraulic pressure is applied via a Power Team SPX pump capable of operating at 10,000 psi. A Texas Instruments controller is connected to a personal computer, which in turn is used to control the test. This controller monitors displacement and force applied by the actuator.

Chapter 4: Test Specimen Design and Testing Procedure

This chapter describes the test specimens and testing methods that were used in this research phase. The primary purpose of this chapter is to describe the experimental methods used in this phase in detail to facilitate understanding and analysis of the experimental data, so that they may be duplicated in future research, if needed.

4.1 INTRODUCTION

The specimen designs used in this phase of research are based on standard HMIP designs of the Texas Department of Transportation (TxDOT 1998). All specimens fabricated thus far for this phase of research were designed based on TxDOT plans for 150 feet tall HMIPs designed for 80 mph winds. Six of the eight specimens were fabricated with full penetration welds without ground sleeves, while the remaining two were fabricated with external collars.

The HMIP designs chosen for testing were based on an inventory of HMIPs in Texas that identified the designs that have the greatest amount of observed cracks at the base and were most prevalent throughout the state (Morovat et al 2015). This inventory indicated that the HMIP of most interest is the 12 sided 150-ft 80 mph design without ground sleeves. Of the HMIPs of this design that were subjected to ultrasonic testing, 100-percent showed the presence of pre-existing cracks. Further, the inventory indicated a large number of HMIPs of this design located throughout the state of Texas. The inventory also showed that 12-sided 80-mph 150-ft HMIP designs with ground sleeves

also showed a high incidence of pre-existing cracks, for the HMIPs subjected to ultrasonic testing.

Previous research explored the fatigue strength of 12 sided 150-ft 80 mph HMIPs without ground sleeves, but this earlier research focused on higher stress ranges (Pool 2010, Belivanis 2014). For the current research, additional; fatigue data was desired at lower stress ranges, on the order of 1 to 6 ksi. Additionally, it tested newly fabricated specimens that have not been repaired after galvanization, thereby emulating behavior of specimens installed at sites spread throughout Texas.

The first six specimens were all 12 sided 150-ft 80 mph HMIPs without ground sleeves. These were fatigue tested until failure at stress ranges of 6, 3, 4, and 2 ksi. Following the completion of the vertical setup, one of the 6 ksi specimens will be reused and tested to evaluate to what extent the static strength of the HMIP shaft-to-baseplate connection has been affected by the presence of a significant degree of fatigue cracking.

The remaining two specimens were 12-sided 80-mph 150-ft HMIP designs with ground sleeves, also known as external collars. The external collar specimens will be tested at a 6 ksi stress range.

For the horizontal test setup, two identical specimens were paired and tested at one time. These specimens are labeled by two successive letters of the alphabet, i.e., A and B or C and D. As previously discussed, the pairing of specimens is necessary to establish a uniform distribution of load. The only differences in the specimens was the location and size of the cracks in the shaft-to-baseplate connection. As these cracks

formed during galvanization of the specimens, it was impossible to control them. Researchers attempted to pair similarly cracked specimens together, when possible, but slight differences in crack patterns remained. This typically resulted in one specimen failing before another. When this occurred, the failed specimen was usually flipped 180-degrees, and testing resumed on the flipped specimen.

For the vertical test, one specimen was tested at a time. This specimen was subject to a full stress reversal. As such, the specimen typically only underwent one failure, as both sides failed at or near the same time.

4.2 SPECIMEN NAMING SCHEME

The naming scheme used in this phase of research is similar to those used in previous research phases at Ferguson Lab. This naming scheme provides a concise means of summarizing the critical geometric details for each specimen. The naming scheme used in this phase of research can be found in Figure 4.1.

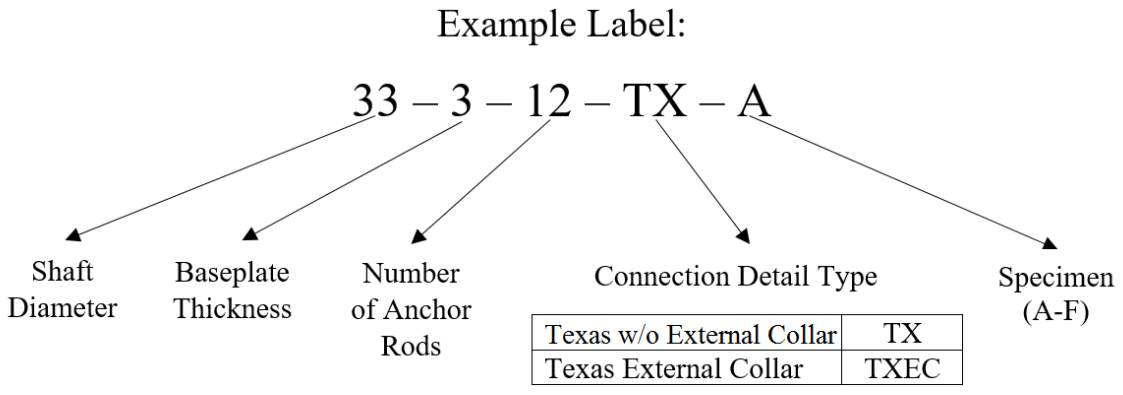

Figure 4.1: Specimen Naming Scheme

4.3 SPECIMEN DESIGN

High mast specimens tested at the University of Texas Ferguson Structural Engineering Laboratory were composed of four major components: a baseplate, a pole shaft, an end reaction plate, and a shaft-to-baseplate connection. These components can be seen in Figure 4.2. At the time of this report, all but one of these components, the connection, had been kept constant between all specimens. The outlier in these components was varied on two of the eight specimens when the connection was changed from having no external collar to including an external collar. For the majority of specimens, researchers opted to vary the tested stress range in lieu of geometric components.

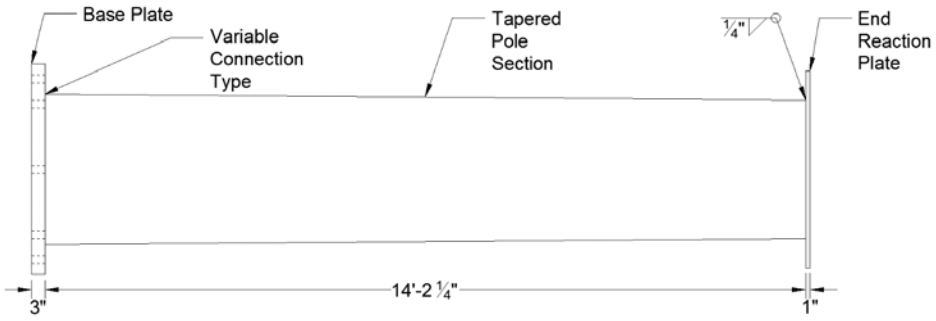

Figure 4.2: Test Specimen Components

To determine the size or type of the major components, researchers worked closely with TxDOT to ensure that the most important configurations were tested. After this deliberation, it was determined that specimens representing the 12-sided 150 foot tall poles rated for 80 mph would be tested. Full penetration welded specimens without an external collar were chosen for the first tests. These tests will be followed by a test of specimens rated for the same conditions, but with the addition of external collars.

In large part, the specimens were designed to TxDOT Standard HMIP-98 (High Mast, 1998). All specimens were dodecagon (12-sided polygon) sections with base diameters of 32-5/8” across the flats. The pole shafts for all specimens were all 5/16” thick for all specimens. External collared specimens added a 3/8” thick collar that connected to the base of the specimen and extended for one foot before being welded to the shaft. Finally, all specimens were tapered at a rate of 0.175 inches in diameter for every foot of the specimen.

When possible, TxDOT standards were followed, but some notable changes were necessary to facilitate testing. These changes include shortening the pole and the addition of an end plate. Occasionally other changes were made to induce a worst case testing scenario. For example, the bolt-hole arrangement in the base plate was modified such that a hole lined up with every bend. This change in orientation resulted in the addition of two anchor rods, but created a stress concentration at the bends. In turn, a worst case loading condition was guaranteed for the specimens and lower bound fatigue life estimates were yielded.

For all specimens, a length of 14’-6 ¼” was used. When the baseplate and end plate thicknesses are removed, the shaft length left is 14’-2 ¼”. This length was dictated by the overall test setup length of 32 feet, which is covered in Chapter 3. Despite their relatively short length, these specimens are capable of adequately representing the bases of the HMIPs.

End plates were added to all specimens for testing purposes. These end plates created a connection location between the specimens and the end supports of the testing

frames. All end plates were made using one inch thick steel plates which were welded to the shaft using a fillet welds. The end plates were drilled with slotted holes to permit connection to the end supports of the test setup. See Figure 4.3 for the shop drawing of these end plates.

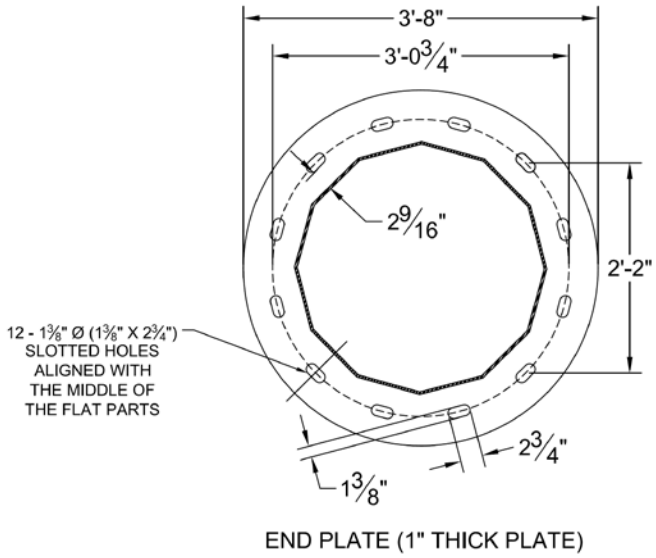

Figure 4.3: Specimen End Plate Connection Details

Finally, the two anchor rods were added to the baseplate bolt pattern. This addition brought the total amount from ten anchor rods, as specified in the standard TxDOT design, to twelve. Prompting this change was the research team's desire to place bends, not flats in the upmost position. Typically HMIP specimens fail at the bends, as there is a stress concentration at these changes in geometry. Anchor rods were aligned with all twelve of the bends allowing specific bends to be tested. This revised orientation was determined to cause an even higher amplification of stresses in the bends of the specimens. A photo of the HMIP base can be seen in Figure 4.4. All base plates were

three inch thick circular plates with a 47 inch diameter and a 22 inch dimeter hole cut out of the middle.

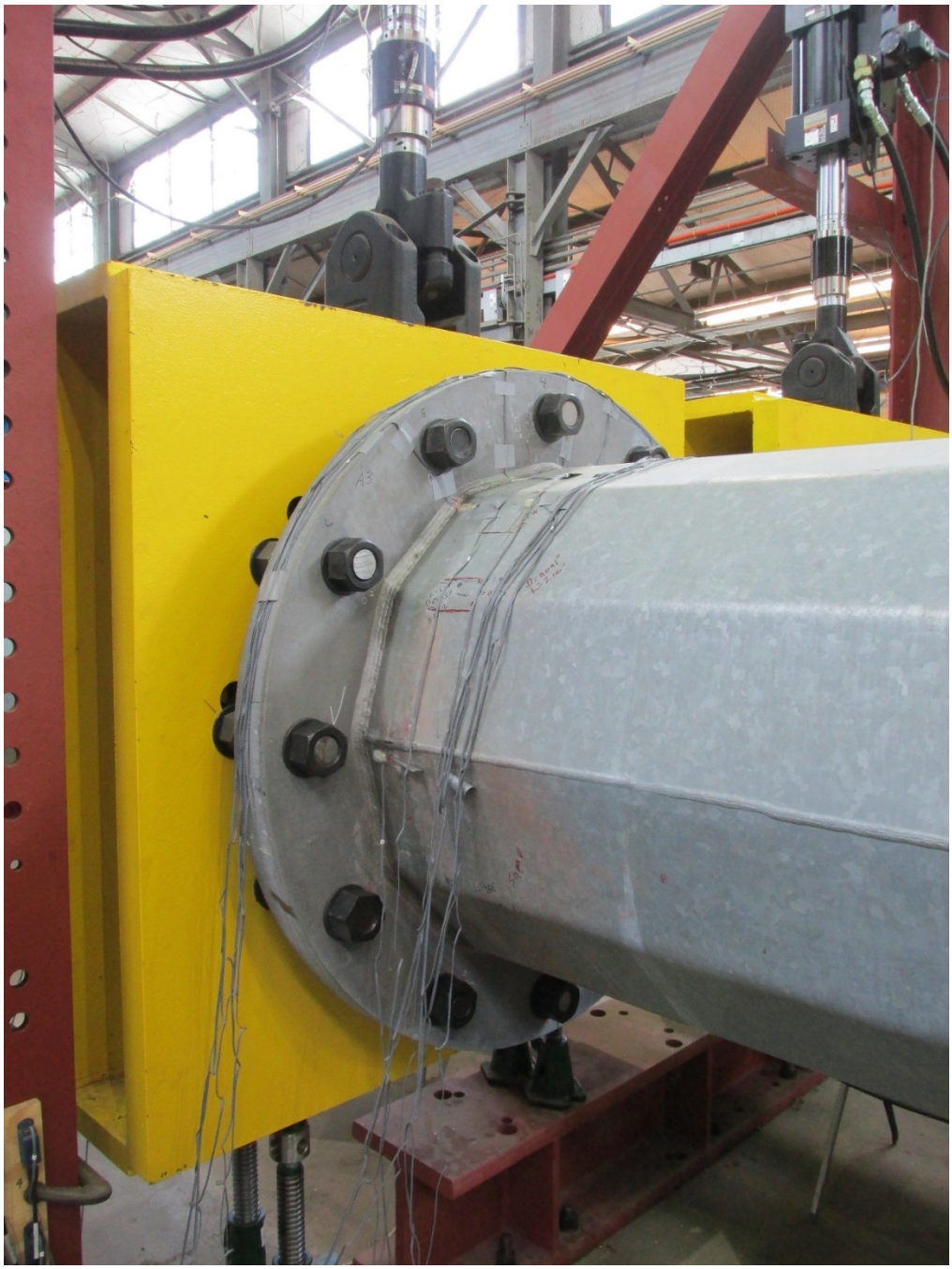

Figure 4.4: Specimen Base

4.3.1 Texas Full Penetration Welded Connection without External Collar

A common connection detail used on existing HMIPs in Texas is a full penetration welded connection between the baseplate and the pole shaft. For this detail, a full penetration weld is run along the outside of the pole to connect the baseplate to the shaft. This full penetration weld is created by beveling the shaft and filling the void with weld material. On the inside, a seal weld is run to seal the seam between the shaft and the baseplate. While this weld provides no significant rigidity to the specimens, it is commonly used to prevent the entrapment of galvanizing slag in the seam between the shaft and the baseplate. Details of this connection can be seen Figures 4.5 to 4.7.

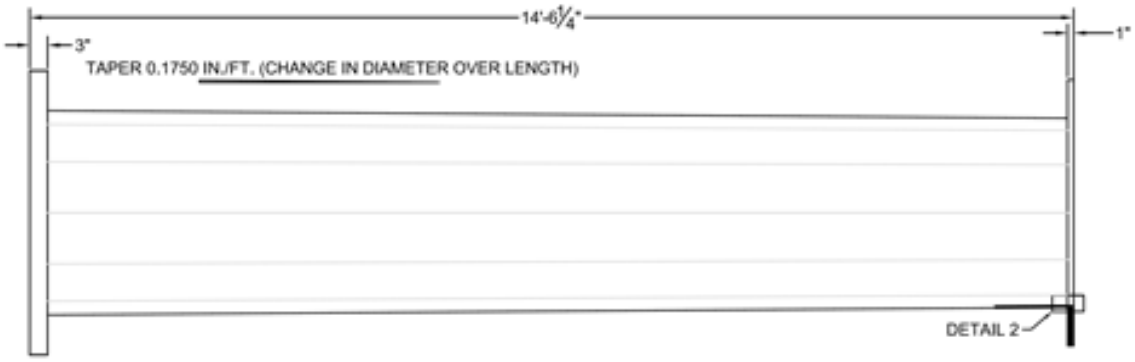

Figure 4.5: Layout of an HMIP specimen with a Full Penetration Welded Connection without External Collar

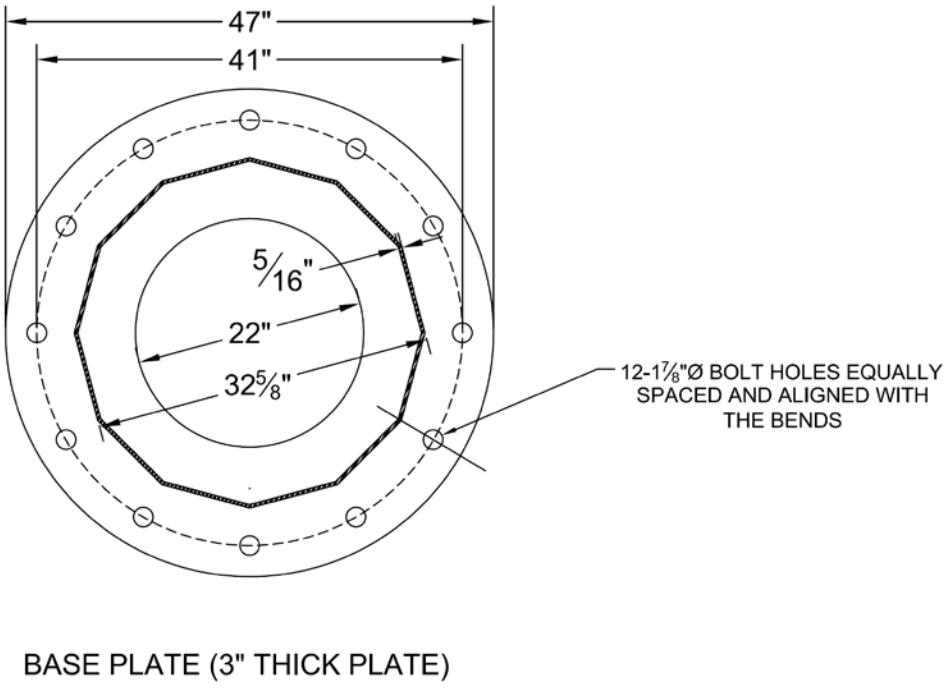

Figure 4.6: Baseplate Details for HMIP Full Penetration Connection without External Collar

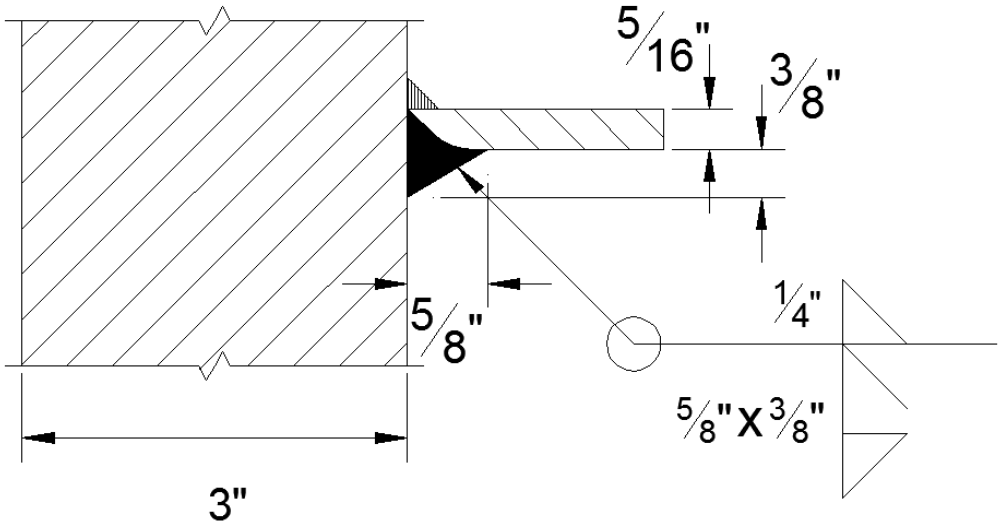

Figure 4.7: Weld Detail for HMIP Full Penetration Connections

4.3.2 Texas Full Penetration Welded Connection with External Collar

Two HMIP test specimens will be tested with a full penetration weld, but with the addition of an external collar, also known as a ground sleeve. This external collar is created out of 3/8” thick by one foot tall steel plate. The steel is bent such that it can be wrapped around the base of pole shaft. This can be seen in Figures 4.8 to 4.10.

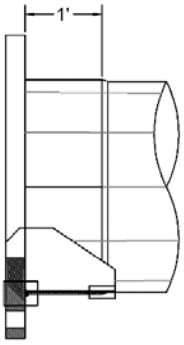

Figure 4.8: External Collar Dimension

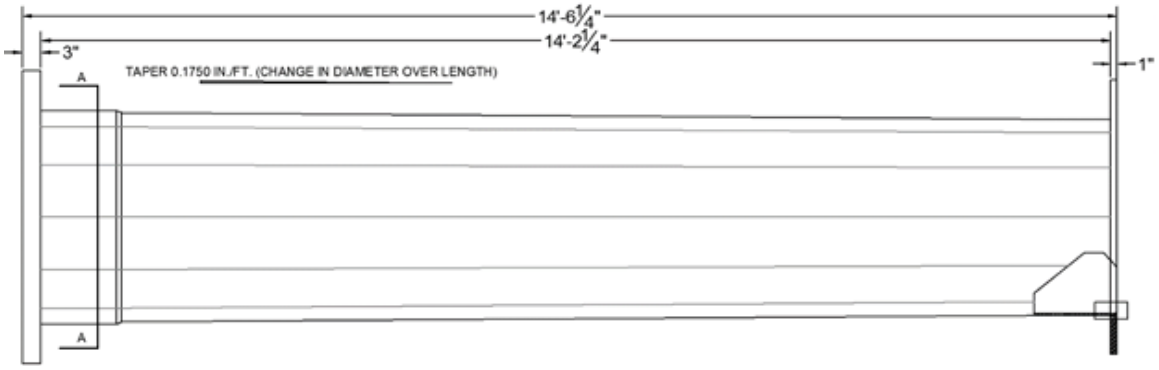

Figure 4.9: Layout of an HMIP specimen with an External Collar Connection

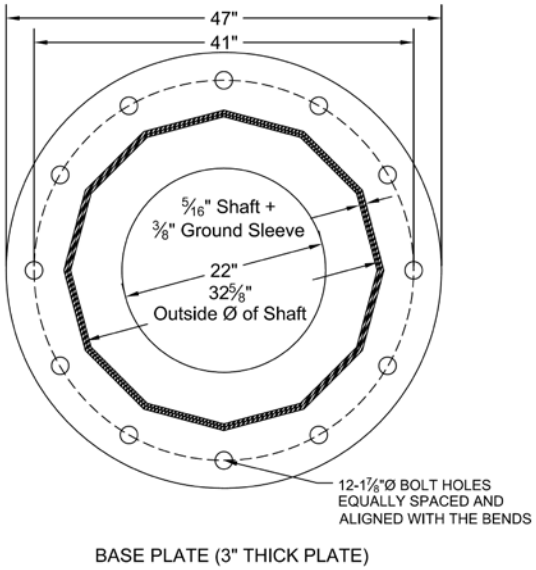

Figure 4.10: Baseplate Details for HMIP External Collar Connection

Like the typical full penetration welded connections, the shaft-to-baseplate connection for the external collar specimens is also a full penetration weld. First, the external collar is installed on the outside of the shaft. Next, the external collar and shaft are both beveled and the beveled void is then filled with weld material. A seal weld is then run along the inside of the specimen to prevent galvanization slag entrapment. Finally, a fillet weld is run along the top of the external collar to seal off the seam between the external collar and the shaft. See Figure 4.11 for the shaft-to-baseplate weld detail and Figure 4.12 for the connection between the external collar and shaft.

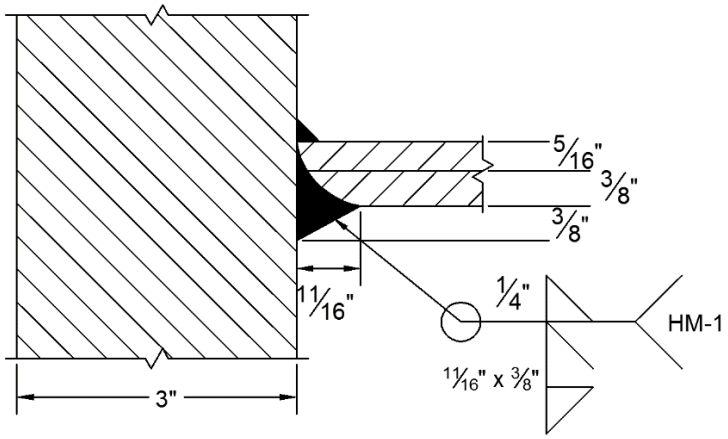

Figure 4.11: External Collar Shaft-to-Baseplate Weld Detail

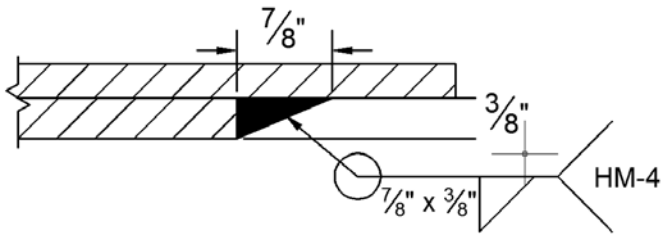

Figure 4.12: External Collar to Shaft Weld Detail

One significant factor worth noting in the design of specimens with external collars is the addition of vent holes. These holes permit the escape of the air from the seam between the external collar and the pole shaft. They must be drilled through the external collar to the shaft such that they can permit the escape of gas. This process must be done before galvanizing, but after pickling, as the pickling process can result in severe corrosion (Pool 2010). The drilling of these vent holes adds an additional step during the galvanizing process, which in turn slows the galvanization process and increases the cost of production. Figure 4.13 shows a specimen with an external from Phase II that experienced bulging due to a lack of vent holes.

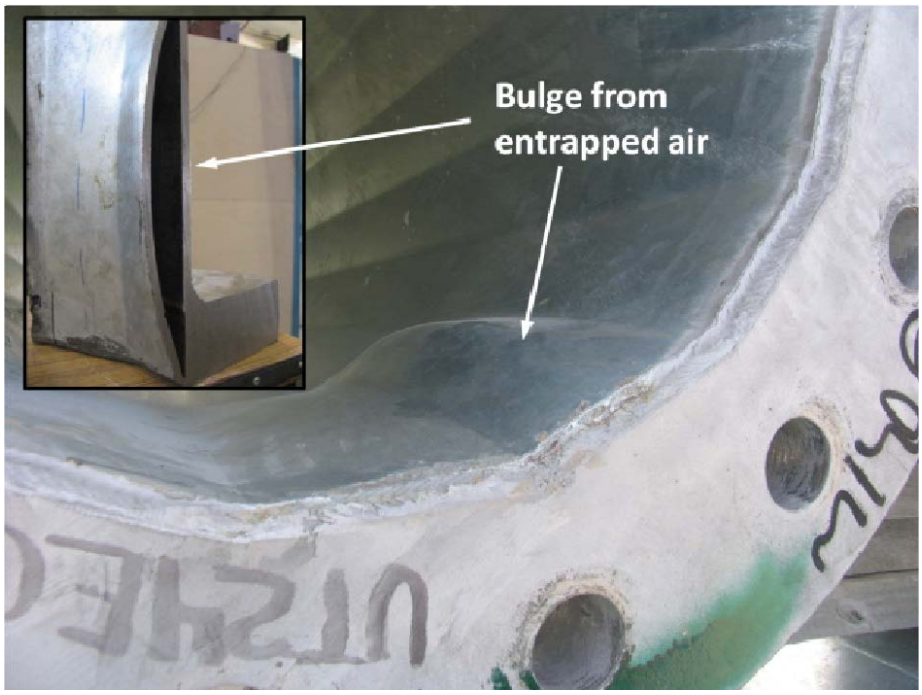

Figure 4.13: Bulging Caused by Entrapped Air (Stam, 2009)

4.4 FATIGUE TESTING PROCEDURE

The testing of High Mast specimens was composed of four distinct phases. These phases were, (1) the measurement and inspection of specimens, (2) the installation of specimens, (3) the installation of strain gauges and measurement of stress at static loads, and (4) the starting of the fatigue test and the adjustment of dynamic loads.

4.4.1 Measurement and Inspection

Prior to testing all specimen were inspected and measured. This was completed prior to installation to increase the ease of access to the baseplate and the interior of the pole. Most dimensions, including length, baseplate thickness, baseplate diameter, bend radius, and pole taper, were checked during this pre-installation phase. Others, including

pole thickness, weld dimensions, and preexisting cracks, were checked by ultrasonic testing during the pre-fatigue test process.

For the first two specimens, a trained TxDOT inspector performed ultrasonic testing around the diameter of the base of the pole. For the remaining poles, inspectors from Reinhart & Associates were contracted to perform ultrasonic tests. The later tests were performed using phase array ultrasonic test (PAUT) instrumentation in lieu of conventional ultrasonic testing instrumentation.

4.4.2 Installation Procedure

Despite the unusual shape of the specimens and their unbalanced weight, the high mast specimens were installed using an efficient procedure developed throughout the project. This procedure was adapted from those used in previous research phases. Detailed accounts of these previous procedures can be found in reports written by Rios (2007) and Stam (2009). The procedure used in this phase of research can be found in Appendix A for the horizontal tests, and Appendix B for the vertical tests.

One of the issues to consider during installation of a specimen was to choose which bend would be located at the top, as the top bend sees that largest stress range during testing. For the first specimen, the longitudinal seam was placed at the top, as this was believed to be the most severe condition for fatigue failure. However, the test results for the first specimen showed that this was not the case. Consequently, for the remaining specimens, the top bend was typically assigned to be the bend that was most critically cracked before the test commences. This designation was made by analyzing preliminary PAUT results to see which bend has the longest and deepest cracks. Usually there is only

one bend that has significant cracking, but when there are multiple bends with significant cracks, the neighboring bends are considered. In this situation, the bend with the most cracking between itself and its neighbors is deemed the top bend.

It should be noted that the nature of this testing method is that only the top bend experiences the specified targeted tensile stress range. The neighboring bends (one on each side) undergo similar but slightly lesser stress ranges. Those stresses in the bends beyond the top three are significantly smaller than the specified tested stresses, as the stress declines when the neutral axis is approached. Above the neutral axis, the bends are in tension, whereas below the neutral axis, the bends are in compression. This means that the specimen can be flipped 180 degrees after its first failure and be tested again.

4.4.3 Stress Measurement and Load Determination

Following the methods of previous phases, all specimen loads were calculated assuming simple beam theory. Specimen stresses were calculated along the top fibers of specimens at the intersection of the shaft to baseplate. At this location, the nominal bending stress is amplified by the notch of the weld toe, which results in a stress concentration. However, as is conventional in fatigue testing, only nominal stresses are considered in determining the stress ranges used in these tests.

The simple elastic bending formula ($\sigma = M_1c/I$) was used to relate nominal bending stresses to bending moments at the baseplate to weld connection. In this, the moment of inertia, I, was calculated by creating the cross-section in AutoCAD and using its cross sectional analysis functions (AutoCAD ‘massprop’ command). Its extreme fiber distance, c, was also calculated in Autocad as the distance from the center of the cross-

section to the exterior side of the top most bend. The bending moment, M_1, is the bending moment at the location of the weld. This moment was determined using simple beam analysis, which can be seen in Figure 4.14.

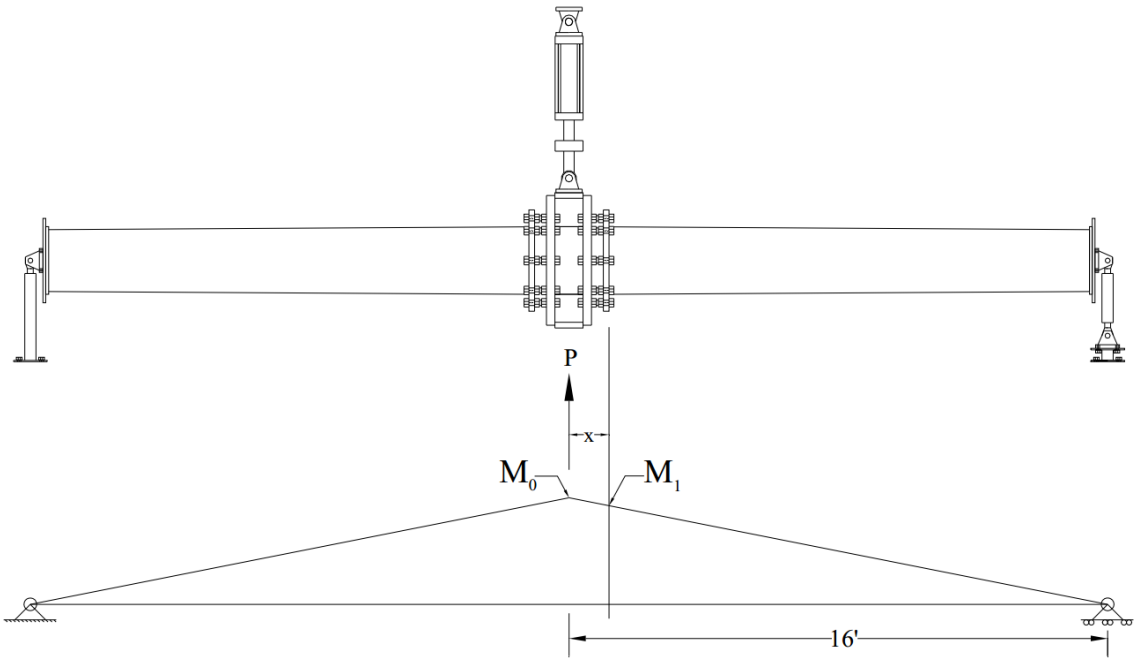

Figure 4.14: Moment Diagram for Calculating Testing Loads (Rios, 2007)

Both stress ranges and mean stresses were selected. All tests completed during the time of this thesis were completed with a mean stress of 6 ksi for consistency. The selected stress ranges varied from 1 to 6 ksi. Once a stress range had been determined, upper and lower stresses were found using the selected mean stress. Then the simple elastic moment relationship above was utilized to solve for the necessary applied moment. Finally, these moments were related to the applied load based on statics. The

applied load, applied moment, M_0, was determined to be a proportion of the maximum value, such that:

$$M_1 = \frac{16 - x}{16} M_0$$

$$Where, \quad M_0 = \frac{P_{req} \times L}{4}$$

$$Finally, \quad P_{req} = \frac{M_1 \times 64}{(16 - x)}$$

For this, the horizontal distance x is the distance from the middle of the actuator to the weld, also known as the standoff distance. It depends on the width of the load box, the spacing between the load box and specimen, and the thickness of the specimen's baseplate. In this phase, the standoff distance was about sixteen inches.

Following this calculation, these load values were compared to the static loads required to meet their corresponding stresses. These stresses were checked using strain gages installed near the weld. A layout schematic of these strain gages can be seen in Figure 4.15. Note that the strain gauges closest to the weld were placed back-to-back to better capture the stresses near the weld. The strain gages placed 6 inches away from the weld were used to monitor the stress at the weld. These strain gages were sufficiently far away from the weld to avoid the stress concentration, but close enough to estimate the stress at the shaft-to-baseplate connection.

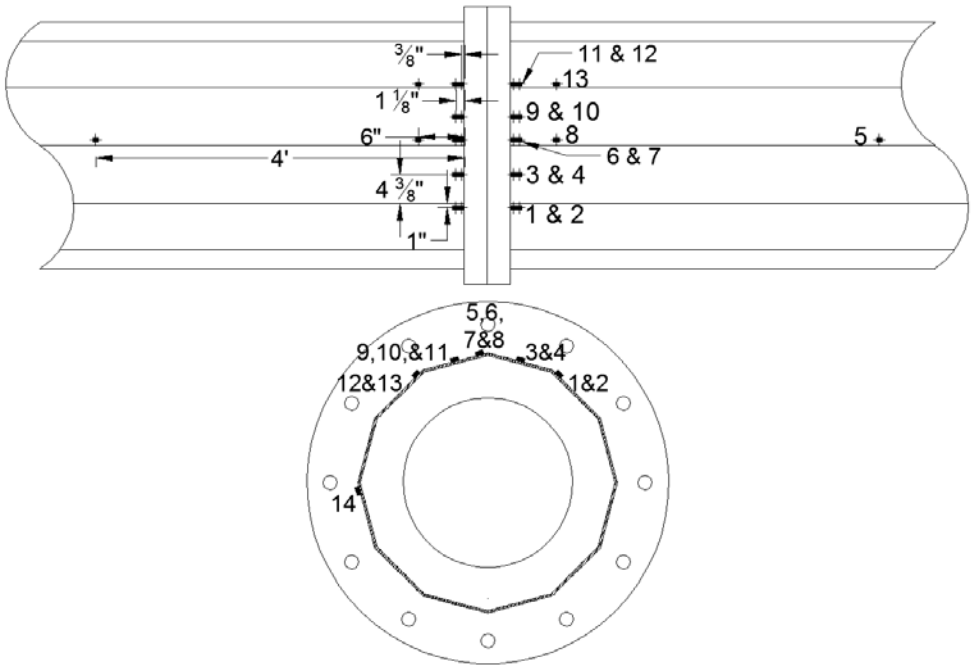

Figure 4.15: Schematic Layout of Strain Gages

Except for minor differences, due to strain gage location, these gages matched the calculated stresses at static loads. At dynamic loads, these strain gages showed stresses lower than the calculated loads. This reduction is the result of dynamic effects caused by the horizontal orientation of the specimens. To counteract this dynamic effect, researchers increased the displacement commands, and therefore the loads, until strain gage 8 measured stresses within 5-percent of the desired stresses. This often involved changing the mean displacement and displacement range. The degree to which these were changed varied from test to test and were heavily dependent on the testing frequency, which varied from 2 to 4 Hz.

4.5 PHASED ARRAY ULTRASONIC TESTING

Before, during, and after fatigue tests were completed, ultrasonic testing was performed on the specimens. This testing was done to provide measurements for length and depth and to monitor crack growth. Unlike previous research phases, this phase of research used Phased Array Ultrasonic Tests (PAUTs) in lieu of conventional ultrasonic tests. Like conventional ultrasonic tests, these tests emit sound waves through a transducer. When a discontinuity, a crack or material property change, lies in the path of the sound waves, they are reflected back and received by the transducer. This received signal is turned into an electrical signal and displayed on the PAUT receiver which is then used to read crack lengths and depths.

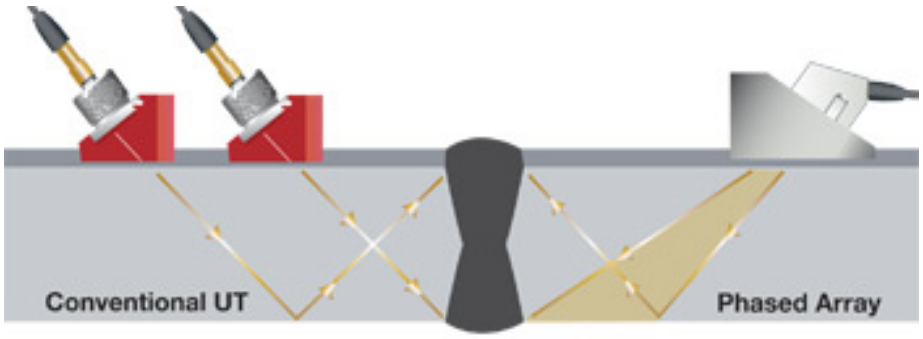

Figure 4.16 Conventional vs. Phased Array Ultrasonic Tests (“Phased Array Tutorial”)

The primary difference between PAUT and conventional ultrasonic tests lies in the transducer. Conventional ultrasonic transducers emit signals at a fixed angle, requiring that the transducer be moved in the direction towards or away from the baseplate-to-shaft connection to fully scan an area. PAUT transducers, on the other hand,

can emit signals across a range of angles. This enables PAUT technicians to leave the transducer at a fixed distance away from the weld and simply sweep it around the perimeter of the pole. During this sweep, it may become necessary to adjust the transducer's range of angles to focus on an imperfection, but this can all be done from the PAUT receiver without adjusting the transducer. Figure 4.16 above shows the difference between conventional and phase array ultrasonic tests. Note how the PAUT transducer can detect the full depth of the weld from one position, while the conventional transducer cannot.

Ultrasonic tests were performed on every specimen tested at the Ferguson Laboratory during this phase of research. Conventional ultrasonic tests were used on the first three readings for specimens A-1 and A-2. These readings were performed by TxDOT inspectors who did not have access to phased array equipment. For these readings, crack length, but not crack depth data is available. Due to time constraints and obligations, the TxDOT inspectors became unable to assist researchers at the Ferguson Laboratory. As such, researchers located a testing firm that was capable of ultrasonic testing. Since that time, tests have been performed by Reinhart & Associates, a nondestructive evaluation testing and engineering firm based in Austin, Texas.

Reinhart & Associates employees carefully measured the length and depth of the cracks existed in the shaft-to-baseplate welded connections of the HMIP specimens. The crack lengths/depths were measured before the start of fatigue tests and periodically during the tests. Reinhart & Associates employees recorded the data from the ultrasonic tests and reported them shortly after work had been performed. With the instruction of

the research team from University of Texas, Reinhart & Associates workers also marked the crack beginning locations, ending locations, and lengths of cracks on the HMIP specimens so that crack growth could be tracked over time. Images of this information were captured and chronicled for later use. These images can be seen in the Chapter 5.

Chapter 5: Experimental Results

In this chapter, the results of the fatigue and ultrasonic tests on HMIP specimens are presented. As of December 1, 2016, four fatigue tests have been completed during the course of this research project. Four others are ongoing. Work is currently ongoing for two other experiments. The first four sections of this chapter will be broken down such that they discuss every experiment based on the specimens tested. The fifth and final section of this chapter will compare the general findings of the fatigue tests during this phase of research.

5.1 Specimens 33-3-12-TX-A and 33-3-12-TX-B – 6 ksi Experiment

The first specimens tested were specimens 33-3-12-TX-A and 33-3-12-TX-B. These specimens were tested at a stress range of 6 ksi and with a mean stress of 6 ksi. As with all specimens tested at the time of this thesis, these specimens were fabricated with a full penetration welded connection and no external collar, as described in Chapter 4.

Only one test was completed on the specimens during this experiment. This test will henceforth be known as test AB-1.

5.1.1 Ultrasonic Test Results

Prior to fatigue testing of the specimens, TxDOT technicians performed ultrasonic tests on the specimens to identify preexisting cracks. These tests showed that every bend had indications of initial cracking, with the exception of the bends that contained the longitudinal seam welds. Despite this finding, bend 1, a seam welded bend, was designated as the top bend.

The initial crack measurements for specimens 33-3-12-TX-A and 33-3-12-TX-B can be seen in Figure 5.1. While the depths of these cracks were not measured, their lengths were measured and recorded for future comparisons. Note that each of these specimens had approximately 10-percent of their 105” perimeters cracked before testing began.

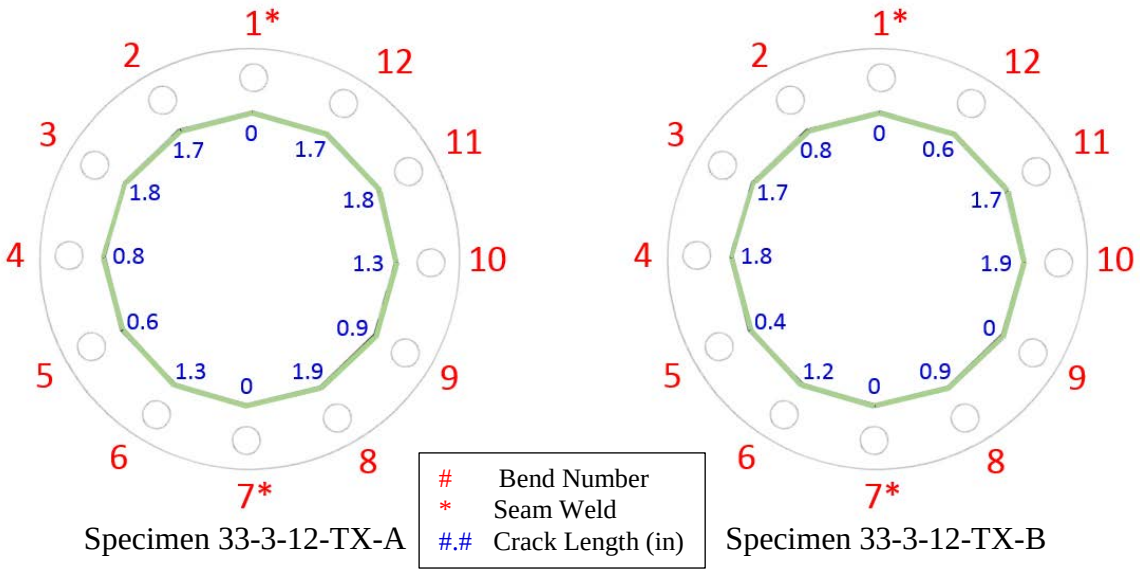

Figure 5.1: Initial Cracks in Specimens 33-3-12-TX-A and 33-3-12-TX-B

Following their initial ultrasonic measurements, Specimens 33-3-12-TX-A and 33-3-12-TX-B were installed into the setup in accordance with the procedure described in Appendix A. These specimens were then tested in the horizontal fatigue setup until their failure. This will be discussed further in the next section.

While fatigue testing was ongoing for these specimens, they were periodically examined using ultrasonic testing. Loading of the specimens was stopped during this ultrasonic testing. These ultrasonic tests were intended to provide data on the increase in

crack length as the number of loading cycles progressed. This successive ultrasonic test data for the first two specimens can be seen below in Figures 5.2 through 5.6.

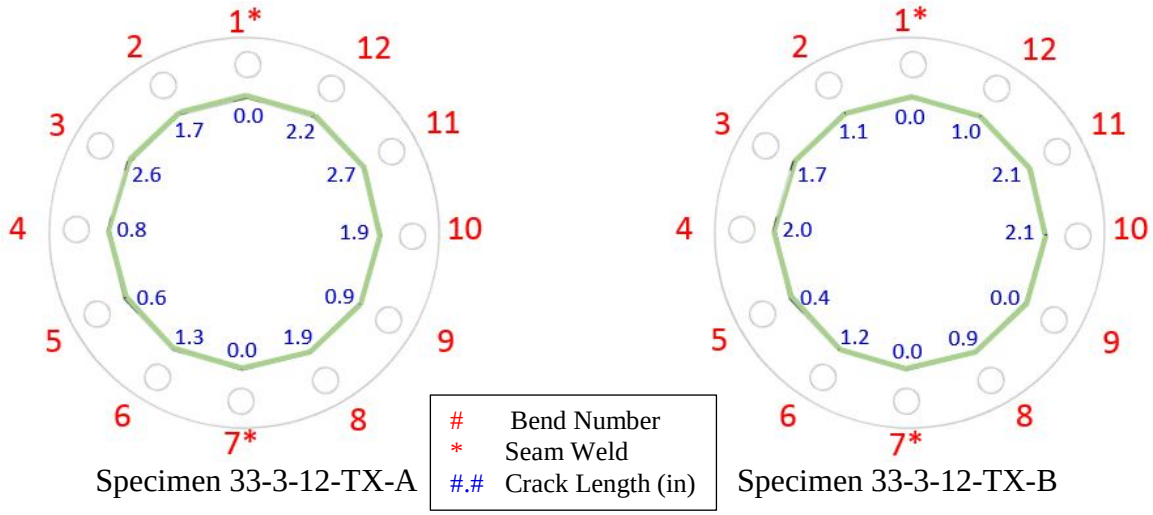

Figure 5.2: Cracks in Specimens 33-3-12-TX-A and 33-3-12-TX-B after 1.6 Million Cycles

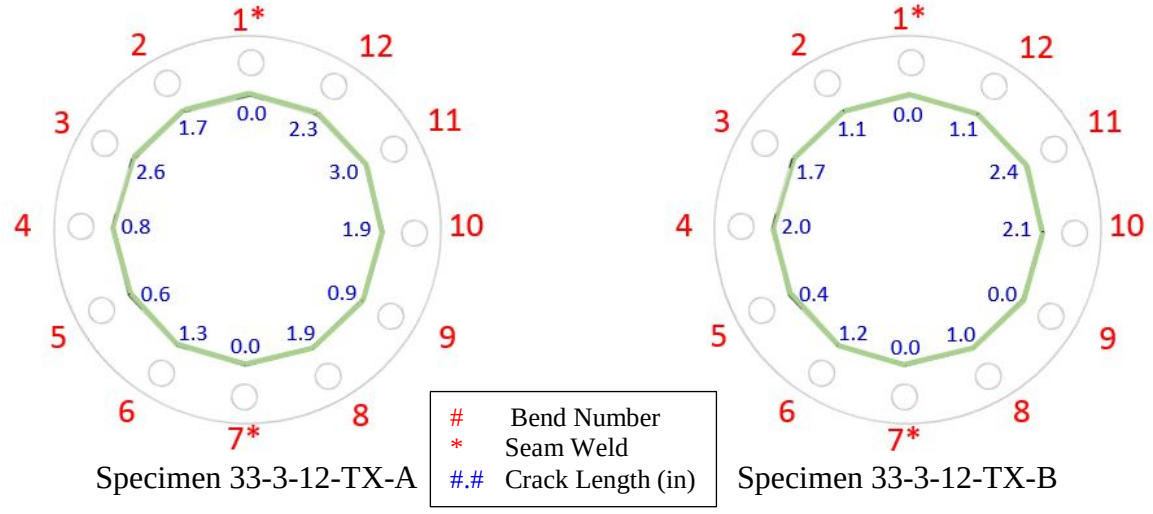

Figure 5.3: Cracks in Specimens 33-3-12-TX-A and 33-3-12-TX-B after 4.0 Million Cycles

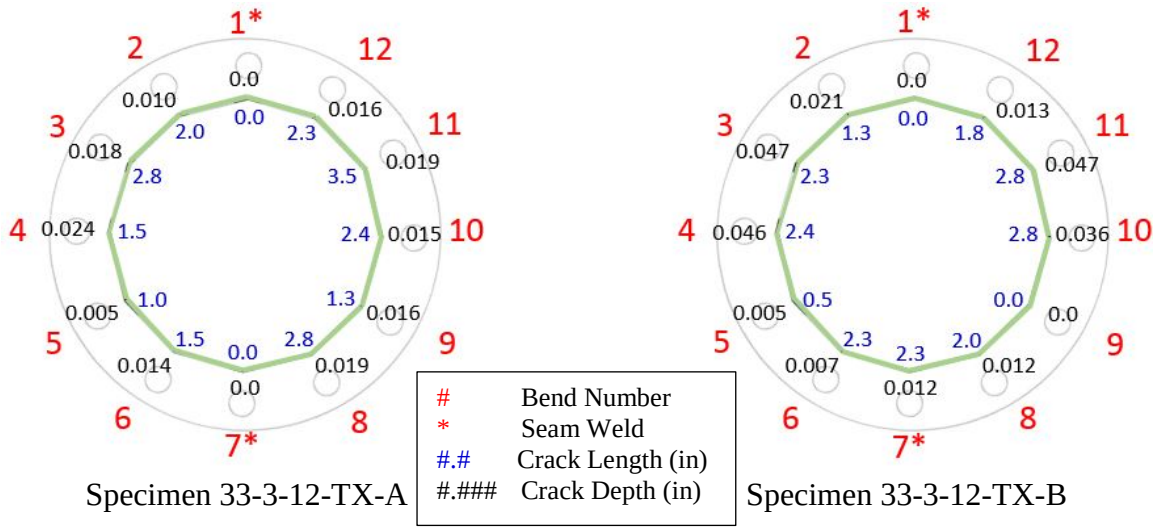

Figure 5.4: Cracks in Specimens 33-3-12-TX-A and 33-3-12-TX-B after 11.9 Million Cycles

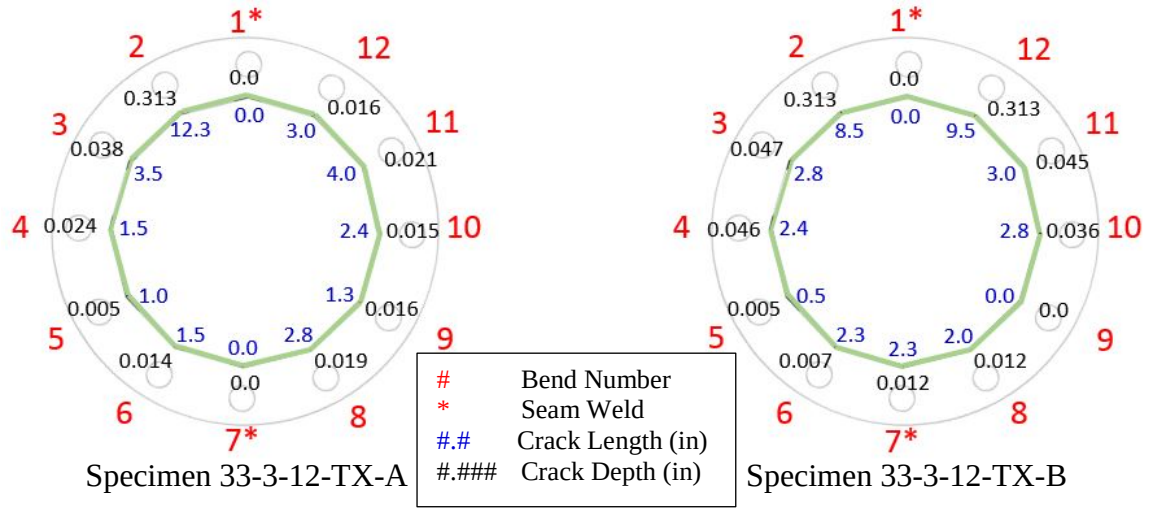

Figure 5.5: Cracks in Specimens 33-3-12-TX-A and 33-3-12-TX-B after 16.8 Million Cycles

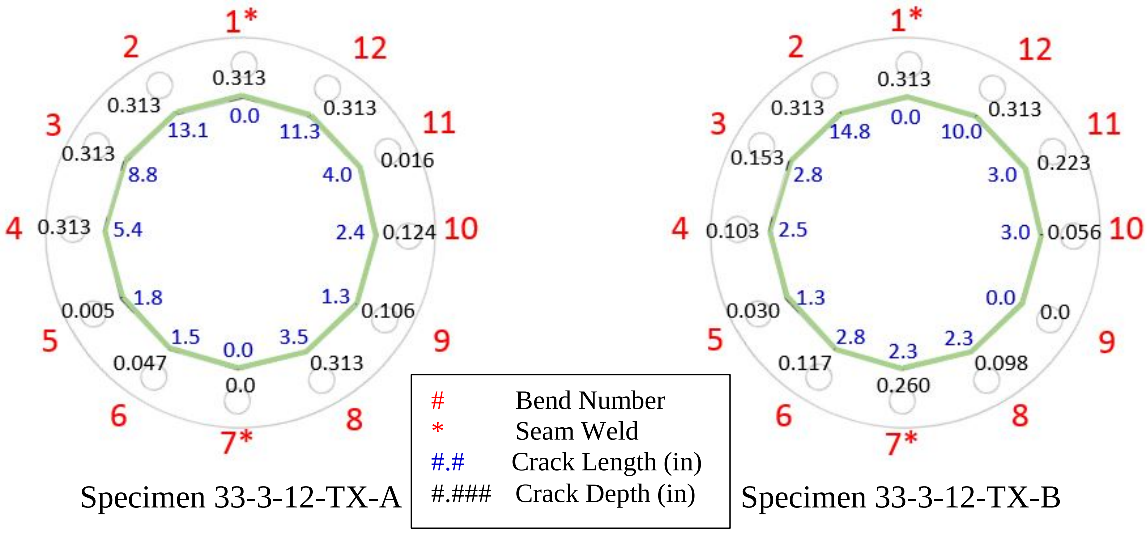

Figure 5.6: Cracks in Specimens 33-3-12-TX-A and 33-3-12-TX-B after 19.4 Million Cycles

A summary of the ultrasonic test results has been plotted in Figures 5.7 and 5.8.

The vertical axis in each plot is the total crack length for all bends of the specimen.

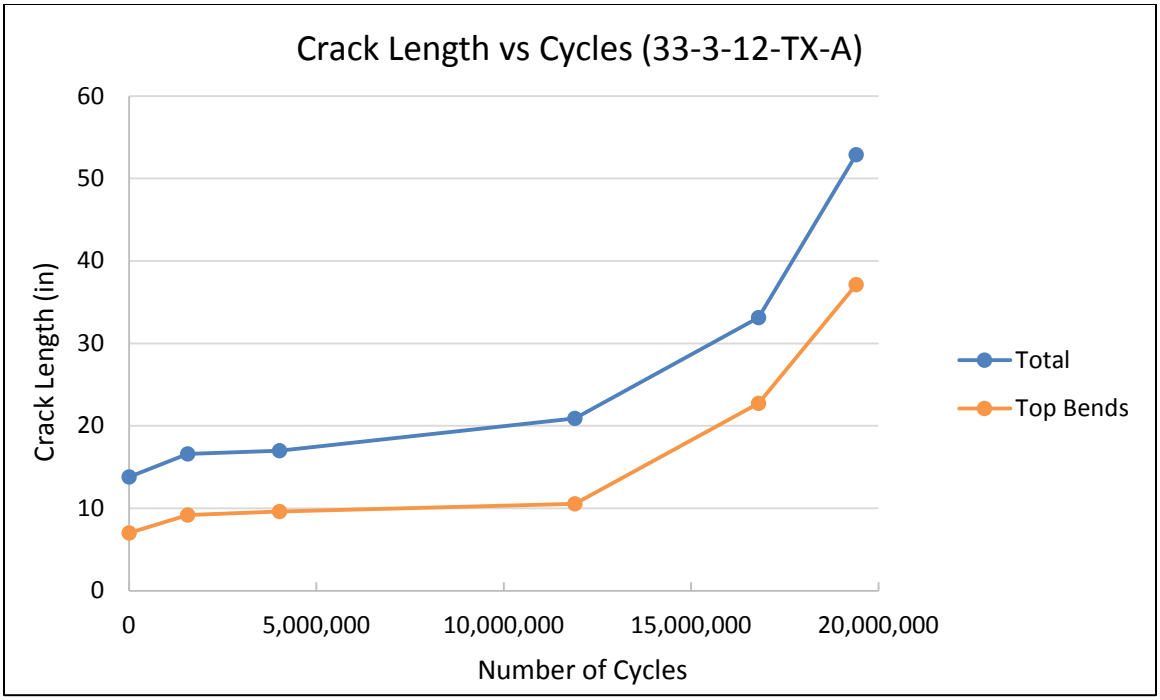

Figure 5.7: Ultrasonic Testing Data for Specimen 33-3-12-TX-A Crack Lengths

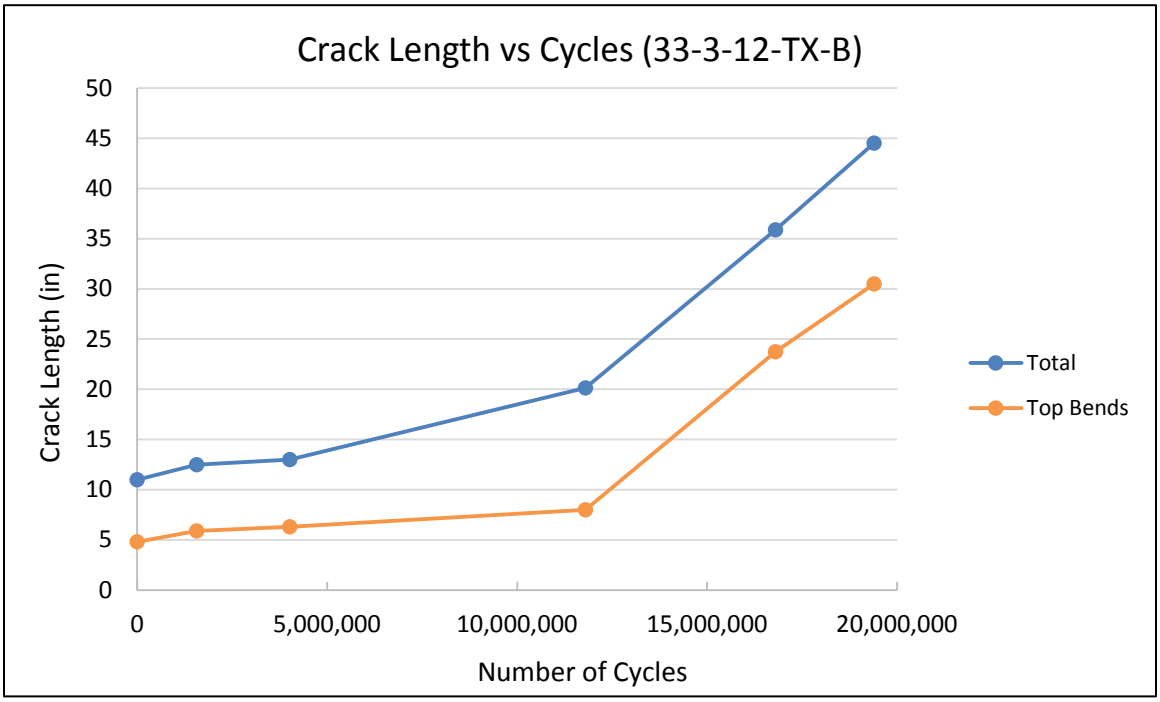

Figure 5.8: Ultrasonic Testing Data for Specimen 33-3-12-TX-B Crack Lengths

For these specimens, ultrasonic tests were performed on every bend of each specimen. After several measurements were taken on these specimens, it was noticed that the crack growth in top five bends nearly paralleled the total crack growth in the specimens. This is because the top five bends, those above the neutral axis, are the only bends in tension. Thus, for future specimens, only the top five bends were measured during phased array ultrasonic tests (PAUTs). This is with the exception of the first and last measurements, during which all bends were scanned. This method of measurement was used for all specimens tested during this phase of research.

Notice that only the crack length data is presented in Figures 5.7 and 5.8. This is a result of the frequency at which the specimens were subjected to ultrasonic tests. At this frequency, depth readings generally remained shallow for most readings before quickly rising to full depth penetration. Intermediate points were often unable to be captured. Also affecting the depth charts for the first two specimens is the lack of data for the first three ultrasonic readings, as depth data was not recorded until Reinhart & Associates began taking PAUT readings.

5.1.2 Fatigue Testing Results

Following initial ultrasonic tests, the fatigue test was begun on Specimens A and B. These specimens were tested at a stress range of 6 ksi to compare results with Phase 3 research (Pool, 2010) and a similar study being simultaneously conducted at the University of Houston. The loading cycles were run at frequencies ranging from 0.5 Hz to 2.0 Hz. Much of the early test was run at a frequency of 0.5 Hz, during which the testing frame and actuator were monitored for resonance and other signs of potential

damage. This loading frequency was gradually increased to 1.5 Hz and then 2.0 Hz. Above this range, maintaining the target stress range became problematic, so no further increases in loading frequency were attempted.

This test was run using the modified displacement control method that was described in Chapter 3. This method began with set displacement commands to obtain the target stress range. As the test progressed and the measured stress decreased, the displacement was increased until the measured stress matched the original target stress. This process was repeated throughout the test until the displacement had to be increased by 10-percent relative to its starting value. This 10-percent increase in the displacement corresponded to a 10-percent reduction in specimen stiffness, which was taken as fatigue failure of the specimen.

When determining the top bend for these specimens, researchers debated whether a pre-cracked bend should be used or whether a seam welded bend should be used. Ultimately it was decided that a seam weld would be placed in the position as the topmost bend. At the beginning of this research phase, it was believed that seam welds were more problematic for fatigue because of imperfections at the seam weld. In placing a seam weld in the top most bend position, researchers explored the effect that the seam weld had on fatigue life. The orientation of the specimens can be seen above in Figures 5.1 to 5.6.

Once the test was started, it was allowed to run largely uninterrupted until failure. Interruptions did occasionally occur, however. These interruptions included the fracture of anchor bolts, the fracture of a spherical rod eye, and the replacement of the spreader beams that connect the end reaction supports to the strong floor. The replacement of the

spreader beams was a one-time delay that was done to strengthen the testing setup. The failure of the spherical rod eye was also a one-time delay, but unlike the spreader beams, it was unplanned. It was the result of an imperfect alignment between the rod eye and the reaction plate. The rod eye was slightly twisted in one direction. This created a torque on

Figure 5.9: A Spherical Rod Eye that Fractured During Fatigue Tests

the rod eye, which gradually fractured it. This fractured rod eye can be seen in Figure 5.9. Like the rod eye, the fractures of the anchor rods were unplanned. These have occurred in previous tests and are simply the result of fatigue tests. While they cannot be prevented,

the frequency of their failures can be reduced through regular tightening of the anchor rod bolts. The anchor rod fractures were often caused by the loosening of their nuts. When these nuts became loose, the anchor rods were free to pivot about the loosened area, creating a stress concentration and ultimately resulting in a fracture. Despite the delays that these fractures caused, they were deemed merely an annoyance rather than a problem. Thus, once the delays were resolved the tests resumed as usual.

Barring the inconveniences mentioned above, the 6 ksi test was completed without significant delay. Researchers regularly searched for cracks at the toe of the welds and once noticed, regularly monitored crack growth. Cracks were not visible by the naked eye until the specimen had undergone nearly 14 million cycles. These cracks were unusual in that they did not begin at the top bend as they had in previous research phases. Instead, the cracks began at the bends on either side of the top bend. This meant that the cracks began at bend 2 and bend 12. They propagated from these bends and toward the neighboring bends, predominately toward the top bend, bend 1. The propagation of one of these cracks in Specimen B can be seen Figure 5.10.

Visible fatigue damage at this stress range had not been observed in previous testing phases. A previous 6 ksi test was run on similar specimens during Phase 3 of the research project (Pool, 2010). That test declared the specimen to be “run outs” at 7.4 million cycles. This “run out” designation meant that the stress range was too low to cause fatigue damage to the specimens, therefore the test was stopped after the specimens reached Category E requirements.

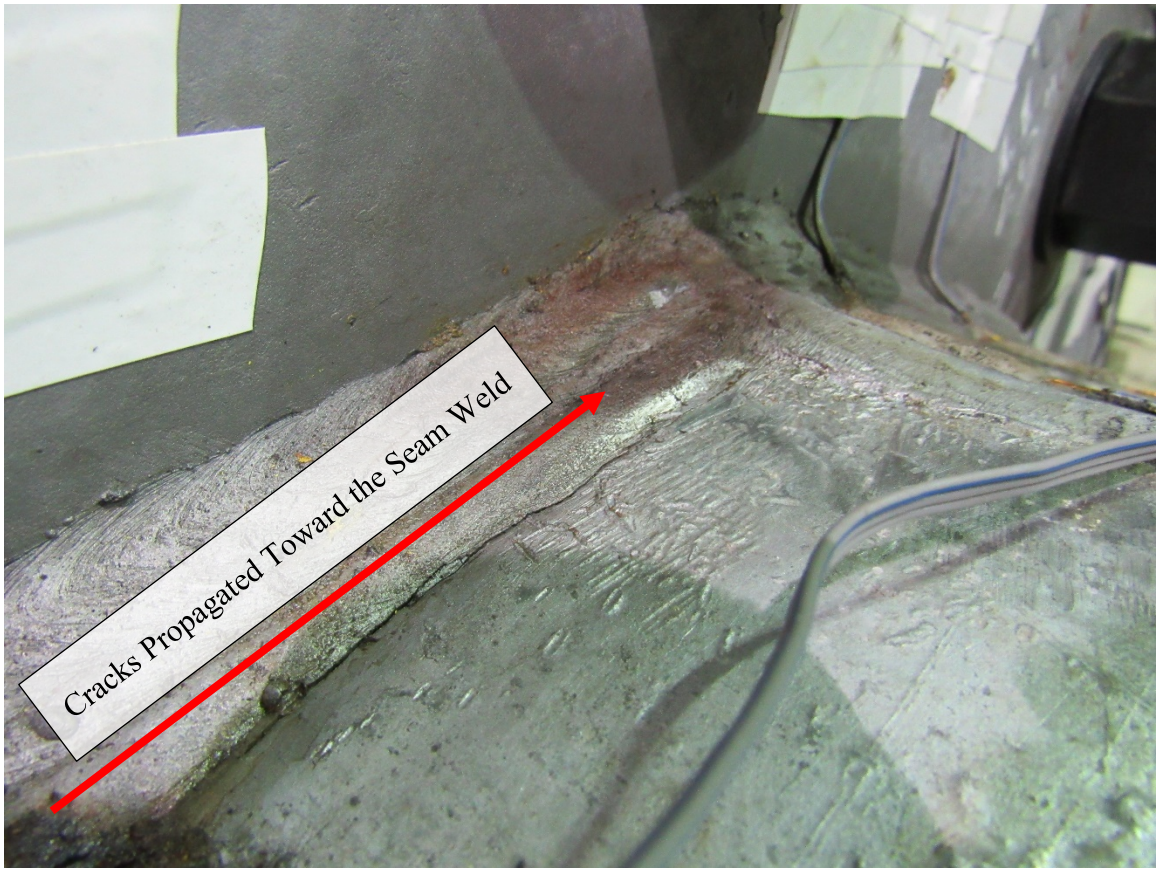

Figure 5.10: Specimen 33-3-12-TX-B Crack Propagation (Photo Taken after 19.4 Million Cycles of Loading)

In this research phase, the test on specimens 33-3-12-TX-A and 33-3-12-TX-B was run until the failure of the specimens. As previously discussed, this failure was marked by a 10-percent reduction is stiffness, as read by a change in loading force. This failure occurred after 17.7 million cycles. To evaluate the remaining fatigue life of the specimens after this stiffness reduction, researchers continued to run until nearly no stiffness remained in the specimens. No specific criteria was made for this point of nearly no remaining stiffness. Researchers decided to stop the test when stability of the specimens became a concern. At this point, cracks had extended beyond the specimen's

original neutral axis. Test AB-1 was stopped at 19.4 million cycles, after it was concluded that the specimens had nearly no stiffness remaining.

At 19.4 million cycles, cracks on Specimen B had propagated from bend 2 and bend 12 toward the top bend, bend 1. As Figure 5.5 above shows, they did not combine to form a large crack across the top of the specimen. They did, however, propagate toward the neutral axis, coalescing with cracks starting at other bends along the way. This severe cracking extended beyond the original neutral axis, thereby causing it to shift.

Like Specimen B, Specimen A underwent severe cracking during the fatigue tests. Similar, but more severe, cracking was noticed at bend 2 and bend 12. Cracks at these bends coalesced to create a large crack spanning across the top bend, between bends 2 and 12. This crack joined those starting from other bends to create one large crack that extended beyond the specimen's neutral axis. This crack can be seen in Figure 5.11 and Figure 5.12.

Figure 5.11: Cracking in Specimen 33-3-12-TX-A's Top (Seam Welded) Bend after 19.4 Million Cycles of Loading

Figure 5.12: Close up of Specimen 33-3-12-TX-A's Top (Seam Welded) Bend after 19.4 Million Cycles of Loading

After considering the stress range and number of cycles at which these specimens were tested, it was determined that these specimens met AASHTO fatigue category E requirements, as shown in Figure 5.13. Typically, after a specimen failure, one or both specimens would be rotated 180-degrees to test the undamaged side of the specimen. However, because cracking extended beyond the neutral axis of both specimens, neither specimen had an undamaged side. As such, neither specimen was flipped and retested.

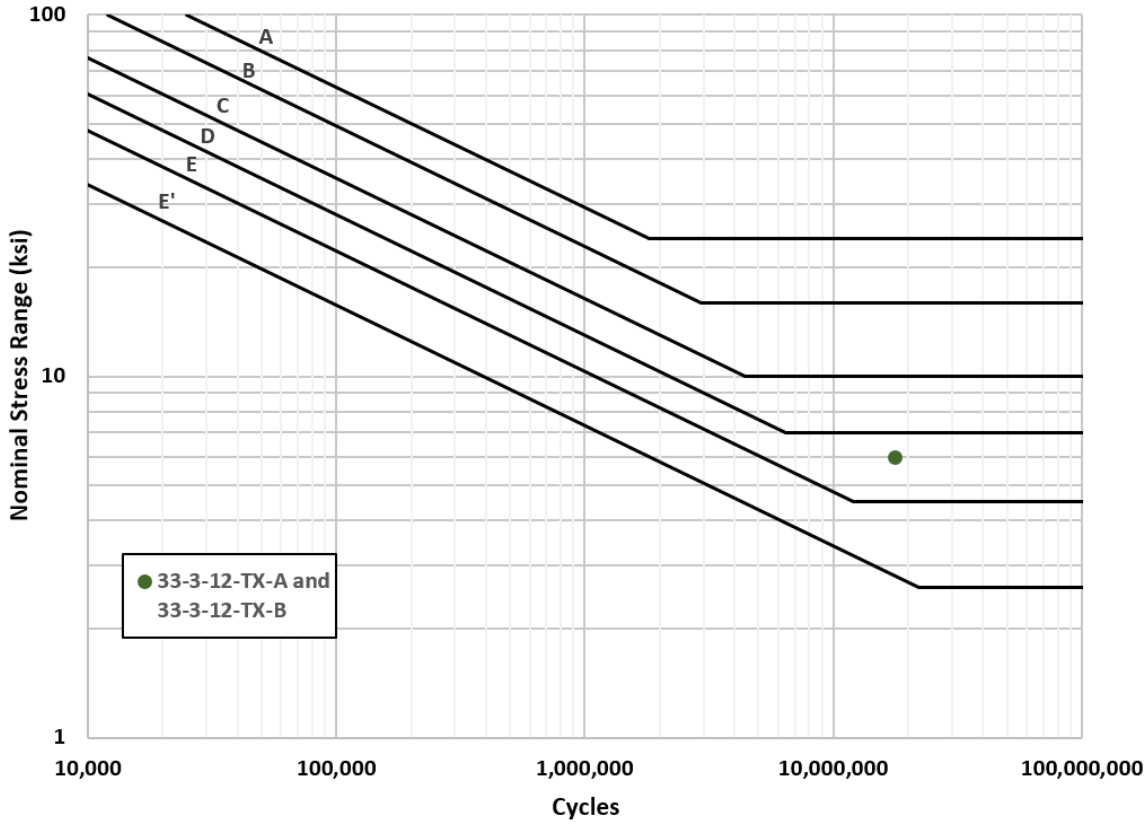

Figure 5.13: Fatigue Life of Specimens 33-3-12-TX-A and 33-3-12-TX-B

5.2 SPECIMENS 33-3-12-TX-E AND 33-3-12-TX-F – 3 KSI EXPERIMENT

The second experiment of this research phase was conducted on specimens 33-3-12-TX-E and 33-3-12-TX-F. The specimens are being at a stress range of 3 ksi and with a mean stress of 6 ksi.

Only one test has been run on each specimen thus far during this experiment. These tests will henceforth be known as tests E-1 and F-1. At this time, tests E-1 and F-1 are currently ongoing. Final results will be reported in other publications.

5.2.1 Ultrasonic Test Results

As with the all other experiments, tests E-1 & F-1 began with the PAUT of the specimens. These phased array tests marked the research team's first work with Reinhart & Associates, a nondestructive testing company based in Austin, Texas.

The PAUT results were used to determine the top bend for each specimen. Unlike the previous tests that have been discussed, the same top bend was not used for each specimen. For specimen E, the top bend was designated as bend 11. The top bend for specimen F was selected to be bend 5. These selections were made based upon the initial PAUT readings which can be seen in Figure 5.16.

Notice that while the top bends are not the same, they are 180-degrees removed from one another. This leaves the seam welds in the same position for each specimen, meaning that their effect on each specimen's fatigue resistance are the same. Despite being arbitrarily labeled differently, the top bends of these specimens are subject to similar external conditions.

The same cannot be said about the internal conditions of the specimens. As Figure 5.14 shows, specimen E was notably more cracked than specimen F. Specimen E had cracks on nearly 25-percent of its perimeter at the beginning of the experiment. Specimen F, on the other hand only had about 8-percent of its perimeter cracked.

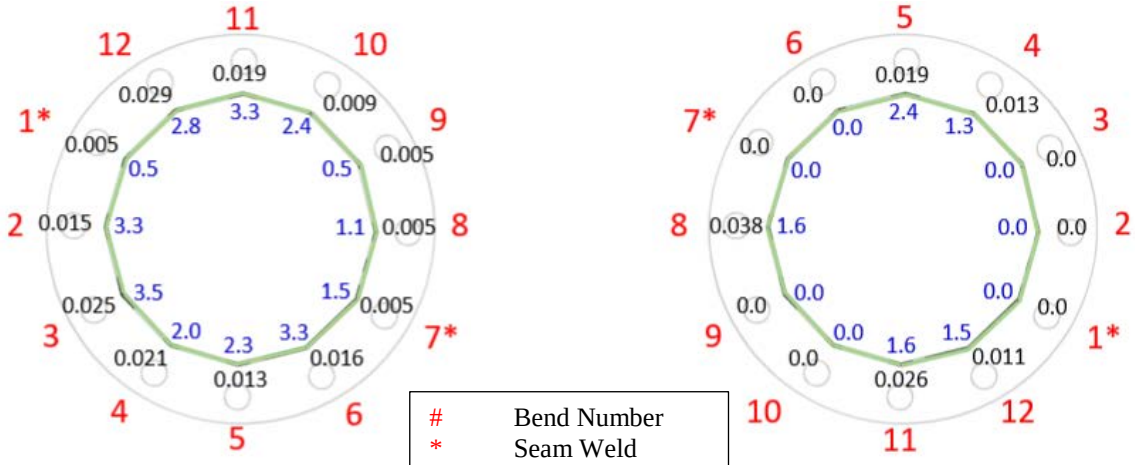

Specimen 33-3-12-TX-E Specimen 33-3-12-TX-F

Figure 5.14: Initial Cracks in Specimens 33-3-12-TX-E and 33-3-12-TX-F

The severe cracking in Specimen E led researchers to believe that it would experience rapid crack growth and quickly fatigue. This has not happened, however. Specimen E has only experienced gradual crack growth in its top bend, as seen in the successive phased array measurements shown in Figure 5.15 through Figure 5.20.

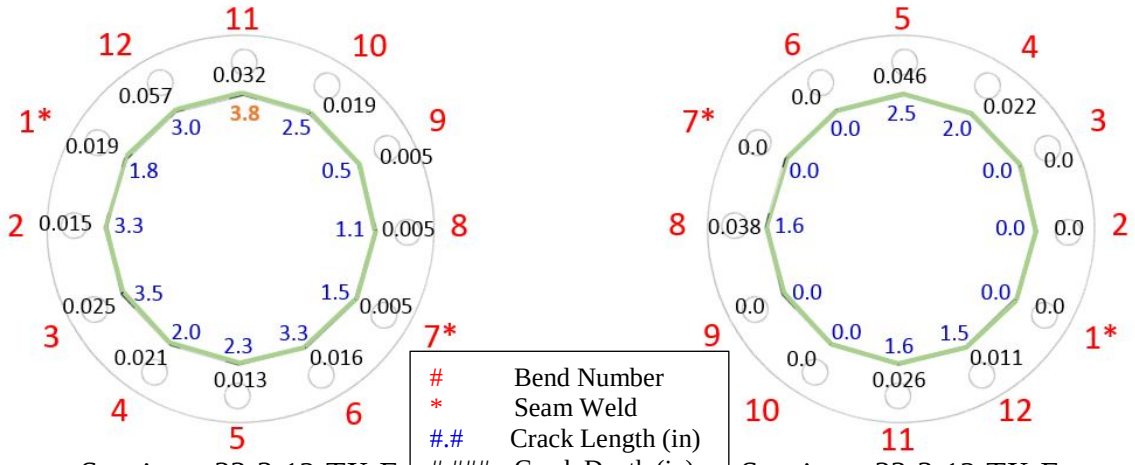

Specimen 33-3-12-TX-E Specimen 33-3-12-TX-F

Figure 5.15: Cracks in Specimens 33-3-12-TX-E and 33-3-12-TX-F after 4.4 Million Cycles

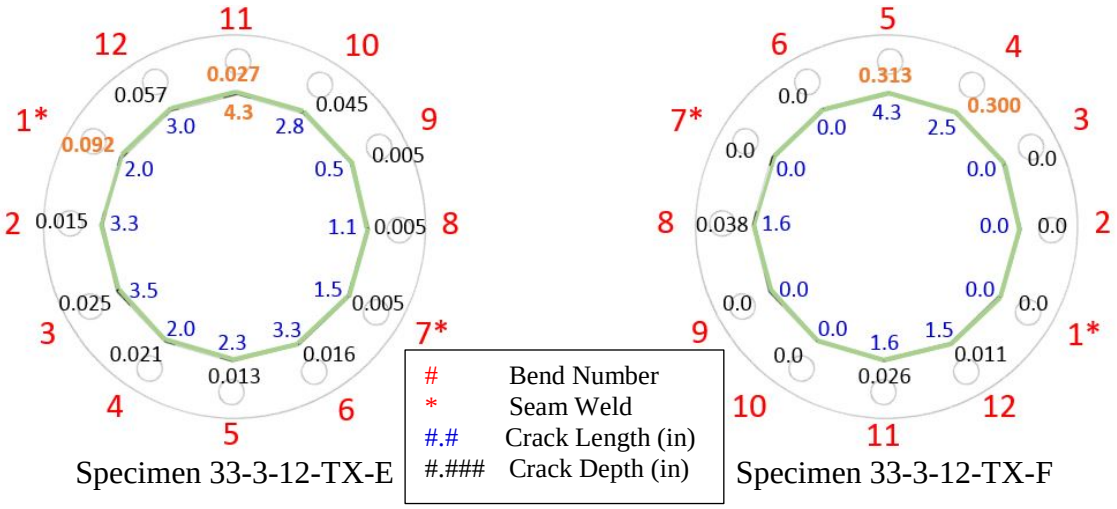

Figure 5.16: Cracks in Specimens 33-3-12-TX-E and 33-3-12-TX-F after 7.8 Million Cycles

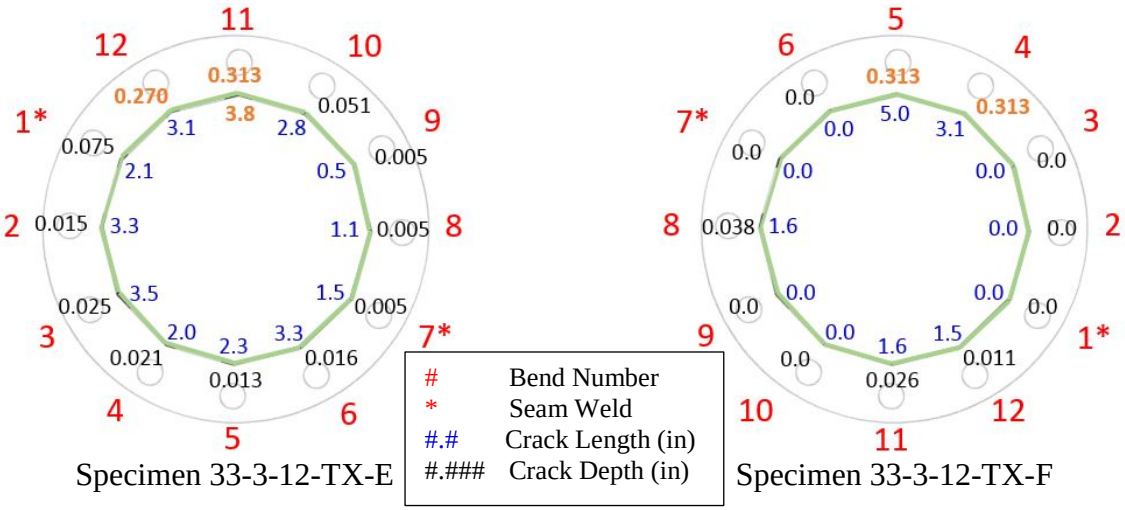

Figure 5.17: Cracks in Specimens 33-3-12-TX-E and 33-3-12-TX-F after 16.8 Million Cycles

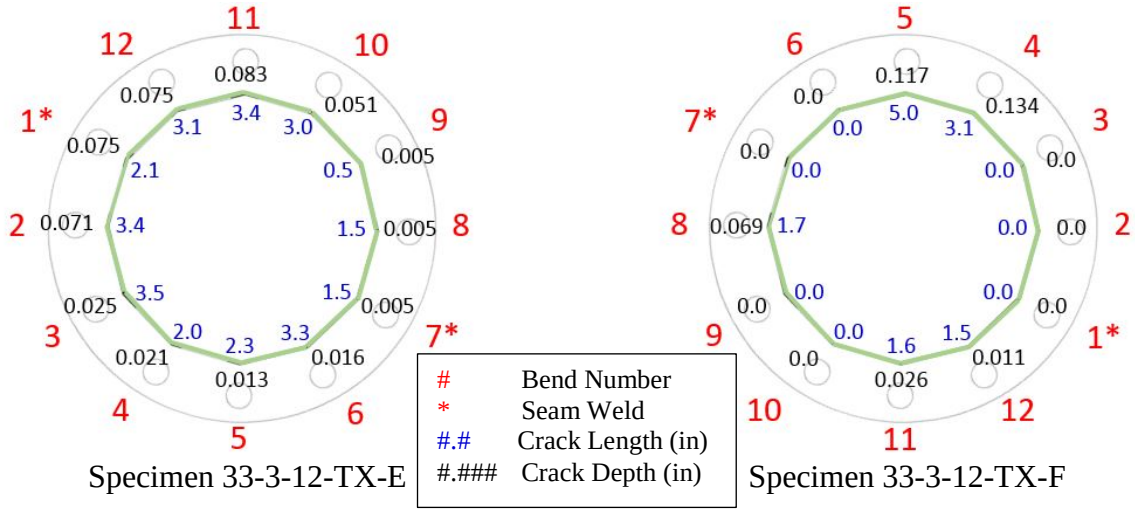

Figure 5.18: Cracks in Specimens 33-3-12-TX-E and 33-3-12-TX-F after 36.7 Million Cycles

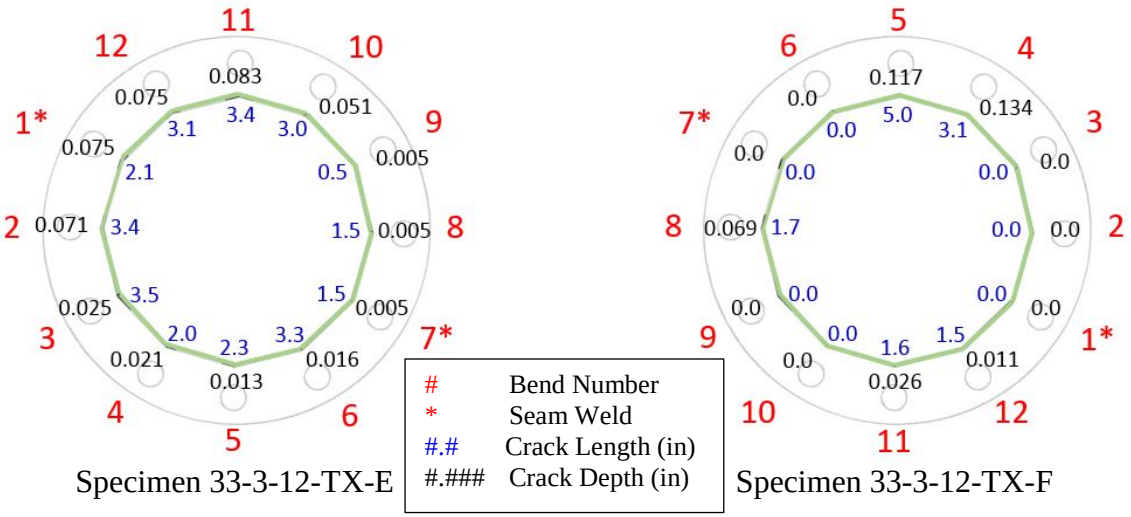

Figure 5.19: Cracks in Specimens 33-3-12-TX-E and 33-3-12-TX-F after 54.9 Million Cycles

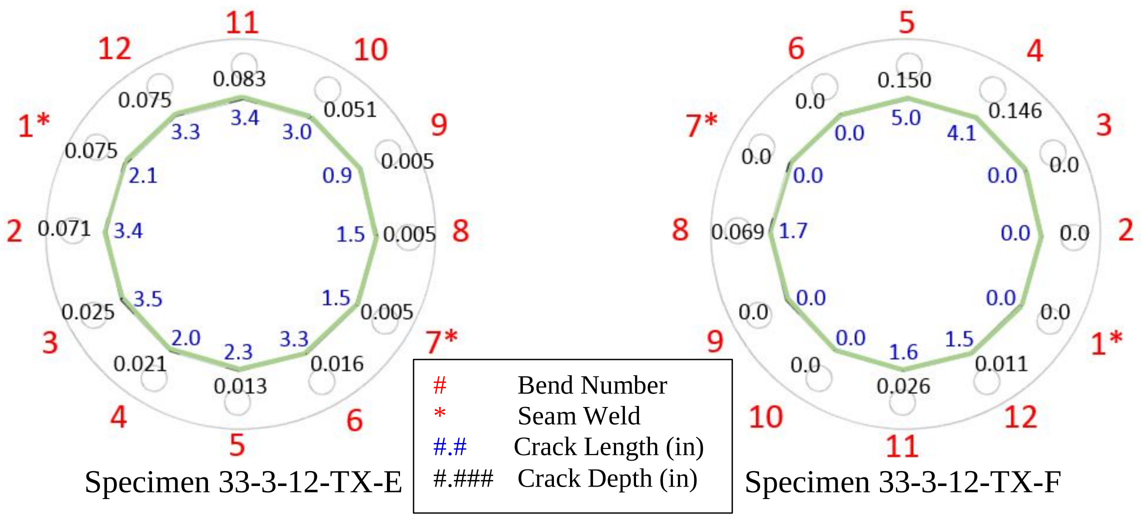

Figure 5.20: Cracks in Specimens 33-3-12-TX-E and 33-3-12-TX-F after 84.0 Million Cycles

Note that a few anomalies are bolded in orange text. After examining trends in the PAUT data for this specimen across multiple tests, some measurements were determined to be anomalies. Through discussions with Reinhart and Associates technicians, it was determined that an error was likely made for these measurements. When this data is plotted, such as in Figures 5.21 and 5.22, it is modified such that the anomalies are removed and replaced with appropriate data from the PAUT preceding the anomalies.

Figures 5.15 through 5.20 show that there has not been much grown of the cracks in Specimens E of F during the course of Tests E-1 & F-1. Still, the top bends have experienced some gradual crack growth over the course of these tests. Figures 5.21 and 5.22 show a gradual, but steady crack growth in the top bends of Specimen E. A similar growth trend can be seen in the early phases for Specimen F, but recently growth has escalated. Previous findings in this research phase have shown that specimens typically fail after nearly 50 inches of their perimeters have cracked. The vertical axis in each plot is the total crack length for all bends of the specimen.

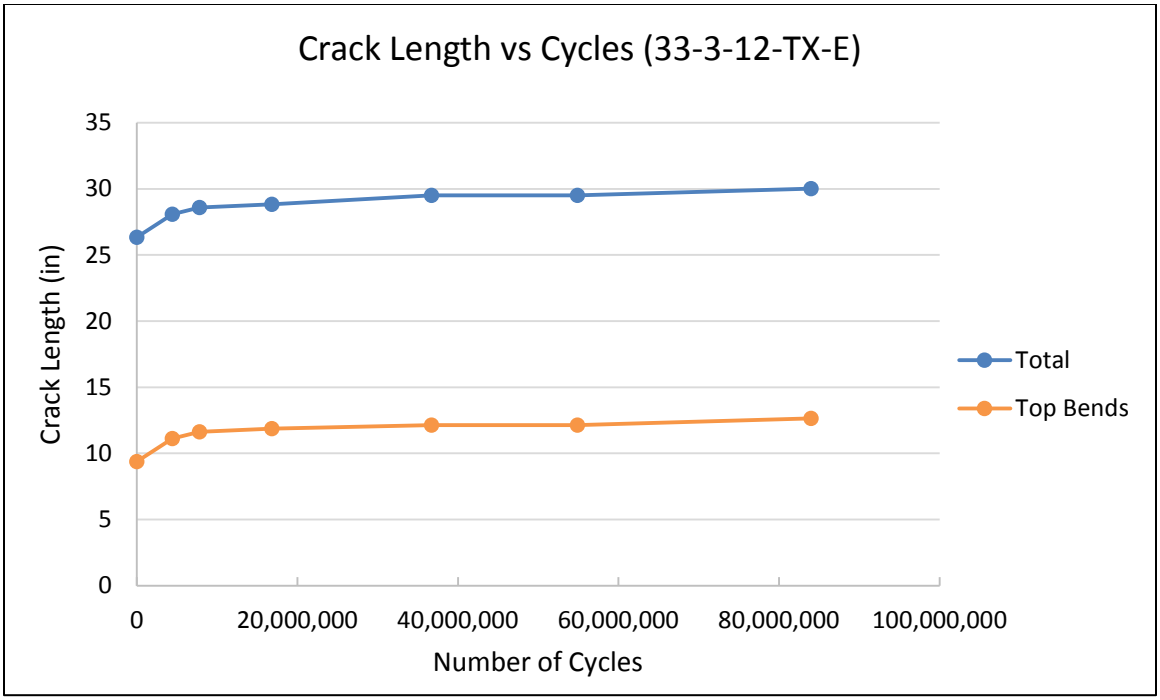

Figure 5.21: Ultrasonic Testing Data for Specimen 33-3-12-TX-E Crack Lengths

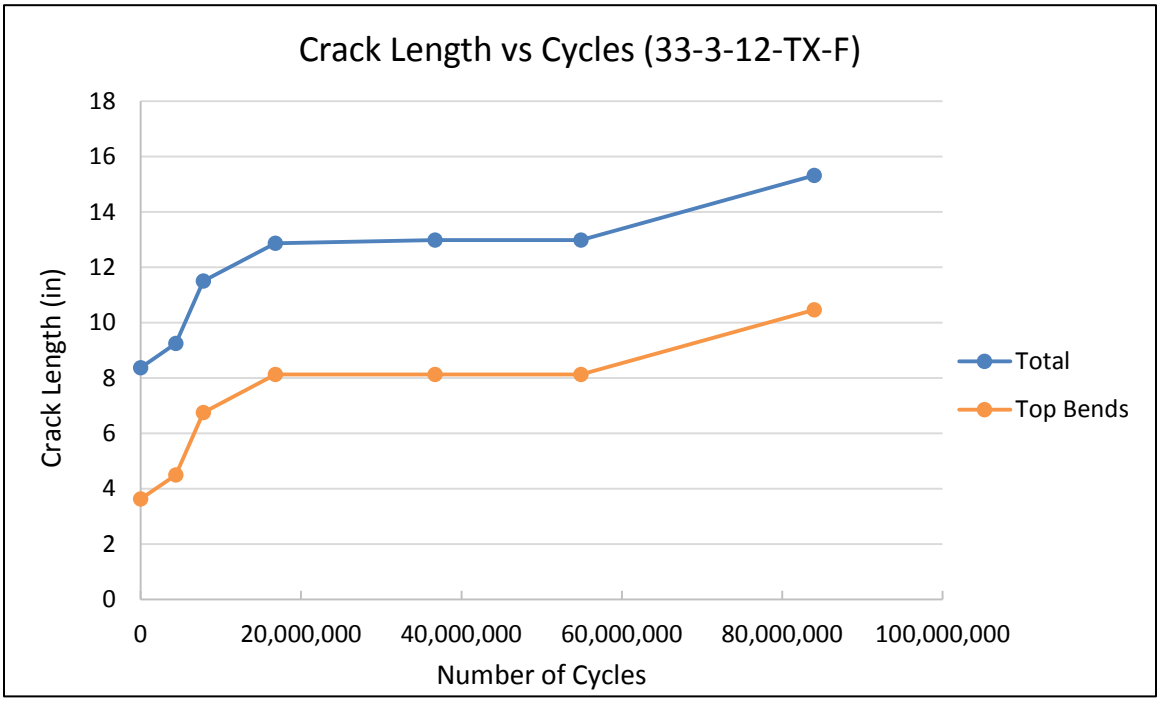

Figure 5.22: Ultrasonic Testing Data for Specimen 33-3-12-TX-F Crack Lengths

5.2.2 Fatigue Testing Results

The fatigue experiment on Specimens 33-3-12-TX-E and 33-3-12-TX-F began mid December 2015. This experiment has been run at a stress range of 3 ksi and with a mean stress of 6 ksi. Initially, the experiment was run with a loading frequency of 2.7 Hz. After monitoring the experiment for approximately a week and a half, researchers opted to increase the loading frequency to 3.5 Hz. This loading frequency has remained since that time.

At the time of the writing of this report, mid November 2016, the first of the fatigue tests on specimens E and F is still underway. After nearly a year of fatigue testing, with minimal interruptions, these specimens have neither failed nor exhibited any signs of significant stiffness loss. Presently, the specimens have exhibited very little crack growth.

Early in the testing of these specimens, researchers were led to believe that Specimen F was beginning to fail. PAUT readings taken after 7.8 million cycles, shown in Figure 5.16, indicated that a crack had penetrated through the depth of the top bend. With this in mind, researchers closely monitored the experiment, specifically Specimen F. Another round of PAUT tests was performed nearly a month after the PAUT readings that showed full depth penetration in Specimen F. These PAUT readings, completed after 16.8 million cycles, indicated full depth crack penetration through the top bend of Specimen F, just as the earlier PAUT readings did. They also indicated full depth penetration through the top of Specimen E. At this point, researchers expected cracks to grow enough to become viewable by visual inspection within weeks, but they did not.

Researchers visually inspected the specimens for two months without seeing any indication of crack growth.

When no cracks had been seen after two additional months of testing, researchers had the specimens ultrasonically tested to discover what had been happening in the specimens. These tests were conducted at 36.7 million cycles. The ultrasonic tests results showed that the cracks had stayed the same lengths, but decreased in depths. This perplexed researchers, as the crack could not decrease in size without being repaired. Researchers considered that an error could have been made in the PAUTs, but were uncertain as to which PAUT was incorrect.

Finally, another phased array ultrasonic test was run on the specimen in after 54.9 million cycles. This PAUT yielded readings nearly identical to the PAUT completed four months before. This led researchers to believe that an error had been made by the phased array technician. After discussing this possibility with Reinhart and Associates technicians, it was determined that a mistake was likely. On the phased array ultrasonic instrumentation being used, it is difficult to determine between the difference between a crack and the interior of the specimen. It takes a trained eye to determine the difference and even then it is possible to make a mistake. These mistakes showed researchers that, despite the science behind it, phased array ultrasonic testing is as much of an art as it is a science.

At the time of this report, the specimens have been cycled for nearly 94.3 million cycles without failing. Final results will be reported in other publications.

5.3 SPECIMENS 33-3-12-TX-C AND 33-3-12-TX-D – 4 KSI & 2 KSI EXPERIMENTS

The third experiment of this research program was run on specimens 33-3-12-TX-C and 33-3-12-TX-D. These specimens were fabricated with a full penetration welded connection and no external collar.

These specimens were tested at two separate stress ranges, 4 ksi and 2 ksi. For all tests on these specimens, a mean stress of 6 ksi was used.

Unlike the specimens of test AB-1, the specimens of these tests did not fail at the same time. As such, this experiment was broken down into tests according to the failures of each specimen rather than a pair of specimens. While the nature of the horizontal test setup mandates that two specimens be tested at one time to satisfy simple beam theory assumption, the specimens have little interaction with each other. As such, each specimen can be split into a separate tests under specific conditions. These conditions included the tested specimen, testing stress range, orientation of bends, and cracking of each bend.

Table 5.1 presents an overview of these tests, while the sections following will go into greater detail.

Table 5.1: Summary of Tests Performed on Specimens 33-3-12-TX-C and 33-3-12-TX-D

Test	Tested Specimen	Top Bend	Stress Range (ksi)	Cycles to Failure ($x10^6$)	Total Cycles ($x10^6$)	Comments
D-1	D	4	4	2.6	3.8	Completion marked by failure of Specimen D
C-1	C	4	4	4.1	5.5	Completion marked by failure of Specimen C
D-2	D (Flipped)	10	4	3.5	6.5	Completion marked by failure of flipped Specimen D
C-2	C (Flipped)	10	4	N/A	4.8	Failure of companion specimen occurred before the test could be completed
D-3	D (Rotated)	12	2	N/A	55.5	Test is ongoing; Approximate cycle count as of December 1, 2016
C-3	C (Flipped)	10	2	N/A	55.5	Test is ongoing; In its current configuration, the specimen was tested to 4.8 million cycles at 4 ksi during test C2

5.3.1 Test D-1

Test D-1 was the first test completed during the 4 ksi experiment. It was run concurrently with tests on Specimen C. The results of this test apply to Specimen 33-3-12-TX-D in the configuration shown in Figure 5.23 This test was run at a stress range of 4 ksi.

5.3.1.1 Test D-1 – Ultrasonic Results

Following the findings of test AB-1, researchers decided to make the seam welded bends a nonfactor. They placed these bends along the neutral axes of the specimen to minimize their effects. This left bends 4 and 10 as the available options for the top bends, as they are both 90 degrees removed from the seam welded bends.

Based on the initial PAUT results, shown in Figure 5.23, researchers decided to designate bend 4 as the top bend for this test. This bend was chosen because it was the most severely cracked before testing began. This bends was not the only ones that was severely cracked, however. Before testing commenced, Specimen D had nearly 16-percent of its perimeter cracked.

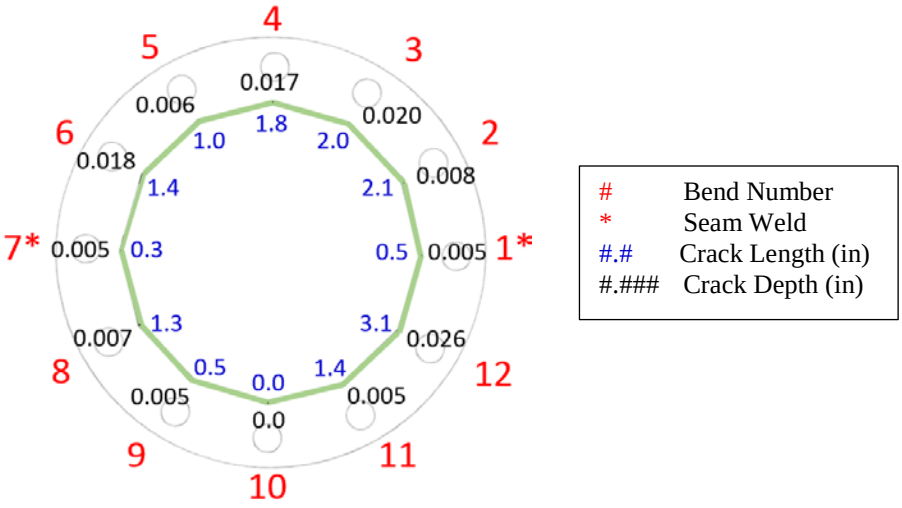

Specimen 33-3-12-TX-D

Figure 5.23: Initial Cracks in specimen 33-3-12-TX-D at the Beginning of Test D-1

Additional PAUTs were performed after 1.7 million cycles, shortly after researchers first noticed fatigue cracks had become visible. The results of these tests can be seen in Figure 5.24 Notice that cracking had penetrated through the wall of the specimen in bends 2 through 4.

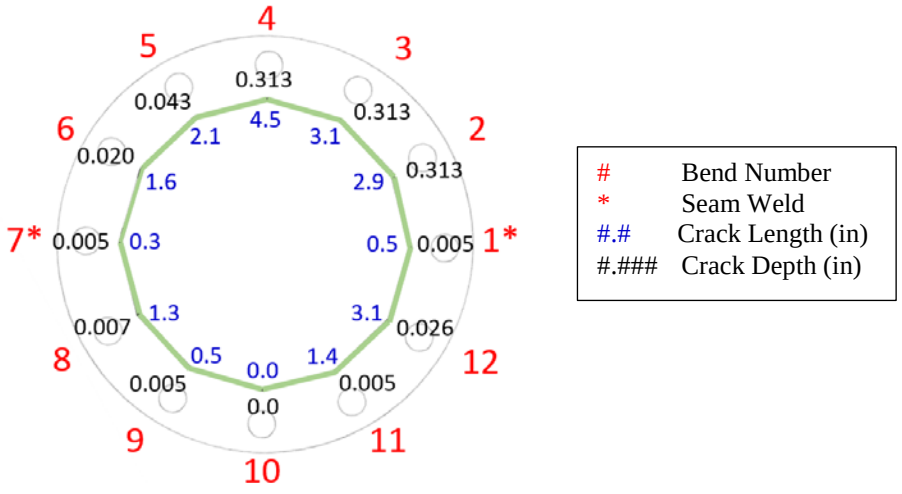

Specimen 33-3-12-TX-D

Figure 5.24: Cracks in specimen 33-3-12-TX-D after 1.7 Million Cycles in Test D-1

The final PAUTs of test D-1 can be seen in Figure 5.25 These PAUTs were completed after Specimen D failed and the test was completed. At this point test D-1 had been run for 3.8 million cycles.

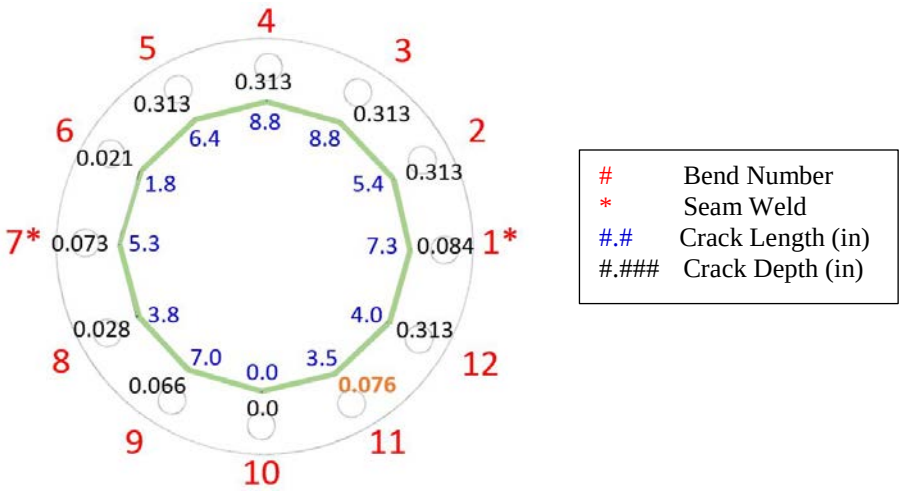

Specimen 33-3-12-TX-D

Figure 5.25: Cracks in specimen 33-3-12-TX-D after 3.8 Million Cycles, the Conclusion of Test D-1

Note that in Figure 5.25, one of the depth measurements has been bolded in orange text. After examining trends in the PAUT data for this specimen across multiple tests, this measurement was determined to be an anomaly. Through discussions with Reinhart and Associates technicians, it was determined that an error was likely made for these measurements. This will be discussed in greater detail in Section 5.3.6.

5.3.1.2 Test D-1 – Fatigue Test Results

After PAUT results were completed, Specimen D and its companion specimen, Specimen C, were installed in the setup and tests were begun. Test D-1 was begun. These specimens were tested at a stress range of 4 ksi. Test D-1 was run at frequencies ranging

from 2.5 to 2.7 Hz, with most of the test having been run at 2.7 Hz. Above this range, maintaining the target stress range became problematic.

This test was run using displacement control, as defined in Chapter 3. This method of test control involved selecting a displacement corresponding to the desired stresses. These displacements were set and retained to maintain the same nominal stress range throughout the test. The test was run until the monitoring strain gauge, gauge 8 in Figure 4.15, measured 0 ksi. Before this stress reduction occurred, the specimen was determined to have failed according to the criteria defined in section 3.1.3.

After the displacement commands and top bend was determined, the test was begun. Unlike test AB-1, researchers did not encounter any delays during this test. They built upon experiences learnt during the tests AB-1, E-1, and F-1 to avoid delays. The steps taken to do this included alignment inspection of baseplates, rod eyes, reaction supports, and specimens and the regular tightening of anchor rods. Without delays due to setup component fracture, test D-1 was completed in a relatively short amount of time

Test D-1 was completed after approximately one month of fatigue tests. Specimen D was deemed to have failed after it had developed sufficient cracking to reduce its stiffness by 10 percent. This reduction in stiffness occurred at 2.6 million cycles. The test was allowed to run to 3.8 million cycles before researchers stopped the test. At this point, the monitoring strain gauge measured 0 ksi. A picture of Specimen D after failure can be seen in Figure 5.26.

Figure 5.26: Specimen 33-3-12-TX-D after the Conclusion of Test D-1 (Photo Taken after 3.8 Million Cycles)

Following the conclusion of test D-1, specimen D was removed from the testing setup. It was then flipped 180-degrees and re-attached to the testing frame. Testing was then resumed, as test C-1 continued, and test D-2 was begun.5.3.2 Test C-1

5.3.2 Test C-1

Test C-1 was the second test completed during the 3 ksi experiment. It was run concurrently with tests on Specimen D. The results of test apply to Specimen C in the configuration shown in Figure 5.27. This test was run at a stress range of 4 ksi.

5.3.2.1 Test C-1 – Ultrasonic Results

To be consistent with test D-1, researchers decided to place the seam welds along the neutral axis of Specimen C to minimize their effects. This left bends 4 and 10 as the available options for the top bends, as they are both 90 degrees removed from the seam welded bends.

Based on the initial PAUT results, shown in Figure 5.27, researchers decided to designate bend 4 as the top bend for this test. This bend was chosen because it was the most severely cracked before testing began. This bends was not the only ones that was severely cracked, however. Before testing commenced, Specimen C had nearly 26-percent of its perimeter cracked.

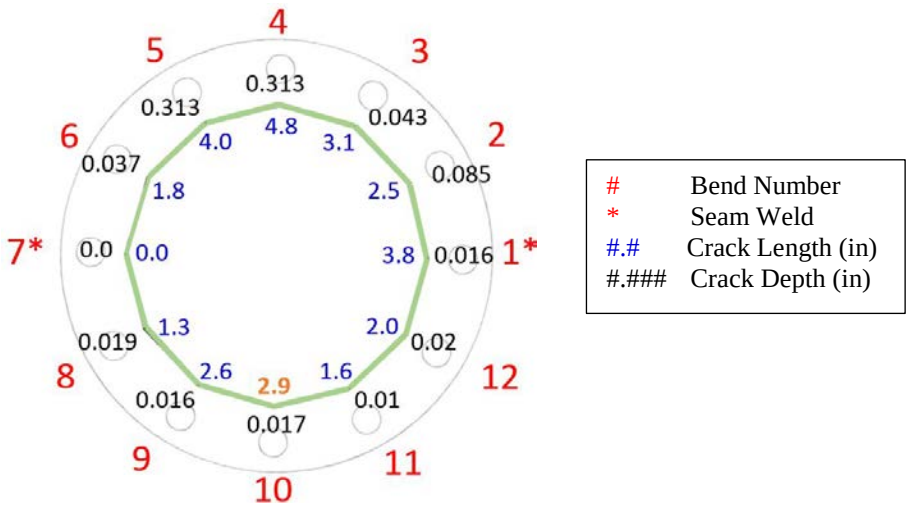

Specimen 33-3-12-TX-C

Figure 5.27 Initial Cracks in specimen 33-3-12-TX-C at the Beginning of Test C-1

Additional PAUTs were performed after 1.7 million cycles, when researchers first noticed fatigue cracks had become visible. The results of these tests can be seen in Figure 5.28.

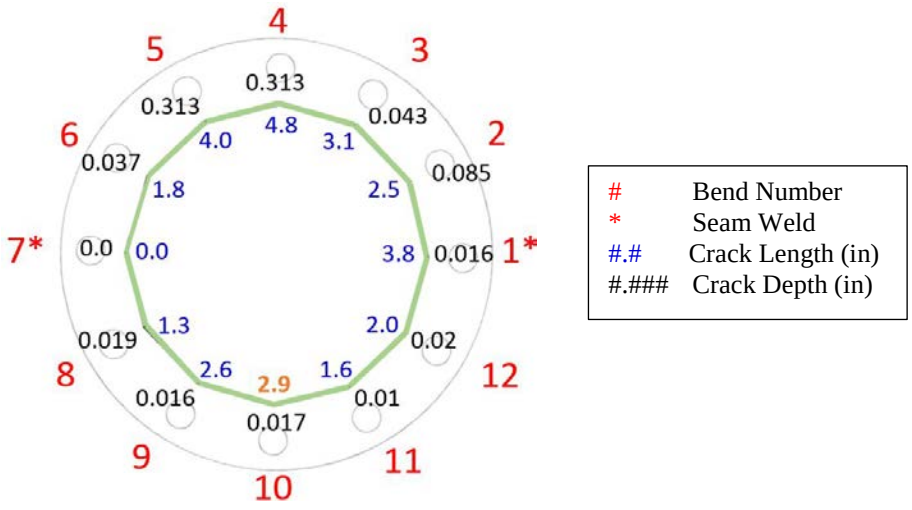

Specimen 33-3-12-TX-C

Figure 5.28 Cracks in specimen 33-3-12-TX-C after 1.7 Million Cycles in Test C-1

More PAUTs were performed when the test on the companion specimen was completed. The results of these PAUTs can be seen in Figure 5.29 At this point test C-1 had been run for 3.8 million cycles.

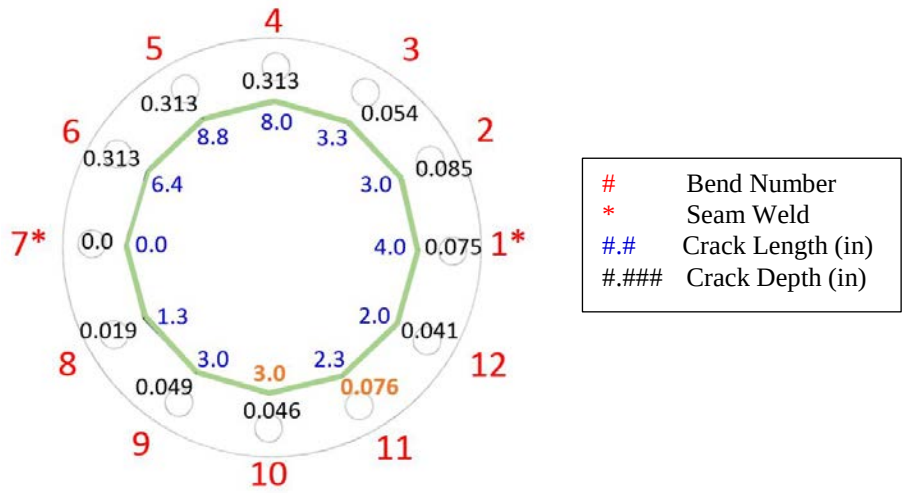

Specimen 33-3-12-TX-C

Figure 5.29 Cracks in specimen 33-3-12-TX-C after 3.8 Million Cycles in Test C-1

The final PAUTs of test C-1 can be seen in Figure 5.30. These PAUTs were run after the test specimen had failed and the test was completed. At this point test C-1 had been run for 5.5 million cycles.

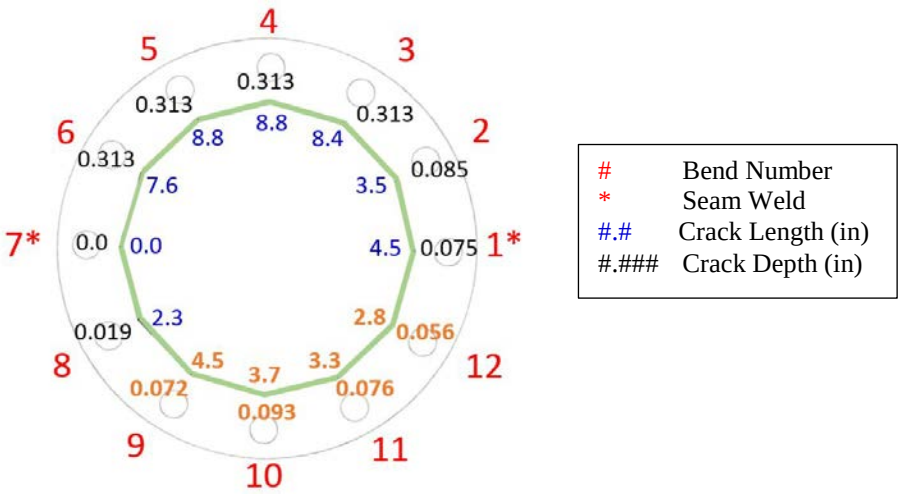

Figure 5.30: Cracks in specimen 33-3-12-TX-C after 5.5 Million Cycles, the Conclusion of Test C-1

Note that in Figures 5.27 through 5.30, many of the length and depth measurements have been bolded in orange text. After examining trends in the PAUT data for this specimen across multiple tests, these measurements were determined to be anomalies. Through discussions with Reinhart and Associates technicians, it was determined that an error was likely made for these measurements. This will be discussed in greater detail in Section 5.3.6.

5.3.2.2 Test C-1 – Fatigue Test Results

Following the completion of PAUTs, Specimen C and its companion specimen, were installed in the setup. Test C-1 was begun. These specimens were tested at a stress

range of 4 ksi. As with test D-1, Test C-1 was run at frequencies ranging from 2.5 to 2.7 Hz, with most of the test having been run at 2.7 Hz. Above this range, maintaining the target stress range became problematic.

Test C-1 was also run using displacement control. For more information on this method of test control, refer to refer to section 5.3.1.2.

The test was run until the monitoring strain gauge, gauge 8 in Figure 4.15, measured 0 ksi. Before this stress reduction occurred, the specimen was determined to have failed according to the criteria defined in section 3.1.3.

After the displacement commands and top bend was determined, the test was begun. The only delay that occurred during this test was the stopping of the test to examine its companion specimen. This stoppage occurred after 3.8 million cycles had been applied. During the stoppage, phased array testing was performed on both Specimen C and its companion specimen. Once phased array ultrasonic testing had been completed, the companion specimen was flipped and test C-1 was resumed.

Test C-1 was completed shortly after. Specimen C was deemed to have failed after it had developed sufficient cracking to reduce its stiffness by 10 percent. This reduction in stiffness occurred at 4.1 million cycles. The test was allowed to run to 5.5 million cycles before researchers declared it to be complete. At this point, the monitoring strain gauge measured 0 ksi. A picture of Specimen C after failure can be seen in Figure 5.31.

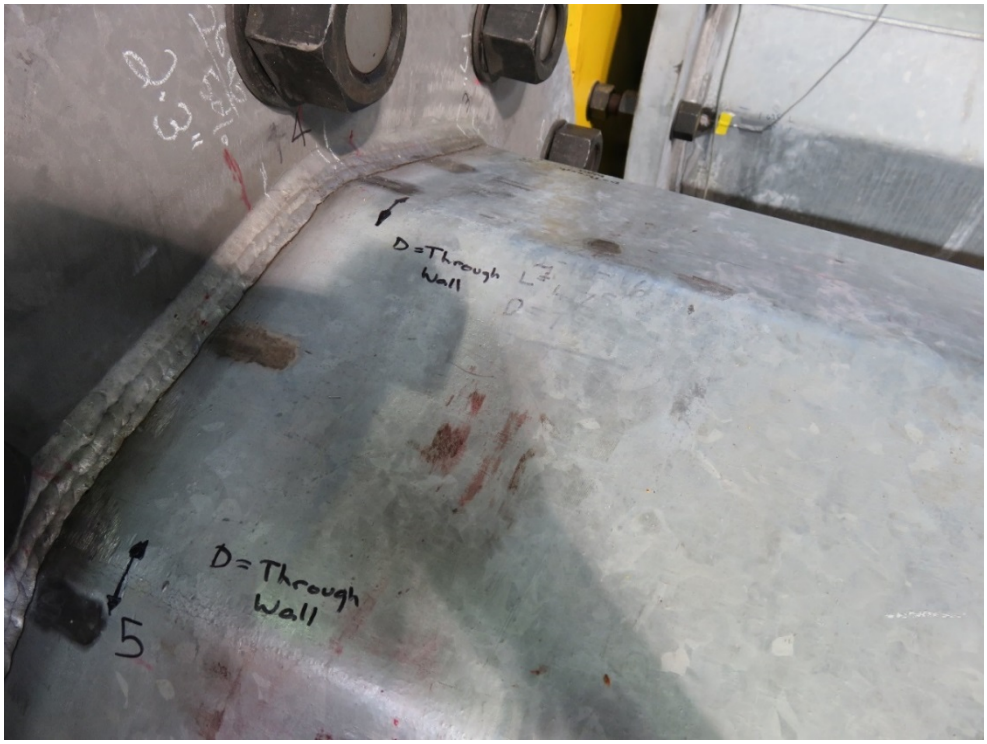

Figure 5.31: Specimen 33-3-12-TX-C after the Conclusion of Test C-1 (Photo Taken after 5.5 Million Cycles)

Following the conclusion of test C-1, Specimen C was removed from the testing setup. It was then flipped 180-degrees and re-attached to the testing frame. Testing was then resumed, as test D-2 continued, and test C-2 was begun.

5.3.3 Test D-2

Following the failure of Specimen D in test D-1, it was removed from the test setup, flipped 180-degrees, and reinstalled. By flipping the specimen, the top bend was changed from bend 4 to bend 10. Test D-2 encompasses the test that was run on Specimen D in its flipped orientation, as shown in Figure 5. This test was run at a stress range of 4 ksi.

5.3.3.1 Test D-2 – Ultrasonic Results

As test D-2 began directly after test D-1, the initial PAUT results for test D-2 are the same as those taken at the end of test D-1. The initial cracking results for test D-2 can be seen in Figure 5.32. Note that this figure reflects the new orientation for test D-2.

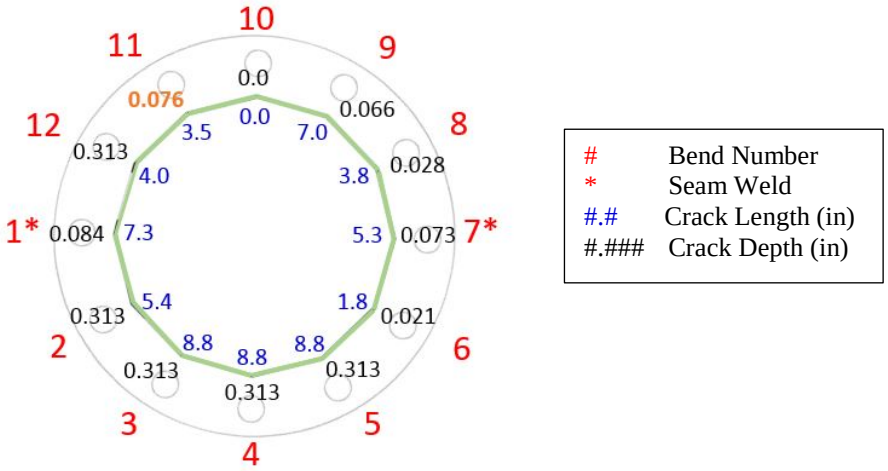

Specimen 33-3-12-TX-D

Figure 5.32: Initial Cracks in specimen 33-3-12-TX-D at the beginning of Test D-2

Test D-2 was only stopped once during its time. This stoppage was the result of the completion of a test on specimen D's companion specimen. Taking advantage of the stoppage, PAUTs were performed at this point. The results of these PAUTs can be seen in Figure 5.33. At this point test D-2 had been run for 1.7 million cycles.

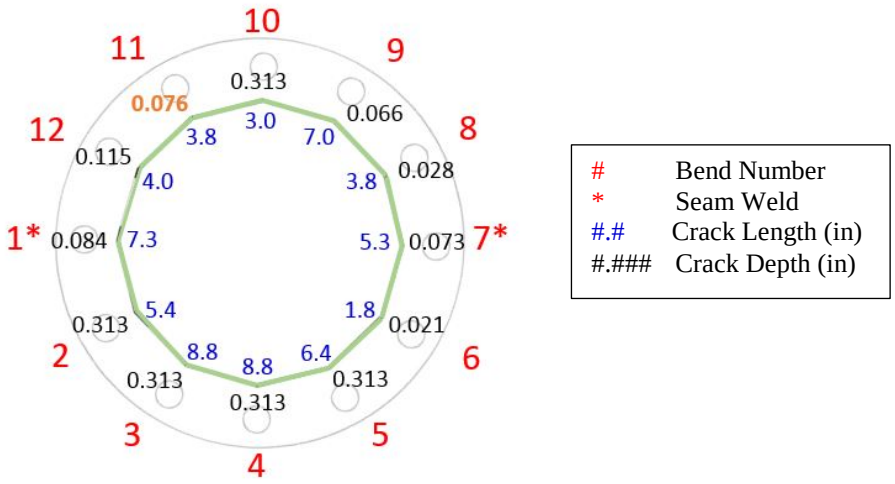

Specimen 33-3-12-TX-D

Figure 5.33: Cracks in specimen 33-3-12-TX-D after 1.7 Million Cycles in Test D-2

The final PAUTs of test D-2 can be seen in Figure 5.34. These PAUTs were run after the test specimen had failed and the test was completed. At this point test D-2 had been run for 6.5 million cycles.

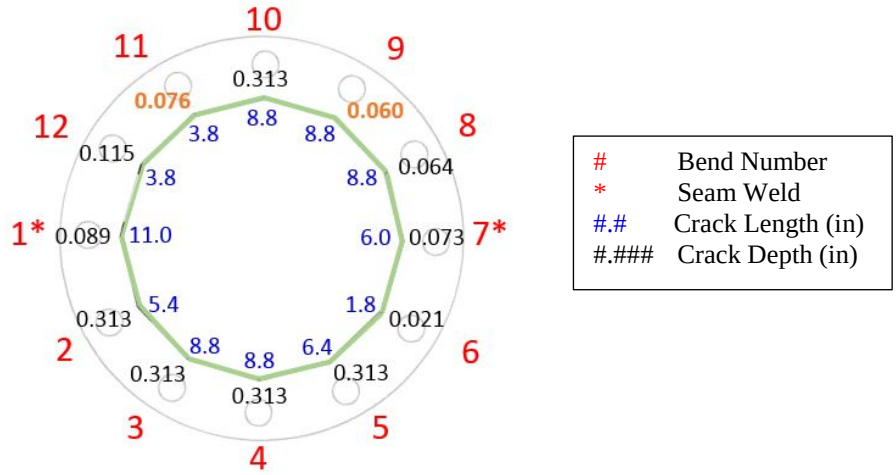

Specimen 33-3-12-TX-D

Figure 5.34: Cracks in specimen 33-3-12-TX-D after 6.5 Million Cycles in Test D-2, the Conclusion of Test D-2

As with previous section, Figures 5.32 through 5.34, display some the length and depth measurements in bolded in orange text. After examining trends in the PAUT data for this specimen across multiple tests, these measurements were determined to be anomalies. Through discussions with Reinhart and Associates technicians, it was determined that an error was likely made for these measurements. This will be discussed in greater detail in Section 5.3.6.

5.3.3.2 Test D-2 – Fatigue Test Results

Following the completion of the initial PAUTs, Specimen D was installed in the testing frame in its flipped orientation. Test D-2 was begun. These specimens were tested at a stress range of 4 ksi. Test D-2 was run at a frequency of 2.7 Hz.

Test D-2 was also run using displacement control. For more information on this method of test control, refer to refer to section 5.3.1.2.

The test was run until the monitoring strain gauge, gauge 8 in Figure 4.15, measured 0 ksi. Before this stress reduction occurred, the specimen was determined to have failed according to the criteria defined in section 3.1.3.

The only delay that occurred during this test was the stopping of the test to examine its companion specimen. This stoppage occurred after 1.7 million cycles had been applied. During the stoppage, phased array testing was performed on both Specimen D and its companion specimen. Once phased array ultrasonic testing had been completed, the companion specimen was flipped and test D-2 was resumed.

Test D-2 was completed shortly after. Specimen D was deemed to have failed after it had developed sufficient cracking to reduce its stiffness by 10 percent. This

reduction in stiffness occurred at 3.5 million cycles. The test was allowed to run to 6.5 million cycles before researchers stopped it. At this point, the monitoring strain gauge measured 0 ksi. A picture of Specimen D after failure can be seen in Figure 5.35.

Figure 5.35: Specimen 33-3-12-TX-D after the Conclusion of Test D-2 (Photo Taken After 6.5 Million Cycles)

The completion of Test D-2 marked the final 4 ksi test in which a specimen was tested to failure. At this point, researchers halted 4 ksi tests and set about testing the specimens at lower stress ranges. This will be discussed further in section 5.3.5.

5.3.4 Test C-2

Test C-2 on Specimen C after its failure during test C-1. After test C-1 was completed, specimen C was removed from the testing frame, flipped 180-degrees, and then reinstalled. By flipping the specimen, the top bend was changed from bend 4 to bend 10. Test C-2 encompasses the partial test that was run in this new orientation, as seen in Figure 5.36. This test was run at a stress range of 4 ksi.

Note that this test was not run to completion. Testing at 4 ksi was stopped after the failure of the companion specimen, Specimen D, during test D-2. The data reported in this section reflects that which was collected up to the stoppage of the test. This occurred after 4.8 million cycles.

5.3.4.1 Test C-2 – Ultrasonic Results

As test C-2 began directly after test C-1, the initial PAUT results for test C-2 are the same as those taken at the end of test C-1. The initial cracking results for test C-2 can be seen in Figure 5. Note that this figure reflects the new orientation for test C-2.

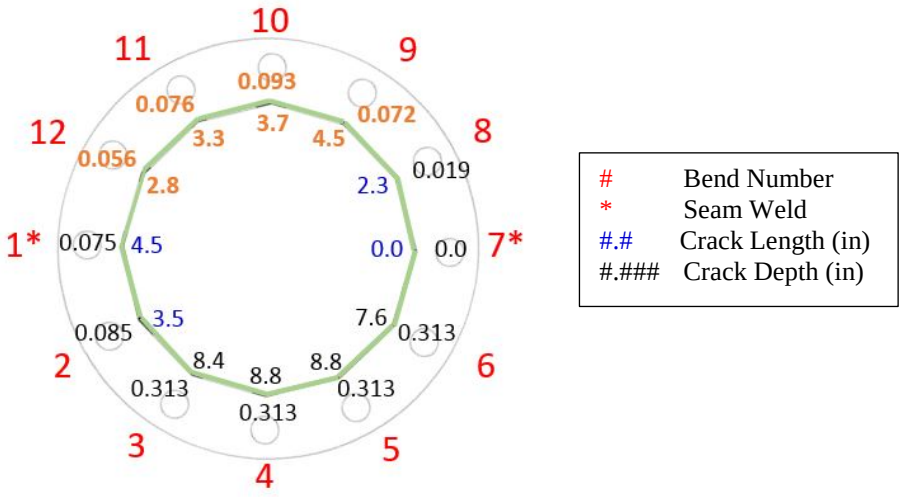

Specimen 33-3-12-TX-C

Figure 5.36: Initial Cracks in specimen 33-3-12-TX-C at the beginning of Test C-2

No intermediate crack measurements were made during test C-2. As such, the second and final PAUT results for this test can be seen in Figure 5.37.

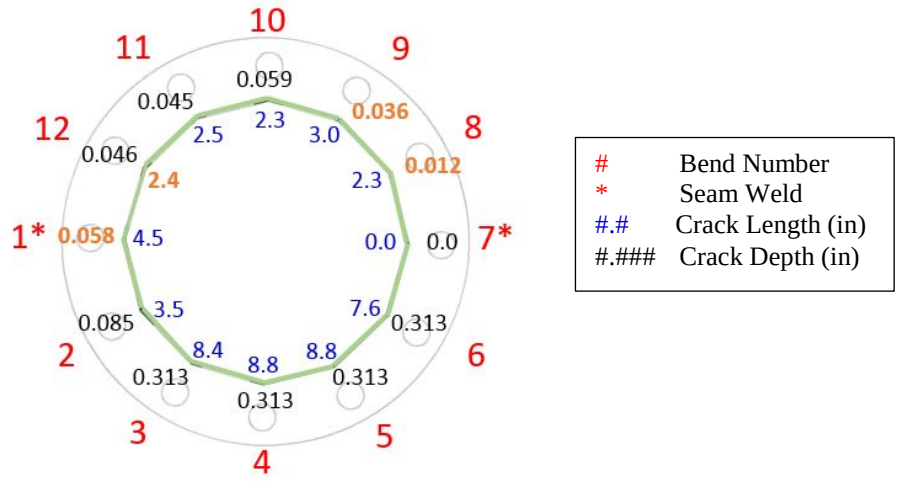

Specimen 33-3-12-TX-C

Figure 5.37: Cracks in specimen 33-3-12-TX-C after 4.8 Million Cycles in Test C-2, the Conclusion of Test C-2

As with previous sections, Figures 5.36 and 5.37 display some the length and depth measurements in bolded in orange text. After examining trends in the PAUT data

for this specimen across multiple tests, these measurements were determined to be anomalies. Through discussions with Reinhart and Associates technicians, it was determined that an error was likely made for these measurements. This will be discussed in greater detail in Section 5.3.6.

5.3.4.2 Test C-2 – Fatigue Test Results

Following the completion of PAUTs, Specimen C was installed in the testing frame in its flipped orientation. Test C-2 was begun. These specimens were tested at a stress range of 4 ksi. Test C-2 was run at a frequency of 2.7 Hz.

Test D-2 was also run using displacement control. For more information on this method of test control, refer to refer to section 5.3.1.2.

As previously mentioned, test C-2 was not run until the failure of Specimen C. It was stopped after Specimen C's companion specimen failed. This occurred after test C-2 had been run for 4.8 million cycles.

Following the termination of test C-2, Specimen C was not removed. Instead, Specimen D was removed, rotated clockwise two bends until bend 12 was the top bend. Specimen D was then reinstalled and another test began. This will be discussed further in Section 5.3.6.

5.3.5 Test D-3 & C-3

Following the completion of the tests D-2 and C-2, researchers began an additional test wherein these specimens that were previously tested at a 4 ksi stress range, were once again tested, but at a lower stress range of 2 ksi. The purpose of this test is

twofold. The first purpose is to see if meaningful data can come from testing a severely damaged specimen. The second is to determine whether or not an analytical model can be made to simulate an ongoing fatigue experiment.

Presently tests D-3 and C-3 are ongoing. Therefore only a brief summary of the results will be presented in this thesis.

5.3.5.1 Test D-3 & C-3 –Results

Following the conclusion of test D-2 and C-2, researchers rotated the failed specimen, Specimen D. Specimen D was removed from the testing setup and rotated clockwise by two bends before being reinstalled. This rotation left bend 12 as the specimen's top bend. The test was run using PAUT measurements taken at the conclusion of the 4 ksi tests. These results can be seen in Figure 5.38.

Note that several bends have cracked lengths of 8.8 inches and depths of 0.313 inches. This is an indication that the bend has become completely cracked. Also note that at the end of test C-2, Specimen C had been tested for 4.8 million cycles, but had not failed. Because of this, the specimen was not rotated at the end of the tests.

Figures 5.38 through 5.40 show representations of the crack lengths and depths as measured by PAUT. The figures represent the PAUTs taken over several months of fatigue testing.

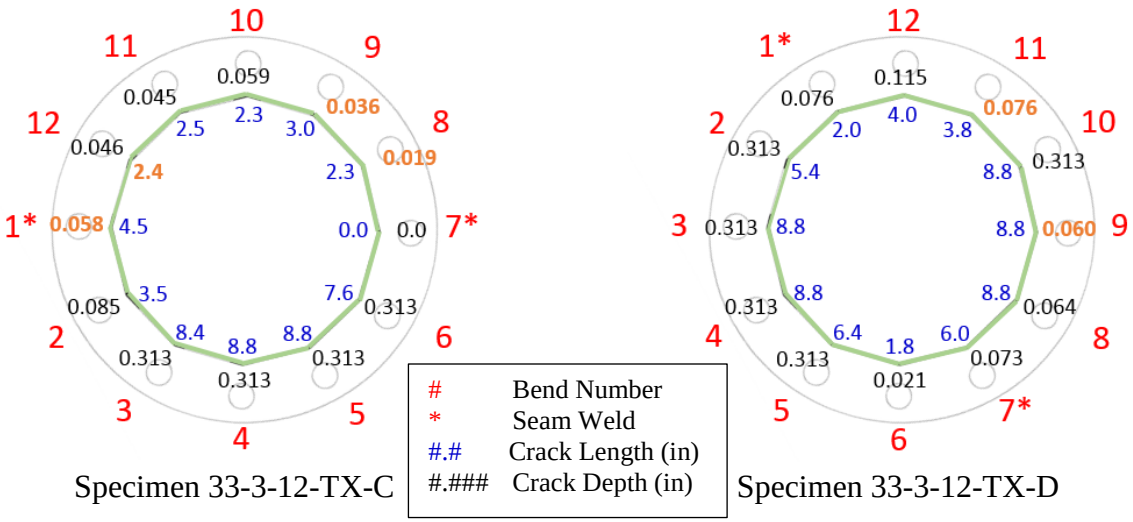

Figure 5.38: PAUT Results for Specimens 33-3-12-TX-C and 33-3-12-TX-D for Test C-3 and D-3 Prior to Start of 2 ksi Testing

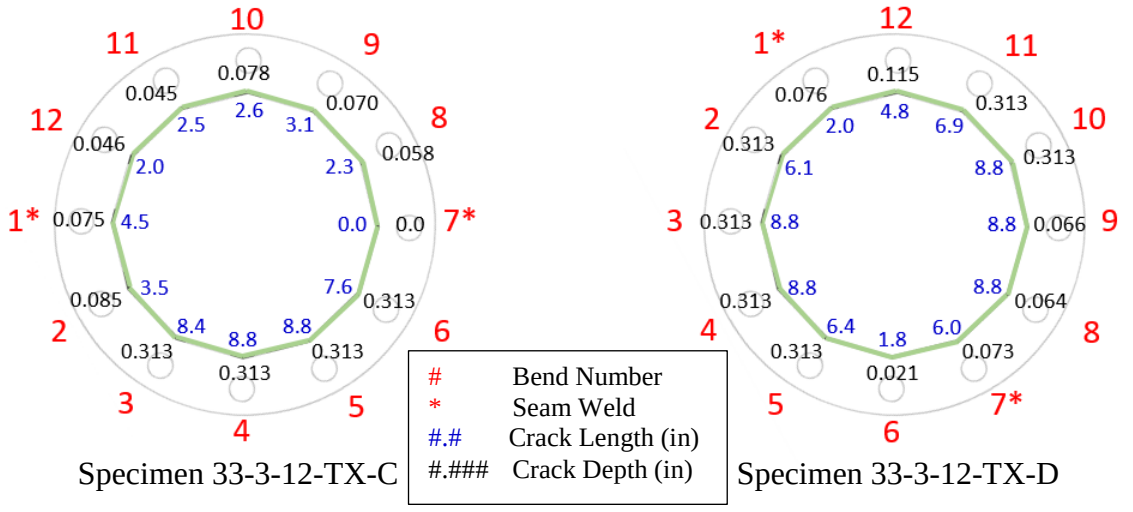

Figure 5.39: PAUT results for 33-3-12-TX-C and 33-3-12-TX-D for Test C-3 and D-3 after 22.6 Million Cycles

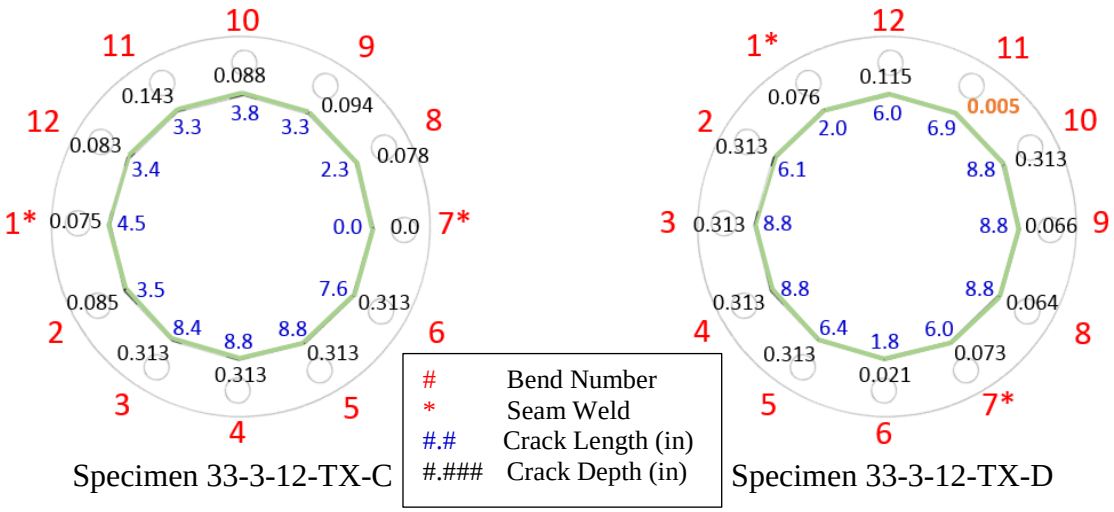

Figure 5.40: PAUT results for 33-3-12-TX-C and 33-3-12-TX-D for Test C-3 and D-3 after 41.0 Million Cycles

The PAUT results show crack growth in both specimens, but at this time, it is difficult to make any conclusions regarding the results of this experiment. Specimen C has shown growth in cracks in the top bends, but these cracks are growing slowly. Specimen D is experiencing crack growth in both the top bend and bends 2 and 11. The test is ongoing, and final results will be reported in other publications.

5.3.6 Summary of 4 ksi and 2 ksi Tests

The total crack growth of Specimens 33-3-12-TX-C and D can be seen in Figures 5.41 and 5.42. These figures present cumulative plots for total crack growth in Specimens C and D through all tests mentioned in section 5.3.

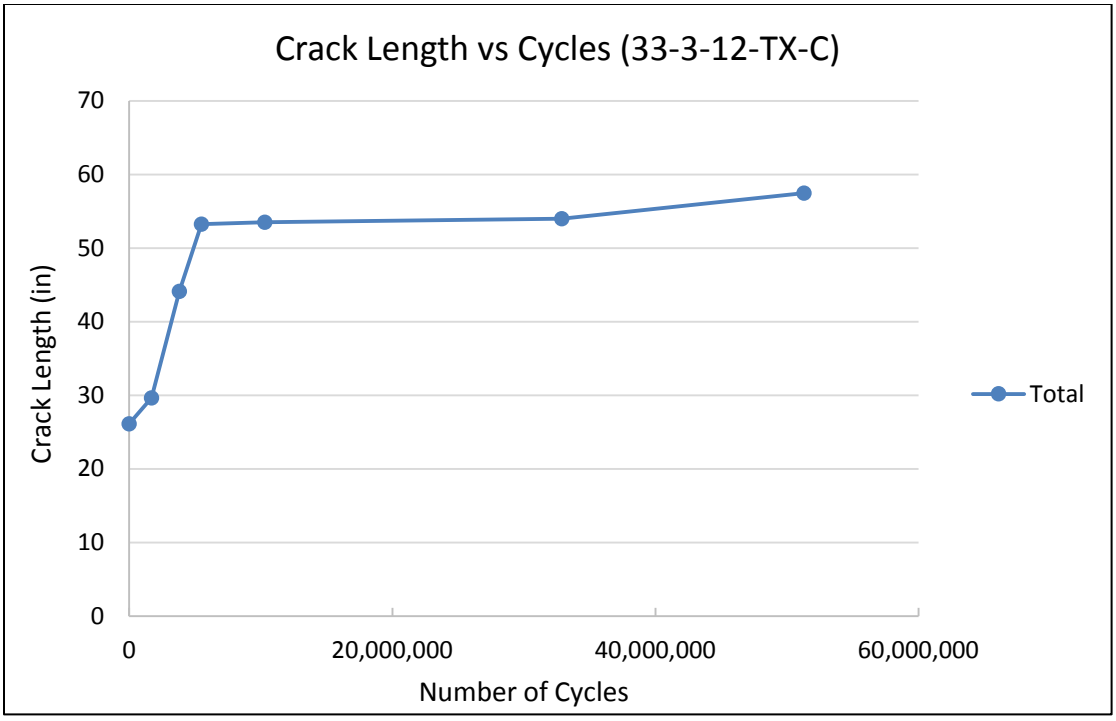

Figure 5.41: Ultrasonic Testing Data for Specimen 33-3-12-TX-C

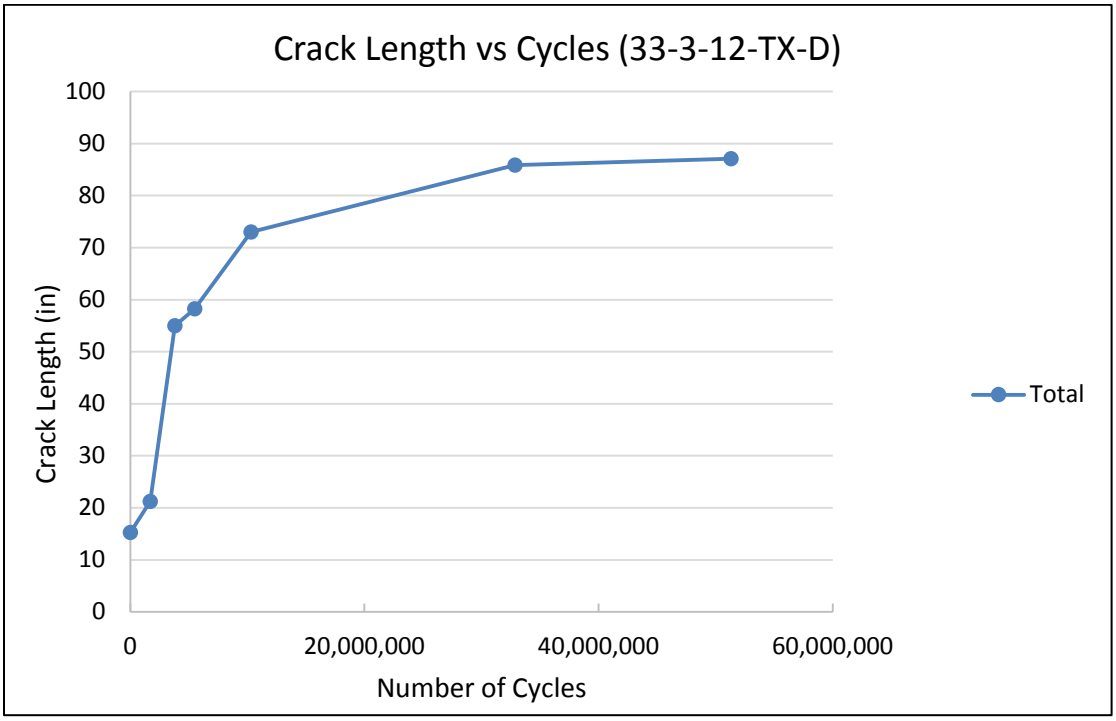

Figure 5.42: Ultrasonic Testing Data for Specimen 33-3-12-TX-D

Note that these plots do not show any reductions in crack length, as the PAUT results in sections 5.3.1 through 5.3.6 may suggest. This is the result of removing the anomalies make it appear as though crack sizes have decreased. When analyzing the PAUT data it is generally very simple to identify an anomaly. When a decrease in size is recorded, researchers must identify the anomaly and remove it. For example, if crack length data consists of five readings of: (1) 3.1 in, (2) 3.25 in, (3) 8 in, (4) 3.25 in, and (5) 3.3 in, it is clear that reading (3) is an anomaly. This readying is then considered to be incorrect, removed, and assumed to match the value of reading (2).

5.4 FATIGUE TEST COMPARISONS

Figure 5.43 shows the results of each specimen's fatigue test results plotted on one S-N plot. As with the previous sections, AASHTO fatigue design curves are included for categorization purposes. Results are also summarized in tabular form in Table 5-2.

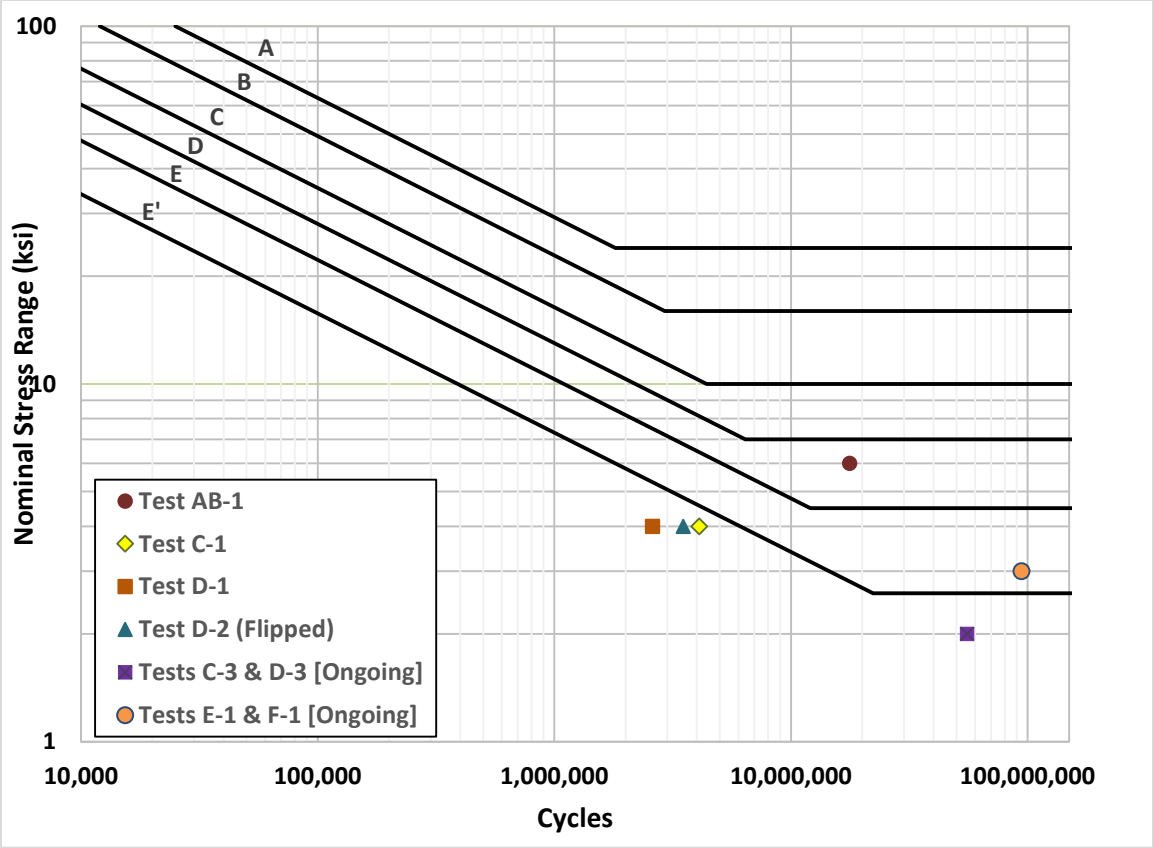

Figure 5.43: S-N Plot for All Specimens

Table 5.2: Summary of Test Results

Test	Tested Specimen(s)	Top Bend	Stress Range (ksi)	Cycles to Failure ($x10^6$)	Total Cycles ($x10^6$)	Comments
AB-1	A & B	1	6	17.8	19.4	Specimens failed simultaneously
E-1	E	11	3	N/A	94.3	Test is ongoing; Approximate cycle count as of December 1, 2016
F-1	F	5	3	N/A	94.3	Test is ongoing; Approximate cycle count as of December 1, 2016
D-1	D	4	4	2.6	3.8	Completion marked by failure of Specimen D
C-1	C	4	4	4.1	5.5	Completion marked by failure of Specimen C
D-2	D (Flipped)	10	4	3.5	6.5	Completion marked by failure of Specimen D
C-2	C (Flipped)	10	4	N/A	4.8	Failure of companion specimen occurred before the test could be completed
D-3	D (Rotated)	12	2	N/A	55.5	Test is ongoing; Approximate cycle count as of December 1, 2016
C-3	C (Flipped)	10	2	N/A	55.5	Test is ongoing; In its current configuration, the specimen was tested to 4.8 million cycles at 4 ksi during test C2

Chapter 6: Summary

The work reported in this thesis is part of TxDOT Research Project 0-6829: *Fatigue Resistance and Reliability of High Mast Illumination Poles (HMIPs) with Pre-Existing Cracks.* The scope of Project 0-6829 includes laboratory fatigue tests on galvanized HMIPs with pre-existing cracks, field studies and measurements to characterize the wind response of Texas HMIPs, the development of a reliability based framework to assess the fatigue life of in-service pre-cracked HMIPs, and recommendations for possible retrofit techniques for in-service HMIPs.

This thesis focuses on reporting research on the task of conducting laboratory fatigue tests of galvanized HMIP specimens with pre-existing cracks at the shaft to baseplate weld. The objective of this work was to collect fatigue test data on pre-cracked HMIPs at low stress ranges, representative of the stress ranges seen by in-service HMIPs subject to vortex induced vibration.

As of December 1, 2016, four fatigue tests have been completed during the course of this research project. Four others are ongoing. These tests have shown that the fatigue life of specimens with pre-existing cracks is highly variable. Many factors affect the fatigue life, including connection detail, testing stress range, seam weld location, and the size of pre-existing cracks. Because of this and the limited test data, no conclusions regarding the tests will be made at this time. The final results and conclusions of this research project will be reported in later publications over the course of the study.

Appendix A: Installation Procedure for Horizontal Tests

1. Start by attaching the actuator to the loading frame and the load box to the actuator. Lower the load box onto the jacks, which can be seen in Figure A1. These jacks were adjusted such that the ends of the specimen would be level when the entire setup was complete i.e., the specimens would not sag.

Figure A1: A Load Box and Specimen Rest on Jacks during Installation

2. Install anchor rods and nuts on the loading box. Leave nuts loose to ease the future mating of the high mast baseplates.

3. Install leveling nuts and washers to a stand-off distance (distance from load box to the baseplate) of 4.5 inches.
4. Position lifting straps around the incoming high mast specimen at the lengths specified in Figure A2.

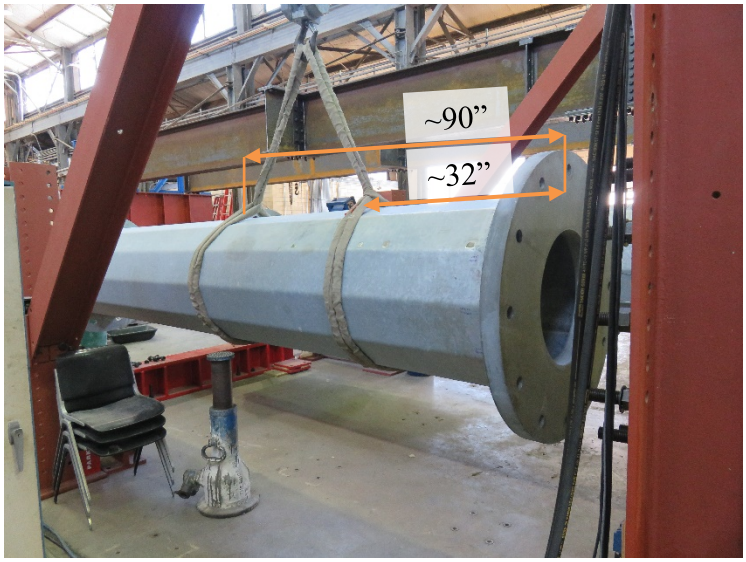

Figure A2: Strap Locations for Lifting Specimens

5. Using a gantry crane, lift the specimen until it is just off of the ground. Place a level on the back side of the baseplate and verify that it is level. After this, use a plum bob to align the top and bottom most bolt holes. This will simplify mating of the specimen to the load box. Adjust the lifting strap positions as necessary. See Figure A3 to see a “leveled” specimen.
6. Beginning on either side of the test setup, mate the first specimen with the anchor rods. It may be necessary to raise and lower the gantry crane or rock the specimen to “walk” it onto the anchor rods. During this process it may be necessary to insert

the remaining rods into the base plate if they do not align perfectly. As the specimen is “walked” onto the anchor rods, begin attaching nuts on the outside of the baseplate to prevent the specimen from sliding off the anchor rods.

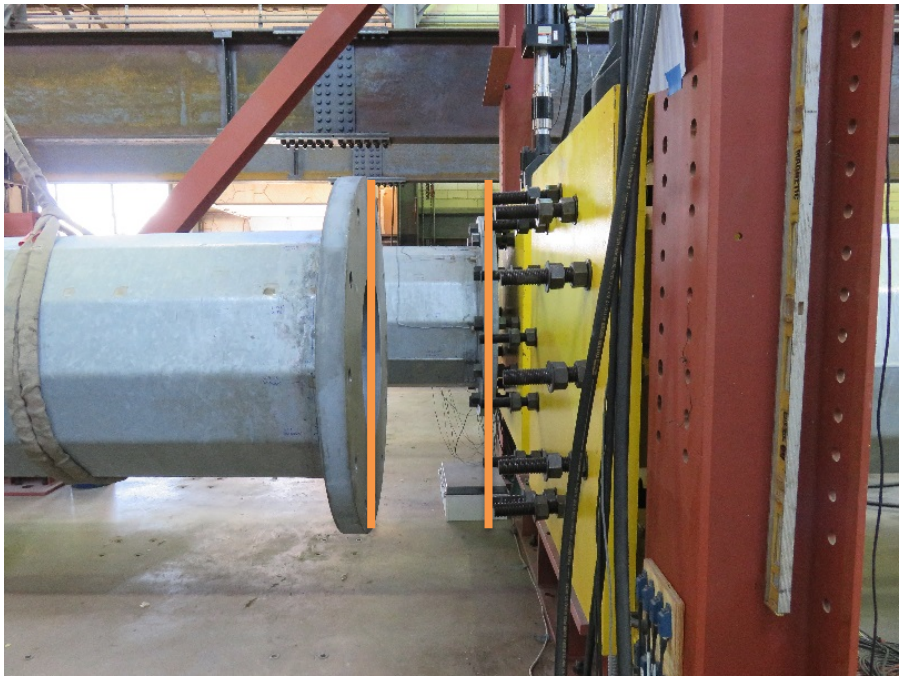

Figure A3: A “Leveled” Specimen is Moved into Place

7. Secure the specimen to the load box by tightening all nuts on the load box and specimen until all are hand tight.
8. While the specimen is still supported by the crane, place a heavy duty jack under the specimen at approximately 1/3rd of the specimen’s length from its free end. Adjust this jack until it supports the specimen. After this is completed, the gantry crane can be lowered and the straps can be removed. See Figure A4.
9. Repeat steps 4 through 8 for the remaining specimen.

Figure A4: An Installed Specimen is Supported by a Jack

10. After both specimens have been installed to the baseplate, use the gantry crane to lift the pinned-end support in place, mating it with the specimen. Tighten bolts between the specimen and pinned-end support plate. Leave the connection between the support's baseplate and spreader beams undone.
11. Repeat step 10 for the roller-end support.
12. Using the hydraulic actuator, lift the loading box, specimens, and end supports until the load box and specimens are no longer supported by the jacks.
13. Acquire three levels and place one on the pinned-end support, one on the roller-end support, and one on the actuator. All of these should be placed on a vertical portion of each support and the actuator such that they show rotation about the long axis of the specimens. See figure A5 for these locations.

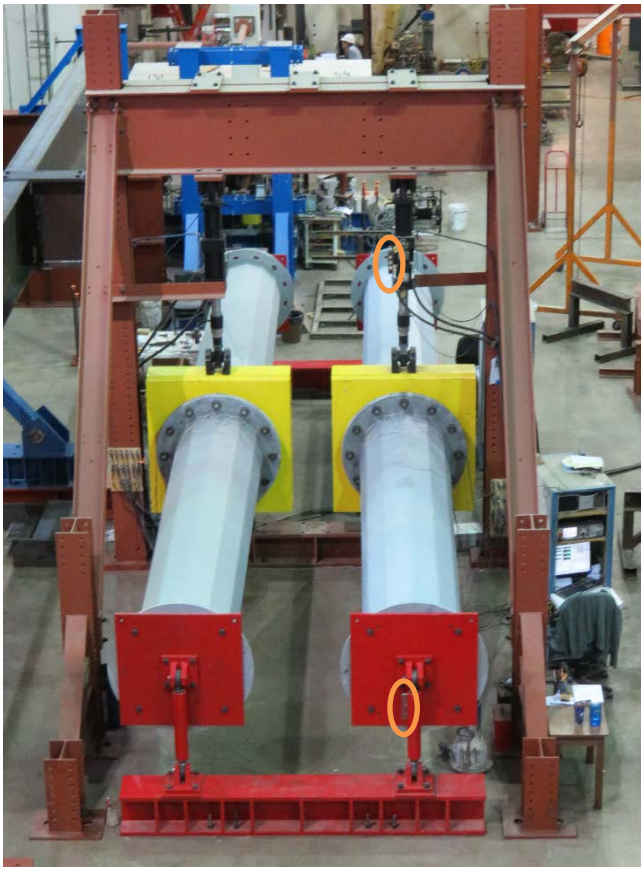

Figure A5: Level Locations

14. With the specimens still supported by the actuator, grab the pinned-end support and rotate the setup (about the actuator's shaft) until the holes of the support's baseplate align with the holes on the spreader beam. Place bolts through a minimum of two of the four holes to limit rotation of the baseplate. Do not tighten these bolts.
15. Verify that the holes between the roller-end support and its spreader beam are aligned. Place bolts through a minimum of two of the four holes to limit rotation of the baseplate. Do not tighten these bolts.

16. Using the hydraulic actuator, lower the load box, specimens, and end supports until the load box and specimens rest on support jacks. At this point the end supports should be resting on their spreader beams. If not, adjust the specimen jacks and/or end supports as necessary.
17. Using the previously installed levels, verify that the actuator and end supports are level.
18. Starting at the pinned-end support, finish installing bolts and tighten the baseplate nuts to approximately 500 ft-lbs torque using a battery powered impact wrench. Repeat for the roller-end support.
19. Secure all load box connections by:
    a. Clamping all load box nuts with approximately 500 ft-lbs torque. This can be accomplished by hitting a slugger wrench with sledge hammer or by placing a five to six foot cheater bar around the slugger wrench and pushing/pulling the cheater bar. Due to the small clearance between the columns and load box. These nuts were tightened from the outside, not the inside of the load box.
    b. Drawing leveling nuts out to a distance of 4.5 inches.
    c. Working in a star pattern, tighten all baseplate nuts using a pneumatic torque wrench at approximately 850 ft-lbs torque. See figure A6 for this pattern.

Figure A6: Tightening Baseplate Nuts (Stam, 2009)

20. The setup is now ready to test.

Appendix B: Installation Procedure for Vertical Tests

1. Start by connecting all major setup systems. These include, connecting the floor beams to the strong floor, connecting all wall beams to the strong wall, connecting the load box to the floor beams, and connecting the lateral support angles to the wall beams. With the exception of the lateral support angles, all connections should be completely tightened.
2. Install anchor rods and nuts on the loading box. Leave nuts loose to ease the future mating of the high mast baseplates.
3. Install leveling nuts and washers to a stand-off distance (distance from load box to the baseplate) of 4.5 inches.
4. Attach double swivel lift plates to the end support plate of the specimen that will be tested. Run straps through the lift plates and attach to the gantry crane.
5. Using a gantry crane, lift the specimen into place on top of the leveling nuts. Hand tighten nuts to prevent movement of the specimen.
6. Secure all load box connections by:
    a. Clamping all load box nuts with approximately 500 ft-lbs torque. This can be accomplished by hammering a slugger wrench with sledge hammer or by placing a five to six foot cheater bar around the slugger wrench and pushing/pulling the cheater bar. Due to the small clearance between the columns and load box. These nuts were tightened from the outside, not the inside of the load box.
    b. Drawing leveling nuts out to a distance of 4.5 inches.

c. Working in a star pattern, tighten all baseplate nuts using a pneumatic torque wrench at approximately 850 ft-lbs torque. This pattern is shown in Figure A6 in Appendix A.

7. Attach double swivel lift plates to the specimen's end support plate, which has previously had a short column bolted to it. See Figure B1 for this plate and column.
8. Lift the end plate and column into place on top of the specimen and secure. Tighten the connecting bolts to approximately 500 ft-lbs using a battery powered impact wrench.
9. Lift the actuator into place between the wall beams and the short column. Connect the actuator to the wall beams.
10. While the actuator is still supported by the crane, hook up all actuator connections to a Power Team SPX pump. Run the pump until the clevis on the free end of the actuator meets the short column on top of the specimen. Connect this clevis to the short column.
11. With the lateral support angles still loosely connected, slide the angles inward, toward the specimen, until each is approximately ¼" away from the specimen.
12. Tighten lateral angle connections to approximately 500 ft-lbs torque using a battery operated impact wrench.
13. Install threaded rod through the slotted holes of the lateral support angles and wall beam. Secure with nuts tightened using a wrench and cheater bar.
14. The setup is now ready to test.

References

AASHTO (2015). LRFD Specifications for Structural Supports for Highway Signs, Luminaires and Traffic Signals. First Edition, American Association of State Highway and Transportation Officials, Washington, D.C.

Belivanis, K. V. (2014). Assessment of Remaining Fatigue Performance of High Mast Illumination Poles. M.S. Thesis, The University of Texas at Austin.

Connor, R. J., S. H. Collicott, A. M. DeSchepper, R. J. Sherman, and J. A. Ocampo. (2012). Development of Fatigue Loading and Design Methodology for High-Mast Lighting Towers, NCHRP Report 718. Transportation Research Board, National Research Council, Washington, DC.

Kleineck, J. R. (2011). Galvanizing Crack Formation at Base Plate to Shaft Welds of High Mast Illumination Poles. M.S. Thesis, The University of Texas at Austin.

Koenigs, M.T. (2003) Fatigue Resistance of Traffic Signal Mast-Arm Connection Details. M.S. Thesis, The University of Texas at Austin.

Magenes, L. (2011). Fatigue Assessment of High Mast Illumination Poles Using Field Measurements. M.S. Thesis, The University of Texas at Austin.

Morovat, M., Chen, Y-C, Eason, M., Engelhardt, M., Manuel, L., Helwig, T., Williamson, E., Clayton, P. (2015). “Fatigue Resistance and Reliability of High Mast Illumination Poles (HMIPs) with Pre-Existing Cracks, Task 2: Survey of Texas HMIPs.” Technical Memorandum, Texas Department of Transportation.

"Phased Array Tutorial - Table of Contents What Are the Advantages?" Olympus - Non Destructive Ultrasonic Test Equipment. Olympus Corporation, n.d. Web. 29 Oct. 2016.

Pool, C. S. (2010). Effect of Galvanization on the Fatigue Strength of High Mast Illumination Poles. M.S. Thesis, The University of Texas at Austin.

Rios, C.A. (2007) Fatigue Performance of Multi-Sided High-Mast Lighting Towers. M.S. Thesis, The University of Texas at Austin.

Roy, S., Y. C. Park, R. Sause, J. W. Fisher, and E.K. Kaufmann. 2011. Cost Effective Connection Details for Highway Sign, Luminaire and Traffic Signal Structures. NCHRP Web Only Document 176 (Final Report for NCHRP Project 10-70). Transportation Research Board, National Research Council, Washington, DC.

Stam, A. P. (2009). Fatigue Performance of Base Plate Connections Used in High Mast Lighting Towers. M.S. Thesis, The University of Texas at Austin.

TxDOT (1998). High Mast Illumination Poles: 100’ – 125’ – 150’ – 175’” Standard HMIP -98, Texas Department of Transportation.

Vita

Mark Eason was born in Orlando, Florida and grew up in Merritt Island, Florida. For his undergraduate education, he attended the University of Florida, where he received his Bachelor of Science Degree in Civil Engineering. During his undergraduate career, Mark was an active member of the University of Florida ASCE Student Steel Bridge Design Team. His experiences with this team helped him discover that he wanted to pursue a master's degree in civil engineering with an emphasis in structures. In fall 2015, he enrolled in the graduate school at the University of Texas at Austin Cockrell School of Engineering to work toward his advanced degree.

Permanent email: easonm.ufl@gmail.com
This thesis was typed by the author.